CAMILA DE SÁ COTRIM

WAVE CLIMATE VARIABILITY ALONG THE COAST OF BRAZIL OVER THE PAST CENTURY

UNIVERSIDADE DO ALGARVE
FACULDADE DE CIÊNCIAS E TECNOLOGIA
2020

CAMILA DE SÁ COTRIM

WAVE CLIMATE VARIABILITY ALONG THE COAST OF BRAZIL OVER THE PAST CENTURY

Master in Marine and Coastal Systems
Work performed under the supervision of:

Theo Moura (Hidromod Ltda.)
Óscar Ferreira (UAlg, CIMA, Faro)

UNIVERSIDADE DO ALGARVE
FACULDADE DE CIÊNCIAS E TECNOLOGIA

2020

Declaração de autoria de trabalho / Declaration of Authorship of work

WAVE CLIMATE VARIABILITY ALONG THE COAST OF BRAZIL OVER THE PAST CENTURY

Declaro ser o(a) autor(a) deste trabalho, que é original e inédito. Autores e trabalhos consultados estão devidamente citados no texto e constam da listagem de referências incluída.

I declare to be the author of this work, which is original and unpublished. Authors and works consulted are duly cited in the text and are included in the list of references.

X

Camila de Sá Cotrim

Faro, 30th of September 2020

Copyright

Acknowledgments

I would like to thank my supervisor, Dr. Theo Moura, for his confidence and support, in addition to providing the data and the main idea of this study. I would also like to thank my co-supervisor, Dr. Óscar Ferreira, for giving me the necessary support in Faro and for guiding me until the result was in the best possible way, maintaining my way of thinking and my ideas.

I would like to acknowledge the coordinators of the Masters in Marine and Coastal Systems (MaCS) and all the professors of the MaCS program who shared experiences and knowledge.

I would like to thank my friends and Oceanography colleagues, Giulia Molina e Laura Verona, for their input on my study and the occasional light conversations. I would also like to thank my friend Emilia Kotiranta for the English corrections and overall review of this document and Ben Mosley for his help with statistics.

I would also like to thank my Faro friends for making these two years so much fun and memorable and a special thanks goes to Jonas Stock and Jasmine Haskell for the amazing Blinding Lights moments.

I thank my sister, Aline Cotrim, my best friend, travel companion and my academic consultant. Thank you for your patience, talks, all the language corrections, suggestions, formatting and the emotional support. Thank you for believing in me, even if you still think I save dolphins for a living.

I thank my parents, Vilma and Cotrim, for their eternal support and friendship, without you nothing would have been possible. Despite the long absence and brief visits, you were always here for me and your confidence was essential for me to be able to follow my dreams. There are no words to describe my gratitude.

Finally, I would like to thank Clara and Laika, for their unconditional love, who even without understanding so many arrivals and departures (often too fast), always received me with the same love and enthusiasm, making my days in Brazil and our video calls always special and with many treats.

Abstract

Changes in the atmosphere and ocean patterns and the intensification of extreme events in the past decades are often suggested as consequences of Climate Change. Understanding the wave climate and its long-term variability is crucial for environmental science and engineering applications. Wave climate studies in the South Atlantic Ocean are limited and there is a lack of observational data. This study aims to describe the evolution of the wave climate along the coast of Brazil in the last century, by performing statistical analysis of critical wave parameters (significant wave height – Hs; peak period – Tp; mean wave direction – Dir). The tool used was the first reanalysis of the 20th century (1900-2010, ERA-20C) developed by the European Centre for Medium-Range Weather Forecasts (ECMWF). Regarding the evolution of the wave parameters, three behavioral groups were established: southern, central and northern regions. Overall, a strong seasonality of waves was observed with the most energetic waves occurred during the Austral winter, with exception of the north region, which showed its most energetic waves during the Austral summer. The analysis of the main South Atlantic climate indices showed that the key ones influencing the wave climate in the southern and central sectors are the Atlantic Multidecadal Oscillation (AMO) and the Tropical South Atlantic Index (TSA) and in the northern region, the Atlantic Meridional Mode (AMM). The most relevant features of the wave climate temporal variability included, peaks of Hs and Tp in the 1910s and 1940s and a positive trend of significant wave height increase starting in the 1970s, with higher increasing rates for extreme waves than for mean conditions. This study concludes that the most likely reasoning behind this rising trend of Hs are the association to the Southern Annular Mode (SAM) and the AMM, the increased hurricane activity, and the upper oceanic warming.

Keywords: wave regime, significant wave height, South Atlantic Ocean, ERA-20C, climate indices

Resumo

Alterações nos padrões atmosféricos e oceânicos e a intensificação de eventos extremos nas últimas décadas são frequentemente sugeridos como uma das consequências das Mudanças Climáticas. Compreender o clima de ondas de um local é imprescindível para a ciência ambiental e as aplicações de engenharia. Os estudos de clima de ondas no Oceano Atlântico Sul são limitados a poucos dados observacionais. Recentemente, o Centro Europeu de Previsões Meteorológicas de Médio Prazo (European Centre for Medium-Range Weather Forecasts – ECMWF) divulgou a primeira reanálise do século XX (1900-2010, ERA-20C). Este estudo teve como objetivo descrever a evolução e variabilidade do clima de ondas ao longo da costa do Brasil no século passado por meio de análises estatísticas de parâmetros de ondas (altura significativa das ondas – Hs; período de pico – Tp; direção média das ondas – Dir). Em relação à evolução dos parâmetros de ondas, foram estabelecidos três grupos comportamentais: regiões sul, central e norte. No geral, foi observada uma forte sazonalidade das ondas e, em alguns casos, um padrão bimodal foi detectado. As ondas mais energéticas ocorreram durante o inverno austral, com exceção da região norte, que apresentou suas ondas mais energéticas no verão austral. Os principais índices climáticos que influenciam o clima de ondas nos setores sul e central do Brasil são a Oscilação Multidecadal do Atlântico (AMO) e o Índice do Atlântico Sul Tropical (TSA) e, na região norte, o Modo Meridional do Atlântico (AMM). As características mais relevantes da variabilidade temporal do clima de ondas no Brasil incluíram os picos de Hs e Tp nas décadas de 1910 e 1940 e uma tendência positiva de aumento de altura significativa de ondas a partir da década de 1970, com taxas de aumento maiores para ondas extremas do que para condições médias. Este estudo concluiu que os motivos mais prováveis para esta tendência crescente de Hs são a associação ao Modo Anular Sul (SAM) e ao AMM, o aumento da atividade de furacões e tempestades tropicais no Oceano Atlântico Norte e o aquecimento da camada superior do oceano como resultado do aquecimento global.

Palavras-chave: clima de ondas, altura significativa de onda, Oceano Atlântico Sul, Brasil, ERA-20C

Resumo Alargado

Alterações nos padrões atmosféricos e oceânicos e a intensificação de eventos extremos nas últimas décadas são frequentemente sugeridos como uma das consequências das Mudanças Climáticas. Estando intimamente ligadas a variações de regimes atmosféricos que apresentam grande variabilidade temporal e espacial, as ondas resultam da transferência de energia da atmosfera para o oceano através do vento. Logo, compreender o clima de ondas de um local é imprescindível para avaliar a erosão costeira e transporte de sedimentos, aplicações na engenharia civil (construção de portos), engenharia naval, maricultura, plataformas de petróleo e embarcações, estimativa da energia de ondas para fins de energia renovável e estudos ambientais. Ademais, o conhecimento do clima pretérito é indispensável para definir a variabilidade do clima das ondas, assim como as tendências associadas às mudanças cíclicas (índices climáticos) e às mudanças climáticas. Igualmente, é fundamental para prever e compreender as tendências futuras, como o aumento da altura das ondas e os impactos dos eventos climáticos nas ondas. Portanto, compreender o clima das ondas e sua variabilidade de longo prazo é crucial para a ciência ambiental, gerenciamento costeiro e aplicações na engenharia.

A área de estudo compreende parte do Oceano Atlântico Tropical, o qual apresenta uma variabilidade climática que varia de sazonal a decadal. A variabilidade sazonal do clima de ondas se deve aos diversos sistemas atmosféricos que atuam na área. O Anticiclone Subtropical do Atlântico Sul (ASAS), a Zona de Convergência Intertropical (ZCIT) e os Anticiclones Polares Migratórios (APM) são as principais forçantes do clima de ondas no Atlântico Sul. Entretanto, os estudos de clima de ondas no Oceano Atlântico Sul são limitados a poucos dados observacionais.

Recentemente, o Centro Europeu de Previsões Meteorológicas de Médio Prazo (European Centre for Medium-Range Weather Forecasts – ECMWF) divulgou a primeira reanálise do século XX (1900-2010, ERA-20C). Esta reanálise se baseia na assimilação de diferentes observações de diversas fontes que documentam a evolução tanto da atmosfera global como do oceano. Sendo assim, as observações incluídas no ERA-20C incluem pressão atmosférica e vento.

Este estudo teve como objetivo descrever a evolução e variabilidade do clima de ondas ao longo da costa do Brasil no século passado, bem como examinar suas possíveis associações com índices

climáticos. Isto foi realizado por meio de análises estatísticas de parâmetros de ondas como altura significativa de onda (Hs), período de pico (Tp) e direção média de onda (Dir). Devido à sua longa extensão, a costa do Brasil foi dividida em seis setores e os dados do ERA-20C foram baixados para um ponto em cada um deles. Os setores são sul (PS), sudeste (PSE), leste (PE), nordeste (PNE), norte 1 (PN1) e norte 2 (PN2). Todos os pontos estão localizados em mar aberto, representando sistemas de águas profundas nos quais a batimetria não interfere na dinâmica de ondas, típico de modelos globais de larga escala.

Neste estudo foi constatada a falta de dados e informações sobre este tema no Oceano Atlântico Sul. Embora apenas dois setores dos seis analisados puderam ter seus dados comparados com dados de boias, foi constatado que o ERA-20C representa o clima de ondas do Brasil suficientemente bem para ser aplicado neste estudo. Os valores modelados apresentam uma subestimativa quando comparados com dados observacionais.

Em relação à evolução dos parâmetros de ondas, foram estabelecidos três grupos comportamentais: regiões sul, central e norte. No geral, foi observada uma forte sazonalidade das ondas e, em alguns casos, um padrão bimodal foi detectado. As ondas mais energéticas ocorreram durante o inverno austral, com exceção da região norte, que apresentou suas ondas mais energéticas no verão austral. Além disso, para os setores PS, PSE, PE e PNE verificou-se que as ondas de E a SW representam o regime de marulho dominante. Por outro lado, para PN1 e PN2, os regimes de marulho vêm principalmente de N e NE.

Os principais índices climáticos que influenciam o clima de ondas nos setores sul e central do Brasil são a Oscilação Multidecadal do Atlântico (Atlantic Multidecadal Oscillation – AMO) e o Índice do Atlântico Sul Tropical (Tropical South Atlantic Index – TSA). Por outro lado, em PN1 e PN2 a situação é mais complexa e, embora o Modo Meridional do Atlântico (Atlantic Meridional Mode – AMM) explique parcialmente o clima de onda da região, nenhum índice climático consegue explicar bem a variabilidade de todos os parâmetros de ondas isoladamente. Além disso, o estudo indicou que o Modo Anular Sul (Southern Annular Mode – SAM) tem alguma influência sobre Hs no Atlântico Sul, com impacto decrescente de sul para norte.

Ao longo dos 110 anos analisados, dois picos de Hs e Tp foram destacados, nas décadas de 1910-1920 e 1940. O primeiro pode estar relacionado ao Oscilação Sul do El Niño (El Niño Southern Oscillation – ENSO) e / ou TSA resultando em picos de Hs para os setores sul e central e Tp no norte. Ou, porventura, este pico seja simplesmente um erro no modelo dada a falta de dados de vento medidos e validados no início do século. Já o pico de Hs na década de 1940 foi detectado ao longo de toda a costa, sendo provavelmente o resultado da combinação de um forte evento de La Niña em 1943 durante uma fase de AMO positiva.

As características mais relevantes das tendências do clima de ondas incluíram variabilidade até a década de 1970 seguida por uma tendência de aumento na qual as taxas de aumento foram mais elevadas para ondas extremas do que para as condições médias. Fora isso, tendências positivas de Hs a partir da década de 1970 foram identificadas para toda a costa, com as taxas mais altas a serem detectadas nos setores do sul e as mais baixas no norte. Os motivos mais prováveis para esta tendência são a associação ao SAM e ao AMM, o aumento da atividade de furacões e tempestades tropicais no Oceano Atlântico Norte e o aquecimento da camada superior do oceano como resultado do aquecimento global.

Por fim, deve ser observado que embora os produtos de reanálise atendam a uma disparidade crítica nas ciências oceânicas e atmosféricas, eles requerem dados adicionais de observação a fim de garantir a precisão e a realidade dos modelos.

Em linhas gerais, este estudo representa um avanço substancial em relação à análise do clima de ondas no Oceano Atlântico Sul e pode servir como uma referência importante para futuras pesquisas na área de estudo.

Palavras-chave: regime de ondas, altura significativa de onda, Oceano Atlântico Sul, ERA-20C, índices climáticos

List of Figures

List of Tables

Table of Contents

1. Introduction

Waves result from the transfer of energy from the atmosphere to the ocean through wind, and are therefore closely related to variations of atmospheric regimes which present great temporal and spatial variability (Cuchiara *et al*., 2006). Understanding the wave climate of a location is important for many different reasons. For example, coastal erosion and sediment transport, civil engineering (construction of harbors, fish farms, oil platforms and vessels), environmental studies and wave energy estimation for renewable energy purposes (WMO, 1998).

Different types of data (measured and/or calculated) can be used to perform wave climate analysis for a specific region. However, since wave measurements are sparse, both in time and space, numerical models are more often used and commonly applied to perform hindcast analysis, where past wave events are simulated based on historical wind data (Pecher and Kofoed, 2017). When it comes to hindcast studies on open ocean, the National Oceanic and Atmospheric Administration (NOAA) WAVEWATCH III (WWIII) is the most used model (Reguero *et al*. 2012; Chawla *et al*., 2013; Silva *et al*. 2015).

Understanding past climate is relevant in defining wave climate variability as well as trends associated with both cyclical changes (climate indices) and climate change. Indeed, this is crucial in order to predict and understand future trends, such as wave height increase and the impacts of climate oscillation on waves (Dodet *et al*., 2010; Kumar *et al*., 2016; Marshall *et al*., 2018).

Wave climate studies off the coast of Brazil are very limited and most of them are focused on a specific region. For instance, Moura (2012) studied the Ceará coast in the north region and Araujo *et al*. (2003) and Sprovieri (2018) analyzed the waves along the south region in Santa Catarina and Rio Grande do Sul, respectively. Hence, the spatial coverage is an important aspect, which is considered in the present study. The data being analyzed here has a 125-km resolution, indicating a meso-scale coverage.

Moreover, in order to be considered a climatology study, the time series to be analyzed must be longer than 30 years. However, the literature review showed a lack of these long-term wave climate analyses along the coast of Brazil. The longest analyses were performed by Silva *et al*. (2015) and Oliveira *et al*. (2019) in the south region, Pereira and Klumb-Oliveira (2015) in the

southeast and Espindola and Araújo (2017) being the only long-term study covering the whole Brazilian coast. Nowadays, the available hindcast data covers a longer period, with the European Centre for Medium-Range Weather Forecasts (ECMWF) being the first to offer a 110-year dataset, called ERA-20C. This reanalysis product was specifically designed for climatic applications with a long temporal scope.

Wave climate researches performed by Pianca *et al*. (2010) and Espindola and Araújo (2017) are the most similar studies to the present work, regarding their spatial coverage and methodology. Based on hindcast analyses, both studies cover the entire Brazilian coast. The first one involves an 11-year WWIII reanalysis data and the latter, a 35-year ERA-Interim reanalysis data. Therefore, the 110-year ERA-20C reanalysis data under examination represents a significant advance in wave climate studies in Brazil, allowing a better representation of shifts and trends, the association to climate indices (such as El Niño and La Niña) and to global climate change.

The present work examines wave climate variability and evolution along the coast of Brazil, in the South Atlantic Ocean (SAO). Ergo, important information regarding the temporal behavior of waves in the area will be addressed. This will improve the definition of the ocean climate, its variability, and possible changes in the evolution of coastal areas, as well as its relevant applications for future environmental and coastal dynamics studies, including wave modelling and risk assessment along the study area, taking into consideration the wave climate change.

1.1. Study Area

The study area covers the coast of Brazil which is located in the Southwest Atlantic Ocean. Due to the different atmospheric systems controlling the climate in Brazil and the extensive coastline with different types of exposure to waves, the study area was divided into six sectors, according to the shoreline orientation. The sectors are south (PS), southeast (PSE), east (PE), northeast (PNE), north 1 (PN1) and north 2 (PN2), as presented in Figure 1. All points are located in the open ocean, representing deep-water systems in which the bathymetry does not interfere in the wave dynamics, typical of large-scale global models.

The regions as divided in this study do not follow the geographical and political classification created by the Brazilian Institute of Geography and Statistics (*Instituto Brasileiro de Geografia e Estatística*) in 1970 (Contel, 2014), but rather a classification based on the wave climate and governing atmospheric systems. For example, here Ceará is inserted in the north region, PN2.

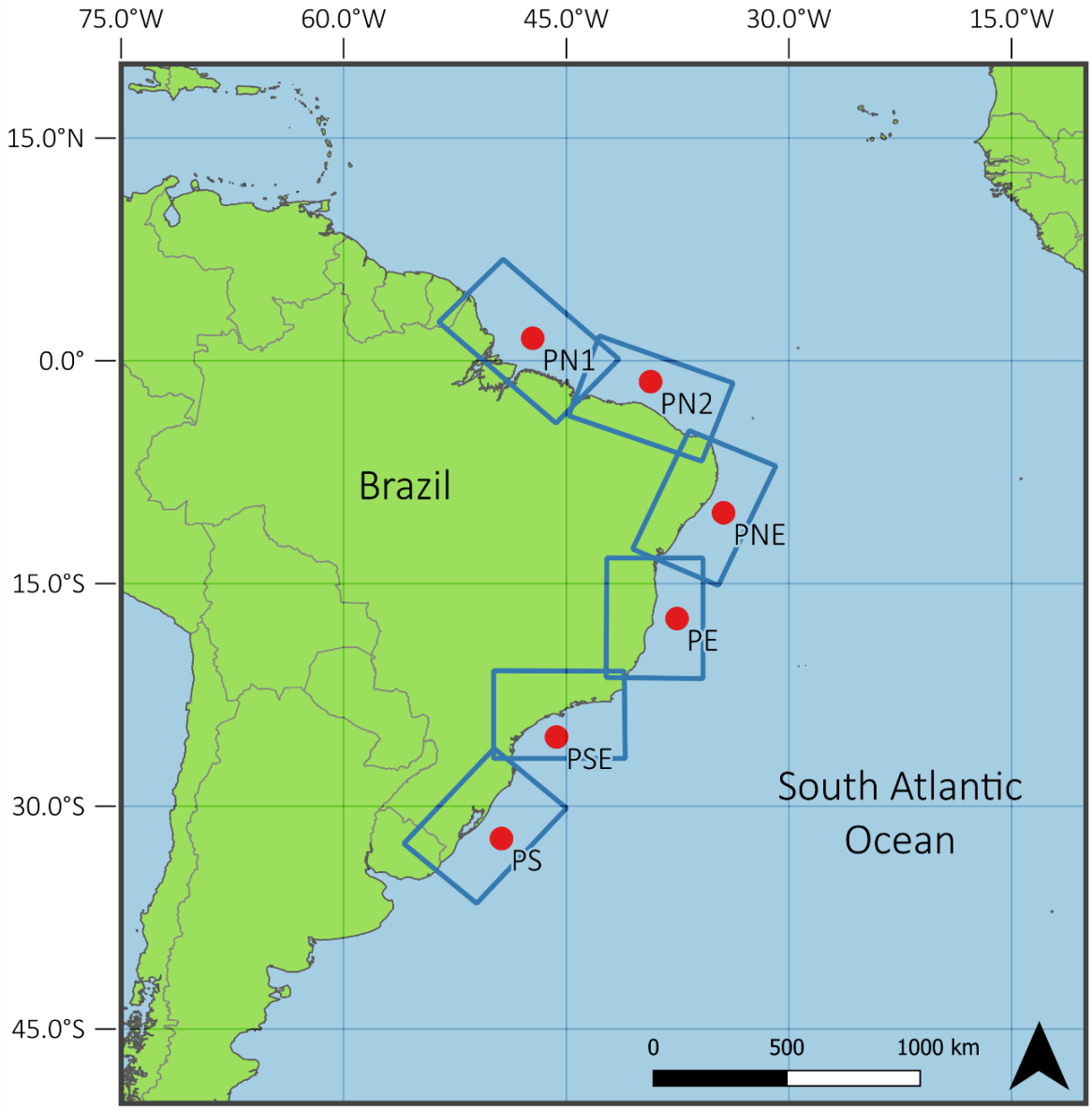

Figure 1 Study area indicating the six points from where data was extracted and their respective regions analyzed in the present study (PS, PSE, PE, PNE, PN1 and PN2).

1.2. Objectives

The aim of the present work is to improve the existing knowledge of the wave climate off the coast of Brazil. This will be achieved by examining its variability through time. The tool to be used is the ERA-20C reanalysis ranging from 1901 to 2010 for six different points on the offshore region of the Brazilian coast made available by ECMWF. The specific objectives, which will allow the main goal to be achieved, are:

- Assessing what has been studied about wave climate in the study area in order to define the regions.
- Describing and characterizing the wave climate patterns in each of the six selected points.
- Understanding the long-term wave climate evolution along the coast of Brazil with monthly, interannual and decadal variability analyses.
- Examining the possible associations between the local wave regime and climate phenomena, such as the El Niño Southern Oscillation (ENSO).
- Performing an analysis focused on extreme wave conditions as well as identifying any existing trends of Hs and Tp that might be associated with climate change or other climatic factors.

The outline of this work is as follows. Section 2 presents the literature review of the topic on wave dynamics and wave reanalyzes. This section also describes the study area climatology, as well as a background of what has been researched in the study area so far. Section 3 introduces the data and methods applied in the study. The results are presented and described in Section 4, followed by a discussion of the findings in Section 5. Lastly, final conclusions and future perspectives for the present study are explored in Section 6.

2. Literature Review

2.1. Wave Parameters

Ocean waves are produced by the transfer of energy from the wind to the ocean. The faster the wind, the longer the time period the wind blows and the bigger the fetch (area over which the wind blows), the bigger the waves. In other words, stronger winds with longer duration generate bigger waves (Stewart, 2005). There are two restoring forces that maintain the progression of surface waves. For waves with wavelength shorter than 1.7 cm, the main restoring force is surface tension, and these waves are termed as the capillary waves. In the case of waves with wavelength above 1.7 cm, the main restoring force is the gravitational force exerted by the Earth, these are the surface gravity waves.

A wind-driven sea is composed of many waves with different heights and periods (Stewart, 2005). This leads to the use of the significant wave height, which is described by the World Meteorological Organization (1998) as "the average value of the height of the highest one-third of all the waves". It is approximate to the visually observed wave height. When working with wave energy spectrum to extract wave parameters, the significant wave height is calculated as four times the square root of the area under the energy spectrum, meaning it is calculated from the total energy content of the wave spectra (Hughes and Miller, 1987). The first definition is usually referred to as Hs and the latter as H_{m0} (equation 1).

$$H_{m0} = 4\sqrt{m0} \tag{1}$$

Here m_0 represents the spectrum variance, which can also be described as four times the standard deviation (Hughes and Miller, 1987).

While wave height is used to determine the size of a wave, the wave period is used to determine the amount of energy it carries. Given that each wave is a combination of several waves, a wave model assumes that the peak period (Tp) corresponds to the highest energy component (WMO, 1998).

Besides Hs and Tp, the third parameter used to describe the wave climate is the mean wave direction (Dir). Wave direction provides a description of the wave spectra and it is useful to calculate the transformations of the wave climate as it propagates to the shore. It is also used to understand where the energy generating the waves comes from. The dominant mean direction of a wave is often directly associated with the peak period (Araujo *et al*., 2003).

However, other parameters can be used to describe wave climate. For instance, Reguero *et al*. (2019) studied wave power as a climate change indicator. Wave power represents the transport of energy from the wind into sea-surface motion. The authors state that such an approach is a better tool to characterize long-term behavior of global wave conditions than simply only using wave height. According to the authors, the success of this indicator lies within the wave power already considering significant wave height and period, and because it represents an accumulation of wave energy over a given period.

2.2. Wave Spectrum

The waves in the ocean can be interpreted as the sum of regular wave components with random phase angles and different frequencies. These various harmonic components can be expressed in a Fourier Series. This combination of components with different periods and amplitudes results in the wave spectrum, which is represented by the frequency domain (Wells, 2012) (Figure 2).

Surface gravity waves are commonly separated into swell and wind sea-state. Swells are composed of waves of longer periods (10 s to 20 s), generated at long distances of the order of thousands of kilometers. Wind sea waves are short-period waves (3 s to 9 s) generated by local winds. These waves are very steep and may present high variability due to changes in the wind intensity and direction. White-capping is a characteristic of sea-state and is closely related to the wind intensity and wave energy saturation at high frequencies (Bigg, 2003).

When long waves travel in the open ocean over a long period of time, they tend to group themselves, due to dispersive properties, depending on their periods. These become sorted into swell of more regular height and eventually arrive at the coast and break (Davidson-Arnott, 2010).

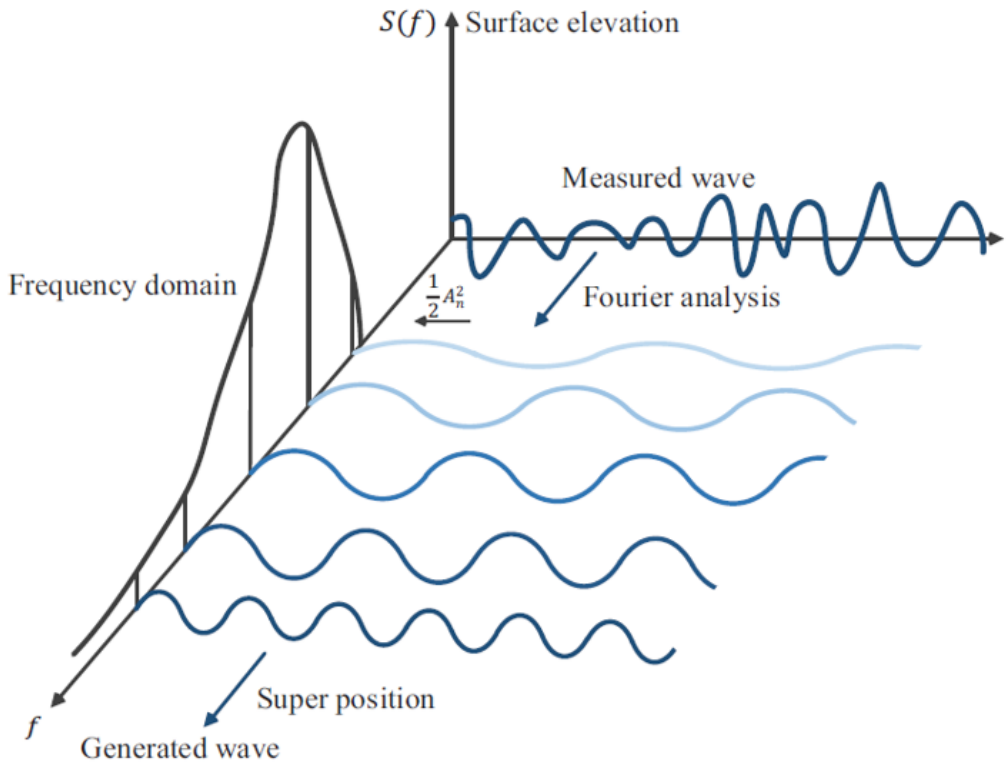

Figure 2 Wave transformation from original to frequency domain, indicating the super-positioning of waves (corresponding to spectral components) to create water surface elevation and the resulting energy spectrum (Vujkov *et al.*, 2019).

2.3. Wave Climate

The knowledge of wave climate has proven itself important to both operational forecasting and the estimation of extremes (WMO, 1998). Ocean waves and their parameters are characterized with observations obtained through records of 15 to 30 minutes. On the other hand, wave climate is the long-term statistics of ocean surface waves and can be characterized by the three parameters mentioned: significant wave height (Hs), peak period (Tp), and mean wave direction (Dir). This means that a wave climate represents the evolution of the wave parameters along time (Holthuijsen, 2007). As wave climate is controlled by meteorological conditions, which generate the winds that produce the waves, it can be analyzed regarding its temporal, directional and spectral characteristics. These include variability and periodicity of wave parameters and their association to climate indices (Pecher and Kofoed, 2017).

There are three major wave-generating storm areas in the world: the Southern Ocean and the northern regions of the Atlantic and Pacific Oceans (Bird, 2008). Given the study area of the present work, the Atlantic Southern Ocean storms are the most important ones regarding the swell regime. Storms in the Atlantic Southern Ocean form SW swells, which travel thousands of kilometers until they reach the coast of Brazil. However, these energetic SW swells are transformed into weaker S and SE swells given the distance they travel and energy they dissipate. In addition, sometimes, the SE swell gains energy with the effect of the trade winds in coastal waters (Bird, 2008). Thus, when analyzing wave climate, it could be useful to divide the wave data in both wind sea-state climate and swell climate analysis. Additionally, these two components of wave climate could also be divided into two or more components each, since a storm may originate from different locations. The same can be interpreted for the wind-sea-state since there could be more than one source of energy for a specific point, such as a hurricane hitting an area usually dominated by trade winds (Holthuijsen, 2007).

Given the possible impacts on coastal systems, extreme waves deserve special attention, as a part of the wave climate of a region. These waves are seen as responsible for the most drastic changes on coastal morphological evolution (Masselink and Gehrels, 2014). Moreover, understanding the patterns behind storm waves is important for any coastal management and engineering activities, not to mention hazard studies. The extreme wave heights (storm waves) are usually associated to high wind speeds generated by meteorological storms (Young ,1999). Additionally, it is important to mention that storm waves are quite frequently combined with storm surges and their impact can be even more disastrous (Marcos *et al*., 2019).

Extreme storm waves are characterized by a significantly higher wave height. The Hs value threshold varies from region to region and is usually calculated as the average of the highest 5 % of all the waves for a given period, or the 95 % percentile (Campos *et al*., 2018) . Nevertheless, this value can be 2 % or 10 %, or even be defined as a specific value for a given location. In the study area, for example, Beserra *et al*. (2007) uses wave power as a way to estimate extreme wave conditions in Ceará while Carvalho *et al*. (2020) uses 3 m as storm wave threshold in Rio de Janeiro.

Another method to study storm waves is through return period analysis, as it is used by Barbariol *et al*. (2019). The authors applied the 50-year return period to compare extreme values and noted

that extreme wave conditions are usually associated with longer wavelengths. They also observed that the difference between the median and the 50-year return values (or the 50^{th} and 99^{th} percentile) is greater at higher latitudes than at the equator.

2.4. Wave Modelling

Waves can be forecasted by using wind results from numerical weather models (Stewart, 2005). There are two main approaches to work with wave modelling in oceanic water: empirical method (parametric) and non-parametric method. The first one is simple and more theoretical and often applied for idealized cases. The second one is applied to arbitrary cases and is widely used for forecasting and for hindcast studies. Additionally, it considers a random-phase/amplitude model where the sea-surface elevation is the sum of several independent wave components (Holthuijsen, 2007). The present study is based on the results of a non-parametric model.

2.4.1. Wave Reanalyses

Reanalysis relies on interpreting, relating, and combining different observations from multiple sources that document the evolution of the global atmosphere, ocean, land surface, cryosphere, and the carbon cycle. Equations of motion and physical processes are used to generate data products based on the assimilated information, which combine a first model result with observations (Buizza *et al*., 2018). The temporal consistency of reanalyses depends on high-quality input observations. These tools have an important role in improving observation systems through the feedback loop, which results from advances in data assimilation and development of better forecast models. The improvement of forecasting systems is largely due to the evolution of observation systems over the last three decades, which is mainly due to the advance of satellite technology (Dee *et al*., 2014; Aarnes *et al*., 2015).

The reanalysis of ocean dynamics strongly depends on the quality of atmospheric fluxes and, consequently, atmospheric reanalyses. However, the application of reanalysis for climate change assessment is controversial, involving difficulties with the representation of low-frequency

variability and trends in the data (Dee *et al*., 2014). Nonetheless, throughout the development of the reanalysis methods, one of the main goals is to guarantee a homogeneous representation of past climate without the effects of the use of different assimilation systems (Dee *et al*., 2011).

These long-term model-based reanalyses were first pursued by NOAA, assimilating only surface pressure which was described as direct and simple to compute (Compo *et al*., 2006). This tool used to be concentrated in the Northern Hemisphere, but its coverage has increased with time, as well as the products' quality. The longest reanalysis was produced by the National Centers for Environmental Prediction, covering 140 years, from 1871 to 2010, by using the Global Forecast System (Dee *et al*., 2014).

The ECMWF started their atmospheric reanalyses in 1979 with the start of the satellite era. Up until the release of ERA-20C, ERA-Interim was the most complete ECMWF product. It covered from 1979 to present with an 80 km resolution. ERA-40 was the first EMCWF product to describe the sea-state by including wave spectra and significant wave height, for example. From ERA-40 to ERA-Interim many technical issues were addressed, leading to considerable improvements (Dee *et al*., 2014). The evolution of forecast and hindcast methods eventually led to the development of ERA-20C.

2.4.2. ERA-20C

ERA-20C is a pilot reanalysis within the framework of the European Union (EU)-funded ERA-CLIM project, which stands for the first of the two European Reanalyses of Global Climate Observations Projects (Poli *et al*., 2016). These projects aim for the development of global climate reanalyses extending back to the early twentieth century. ECMWF leads the project, which includes several EU members, Russia, and Chile. The first phase of this project focused on data rescue of early *in situ* observations, preparation, and reprocessing of satellite datasets (Dee *et al*., 2014).

ERA-20C was produced using the Integrated Forecast System (IFS) at a 125 km resolution, meaning a horizontal resolution of 1.125 ° and 91 vertical levels, as an ensemble of 4-dimensional variational assimilation system (4D-Var) (Poli *et al*., 2013). The use of a 4D-Var technique is mainly

beneficial where data observation is sparse, due to its ability to extract physical information from the model equations (Dee *et al.*, 2011).

The observations included in ERA-20C are surface pressure and marine wind from the International Surface Pressure Databank (ISPD 3.2.6) and the International Comprehensive Ocean-Atmosphere Data Set (ICOADS 2.5.1) (Poli *et al.*, 2016). Hersbach *et al.* (2015) specifies the boundary conditions as well as the atmospheric composition and solar radiation of the atmospheric general circulation model configuration included in the IFS applied to the ERA-20C.

ERA-20C products include a model-only simulation (ERA-20CM) and a 25 km global land surface product (ERA-20CL) (Dee *et al.*, 2014). Prior to including the observational records, ERA-20CM provided results of the reanalysis for the whole time series solely with the model running ten times. This way, a precise assessment of the assimilation of observational data could be performed, which includes the changes of instrumentation and data coverage. Hence, it was possible to separate the impact of the model and the observations in ERA-20C (Hersbach *et al.*, 2015).

The observation quality control in ERA-20C is composed of four steps and aims at limiting the assimilation of bad observations as described by Poli *et al*. (2013). The first one consists of rejecting all observations that are not part of ISPD 3.2.6 or ICOADS 2.5.1 databases, as well as variables other than surface pressure, surface geopotential and wind. The difference between the two databases is that the first database provides atmospheric surface pressure observations while the latter is composed of atmospheric surface pressure above oceans and includes additional geophysical parameters such as atmospheric and oceanic temperatures and atmospheric near-surface winds. The second step in the quality control process involves removing redundant mass information. For example, the model gives preference to surface pressure over pressure reduced at sea level. Background, or first-guess check, is the third step, which compares observations to the first set of results the model outputs. The final step of the quality control process is the variational quality control as there are some specific cases of rejected observations, which may vary with time.

Given that ERA-20C is a reanalysis which includes assimilations of observations, the quality of the model improves with time as more observations become available. For instance, according to Poli *et al*. (2013), the final step of the quality control process rejected around 2 % of surface pressure at the start of the time series and by the 2000s this value decreased to less than 1 %. Additionally, it is estimated that from 1900 to 2010 the number of surface pressure observations per month increased from 30,000 to 3.6 million. Even though, it is not well understood whether this method deteriorates the low-frequency representations of the model, another advantage of working with data assimilation is the inclusion of some realistic information regarding climate and weather events (Poli *et al*., 2016).

Overall, the model represents a great achievement towards the long-term objective of improving extended climate reanalysis by applying instrumental records (Dee *et al*., 2014). The climate fidelity of ERA-20C was investigated by comparing it to several climate indices, among them the Southern Oscillation Index (SOI) and the Oceanic Niño Index (ONI), to name a few. Based on ONI analysis, the most significantly strong El Niño events were identified in 1982/83 and 1997/98 whilst strong La Niña events were observed in 1916-18, 1973-76 and 1988/89. Regarding the SOI analysis, it was found that prior to 1940s, ERA-20C tended to higher values, mainly during the first decade of the twentieth century. The inverse correlation between both indexes implies that the SOI is influenced by the specified sea surface temperature (SST). In general, all climate indices analyzed with ERA-20C exhibited excellent agreement with other products, such as ERA-Interim (Poli *et al*., 2016). Furthermore, D'Agostino and Lionello (2016) compared the atmospheric representation of the Hadley Cell behavior of ERA-20C, ERA-20CM and ERA-Interim. It was concluded that the few assimilated data in the first half of the 20th century by ERA-20C might be a negative aspect of the product. Yet, ERA-20C has been applied to several wave climate studies around the world. For instance, Kumar *et al*. (2019) identified a weak connection between ENSO and wave variability in the North Atlantic by considering that wave conditions can vary significantly depending on the possible co-occurrence of climate modes.

Additionally, ERA-20C has been compared to other atmospheric reanalyses. Befort *et al*. (2016) assessed the representations of ERA-20C and NOAA 20-CR on extra-tropical cyclones and windstorms. The two products agree well on high-frequency variability but not on low-frequency

variability, especially in the first half of the 20th century. The authors associate this difference to the fact that in contrast to NOAA 20-CR, ERA assimilates near-surface winds over the oceans.

2.5. Atmospheric Systems

The two main climatic phenomena involving large-scale interaction between the ocean and the atmosphere in the SAO, and thus influencing the South Atlantic dynamics, are the atmospheric systems and the ENSO phenomenon. Both aspects exist on a permanent, or quasi-periodic, occurrence and are based on the strong air-sea physical coupling (Bigg, 2003).

The Tropical Atlantic Ocean presents a climate variability, which fluctuates from interannual to decadal. The climate and its seasonal variability within each year is due to the various atmospheric systems acting in the area and is further discussed in Section 2.5.1. Moreover, there is a variability of interannual scale (decadal) associated with atmospheric oscillations (indices) like the ENSO (Cavalcanti *et al.*, 2009) (see Section 2.5.2).

The South Atlantic Subtropical Anticyclone (SASA), the Intertropical Convergence Zone (ITCZ) and Migratory Polar Anticyclones (MPA) are the main atmospheric drivers for the wave climate in the SAO and can be seen in Figure 3.

The SASA represents a permanent system of high atmospheric pressure in which the mean sea level pressure (SLP) decreases from the center to the periphery. It is the result of the descending arm of the Hadley cell at around 30° S, which raises the pressure and causes surface divergence (Reboita *et al.*, 2019). This system is usually located between 20° S and 30° S and it governs the climate and its variability in the SAO by originating the easterly winds, or trade winds (Vizy and Cook, 2016). According to Pianca *et al*. (2010), the SASA controls most of the wave climate from the south to the northeast sectors of Brazil, with the exception of winter months which are controlled by cold fronts.

The wind systems of the north and south hemispheres meet in the tropics, leading to the convergence of the trade winds which then results in the formation of a semi-continuous line called the ITCZ (Bigg, 2003). The ITCZ position follows the path of the sun and could be described

as the thermal equator, which is the zone with maximum SST (Wells, 2012). The convergence of winds results in an ascending arm of the Hadley cell, leading to a perpetual low-pressure zone.

The ITCZ's main impact on the wave climate of Brazil can be observed on the northern coast. Depending on the position of the ITCZ there might be N and NE storm waves from the Northern Hemisphere reaching the coast. For instance, Pianca *et al*. (2010) detected a clear seasonality pattern along the Equatorial Brazilian coast, which could be associated to the trade winds' influence with the seasonal migration of the ITCZ.

The MPA represents the high-pressure cells responsible for the arrival of the polar fronts. Cold fronts bring polar air masses from Antarctica to warmer latitudes and strong southerly winds to the south and southeast coasts of Brazil (Campos *et al*., 2018). However, Pianca *et al*. (2010) evidenced the cold fronts presence all the way to the northeast coast. Regarding the resulting wave pattern, the main result is the existence of extreme wave heights given the storm generating area located in the Southern Ocean.

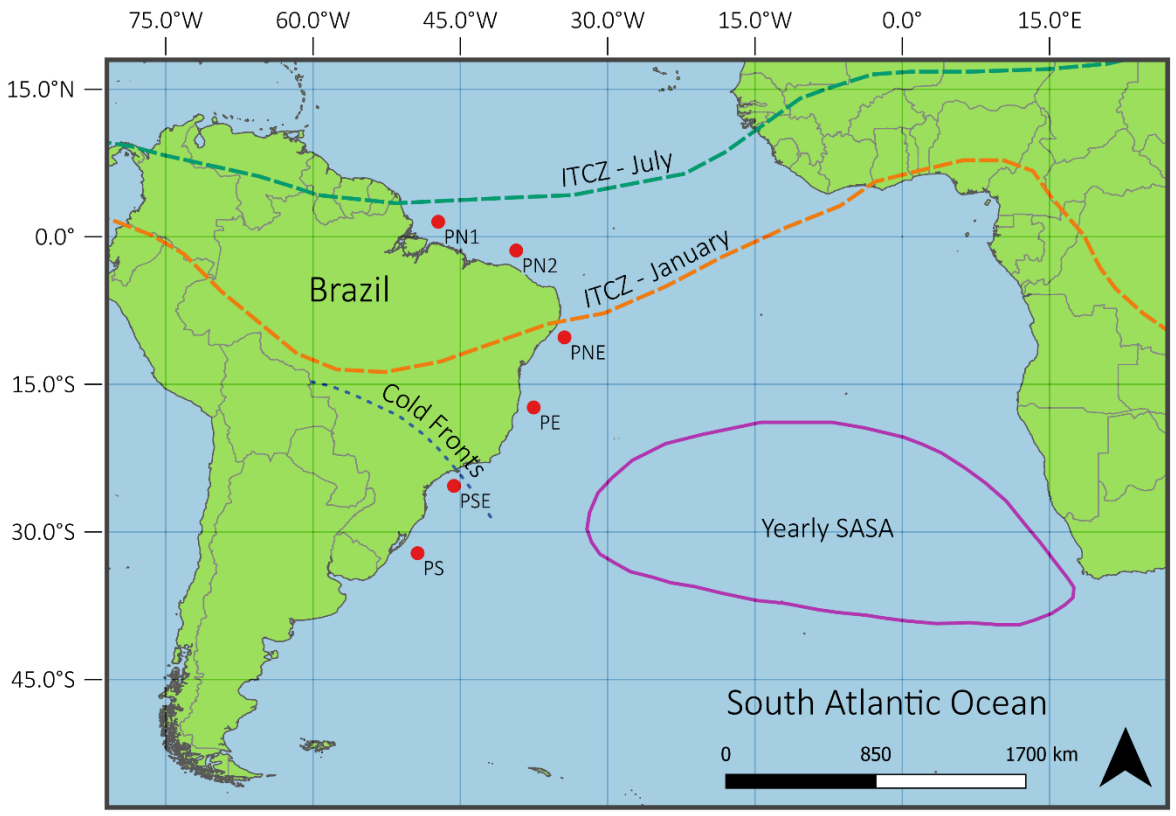

Figure 3 Main features of the atmospheric drivers over the South Atlantic Ocean and the position of each ERA-20C point used in this study.

2.5.1. Annual Variability of SAO

Depending on the solar radiation which varies throughout the year, SASA has a meridional and zonal oscillation (Figure 4). During Austral winter, SASA is more intense and shifts to the west, reaching the southeast coast of Brazil. During Austral summer, SASA moves southward and eastward and is less intense (Tessler and Goya, 2005; Gilliland and Keim, 2018). In other words, the SASA positioning and intensity during winter is influenced by the Hadley Cell and heat sources from the Northern Hemisphere. During summer, monsoons combined with SST and air-sea interactions determine its position (Miyasaka and Nakamura, 2010; Reboita *et al*., 2019).

Due to the SASA position during Austral winter, southeast winds become more intense pushing the ITCZ to the north, close to 5° N. Thus, the same latitudinal shift observed for SASA happens to the ITCZ and the trade winds converge close to the Equator (Tessler and Goya, 2005). Ergo, the ITCZ position shifts with summer/winter regimes being located around 2° N during the Austral summer and 10° N during the Austral winter (Vizy and Cook, 2016). The resulting anti-clockwise atmospheric circulation from SASA arrives on the Brazilian coast with winds from the north and the east quadrants. However, this is only valid south of 10° S. North of that, the ITCZ becomes the main climatic driver (Cavalcanti *et al*., 2009).

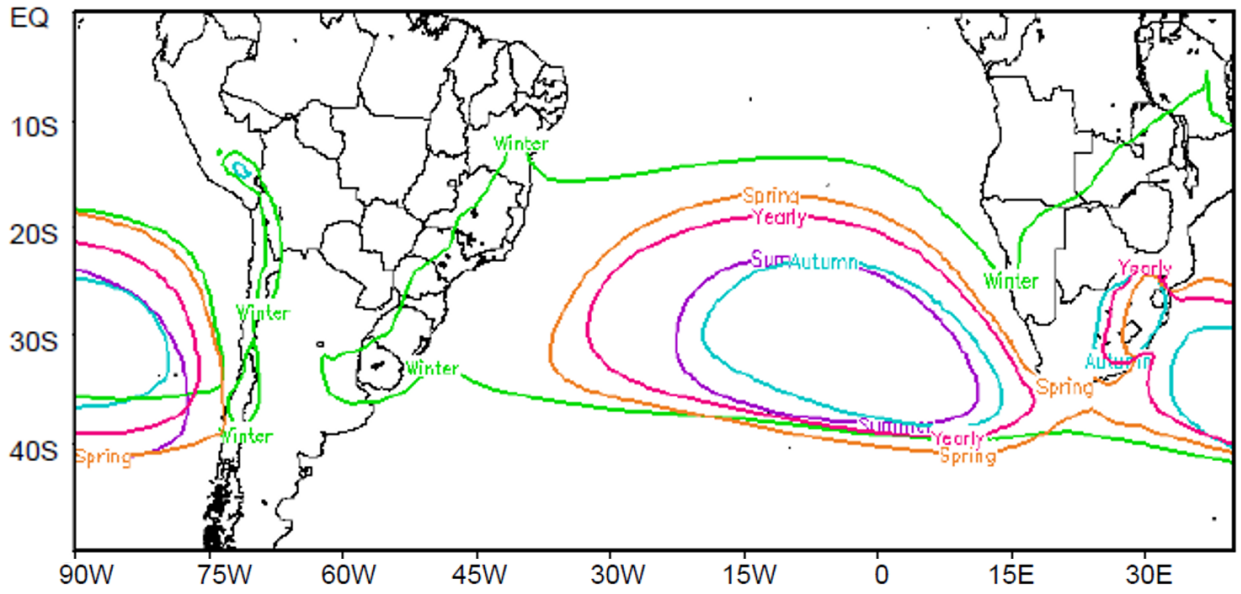

Figure 4 Seasonal and annual climatology of the 1018 hPa isobar in the present climate (1979–2005) from ERA-20C (Reboita et al., 2019).

As mentioned, cold fronts have a great impact on the climatology of part of Brazil and are important drivers of the wave climate in the southern region (Stech and Lorenzzetti, 1992). They are more frequent from May to September and there is a decreasing gradient of the number of cold fronts occurrences across South America and its adjacent oceans. They are more frequent between 30° S and 25° S and rare north of 20° S. In fact, only one to five cold fronts arrive to the Amazon region per year (Cavalcanti *et al*., 2009).

To summarize, the ITCZ is responsible for the circulation along the northern coast of Brazil. SASA, which is the high-pressure cell generating the trade winds, controls the circulation at lower latitudes, from northeast to south regions. The MPA represents the high-pressure cells responsible for the polar fronts' arrival to lower latitudes, which act mostly on the south and southeast regions of the coast during Austral winter (Tessler and Goya, 2005).

2.5.2. Interannual Variability of SAO

Global climate phenomena with interannual and annual climate variability can have strong direct effects on atmospheric and oceanic circulation. Associations between wind and wave climates and climate modes/oscillations are becoming more common with the link of these phenomena and climate change. The importance of these events on wave climate was proven by Dodet *et al*. (2010) and numerous others, when the authors discovered the control of the North Atlantic Oscillation (NAO) over the Hs of the North Atlantic Ocean. Hemer *et al*. (2010) also showed evidence of correlation between wave climate and atmospheric variability. Further, a relationship between the Pacific basin wave climate and ENSO could be observed, as well as a strong positive correlation between Hs in the Southern Ocean and the Southern Annular Mode (SAM).

Furthermore, according to Sun *et al.* (2017), SASA has great variability depending on the present climate mode. For instance, the authors determined the variability of the central position of the SASA in relation to SAM. When SAM is in its positive phase, SASA is shifted to the south and to the north when it is negative. Regarding ENSO, the authors determined that during periods of La Niña, SASA is displaced to the south. These shifts dependent on climate modes are not so clear during winter months as they are during summer.

So far, a restricted number of studies correlating wave climate to climate modes have been conducted in the SAO. For example, Dragani *et al*. (2010) compared *in situ* and satellite Hs data from 1993 to 2006 and neither displayed statistically significant trends of Hs, nor a relationship between interannual Hs variability in the SW Atlantic Ocean and ENSO. On the other hand, Pereira and Klumb-Oliveira (2015) evidenced the impact ENSO has on the wave climate variability along the southeastern coast of Brazil by indicating a decrease of Hs in El Niño years and an increase in La Niña, with a delay of 4 months. However, it is likely that the temporal scope of the first study mentioned (13 years) was not enough to identify such relationships, while the second study was 35 year-long.

Moreover, through global teleconnections, these climate modes can interact between themselves and result in more intense responses from both wind and wave regimes (Nobre and Shukla, 1996; Vimont and Kossin, 2007; Kayano and Capistrano, 2014; Wang, 2019).

2.5.2.1. El Niño Southern Oscillation – ENSO

Among the global phenomena, with marked interannual variability, ENSO is the most discussed feature when it comes to global temperature and climate change. It is centered in the equatorial Pacific Ocean, but its influence has been proved globally (NOAA, 2019). Rodríguez-Fonseca *et al*. (2009) showed that the Atlantic Ocean can influence the ENSO and that there are interrelationships between large-scale phenomena.

The inversion of the high- and low-pressure zones in an El Niño year causes a strengthening of the equatorial current from west to east in the Pacific Ocean and a weakening of the trade winds can be observed. Therefore, the upwelling on the coast of Chile faints and SST rises. The La Niña situation is defined as an amplification of the normal situation causing an increase in the western trade winds and a cooling effect in the eastern tropical Pacific Ocean (NOAA, 2019). ENSO can be examined both through ocean anomalies and atmospheric anomalies. The first one, if estimated with the Niño 3.4 Index, is also called ONI. This index provides an indication of the influence of the ocean on the atmosphere by calculating SST anomalies in the Equatorial Pacific Ocean. On the

other hand, the SOI is a measure of the atmospheric component and is calculated from the anomaly of atmospheric surface pressure difference between Tahiti and Darwin (NOAA, 2017).

Through teleconnections between ENSO and the Walker Circulation, during El Niño years (+ONI), there is an intensification of the SASA and the increase of occurrence of subtropical jets, which block the cold fronts coming from the Southern Ocean. Hence, the waves do not receive as much energy during El Niño phases, which leads to a decrease of Hs and storm waves. On the other hand, the opposite situation happens in La Niña years (-ONI) with a likely increase of Hs in regions where cold fronts affect the wave climate, such as the south and southeast coasts of Brazil. Pereira and Klumb-Oliveira (2015) proved this by showing an increase of S and SW waves in Rio de Janeiro during La Niña years, which represent an increase in storms and swell waves.

2.5.2.2. Tropical South Atlantic Index – TSA

The TSA (or Tropical South Atlantic Index) is an indicator of SST anomaly in the Gulf of Guinea, the eastern tropical SAO, which is highly dependent on the ITCZ position. Along with the Tropical North Atlantic Index (TNA), it was first described by Enfield *et al*. (1999) as an anomalous meridional gradient of SST over the Tropical Atlantic Ocean. Both TSA and TNA present an 8 – 12 year-periodicity for Austral summer/autumn and 2 – 3 year-periodicity for Austral winter/spring.

It is possible to observe the different wind regimes between the two possible TSA scenarios in Figure 5. During +TSA, when ITCZ moves southward, SE trade winds are weaker and SST warmer. In contrast, during -TSA, with the north shift of ITCZ, the winds from SE are the dominant ones reaching the north coast of Brazil and intensifying the easterly wave disturbances which propagate westward over the tropical SAO (Utida *et al*., 2019).

Interactions between diverse climate modes have been observed around the world and they can intensify oceanic and atmospheric variabilities. For instance, evidence has been shown regarding ENSO's influence over TSA's behavior. A cold ENSO phase (La Niña) is usually associated with a positive TSA, resulting in warmer SST and lower SLP in the tropical SAO (Nobre and Shukla, 1996).

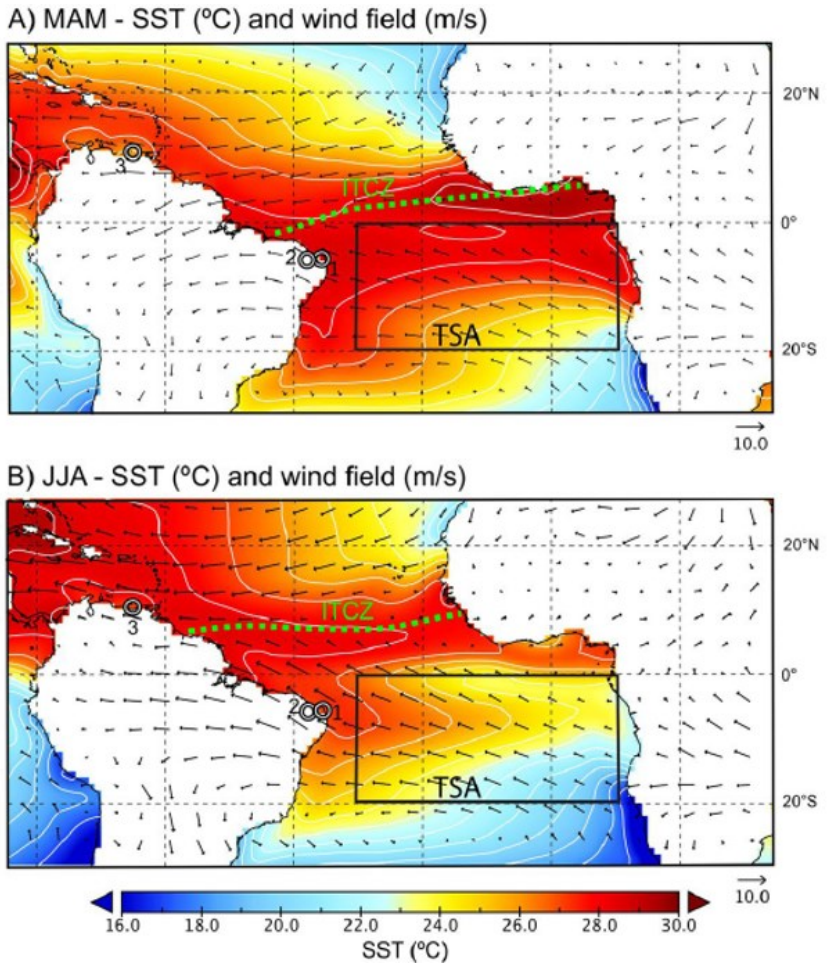

Figure 5 Tropical Atlantic climatology. Mean climatological SST (°C) and 850 hPa wind field (m/s) over the tropical Atlantic Basin for (A) +TSA during March, April and May (MAM) and (B) -TSA during June, July and August (JJA), (Utida *et al*., 2019).

2.5.2.3. Atlantic Multidecadal Oscillation – AMO

The AMO, also known as Atlantic Multidecadal Variability (or Oscillation), represents the SST anomaly between 0° – 80° N in the North Atlantic Ocean, with a periodicity of 60 – 80 years (Trenberth *et al*., 2019). AMO has been in a positive phase since the 1990s and the values are similar to the last positive phase, 1930 – 1960 (Figure 6) (Enfield *et al*., 2001). Moreover, it has been projected that AMO's low-frequency time scale could be linked to thermohaline circulation variations and/or to anthropogenic forcing (Kerr, 2000).

AMO is driven mainly by the atmosphere and changes in the intensity of the westerlies are associated with variability in the southward extension of SASA. Therefore, an increase in SLP

around 40° S implies a southward extension of SASA with an associated weakening of westerlies along the same latitude (Wainer and Venegas, 2002). During +AMO, there is an associated low SLP in the subtropical SAO (Alexander *et al*., 2014).

This climate index has been associated to climate impacts such as hurricane activity, Arctic sea ice anomalies, northern hemispheric mean surface temperature and rainfall in the northeast of Brazil. Thus, one of the ways AMO can affect wave regimes is through its effect over Atlantic storm formation. For example, during -AMO, the cyclogenesis reduces in the Atlantic Ocean (Knight *et al*., 2006). Goldenberg *et al*. (2001) attributed this reduced storm formation during cold phases of AMO to decreased SST and high tropospheric vertical wind shear because of changes in tropical atmospheric circulation. As a result, wave heights are likely to decrease in the northern coast of Brazil due to reduced storm activity.

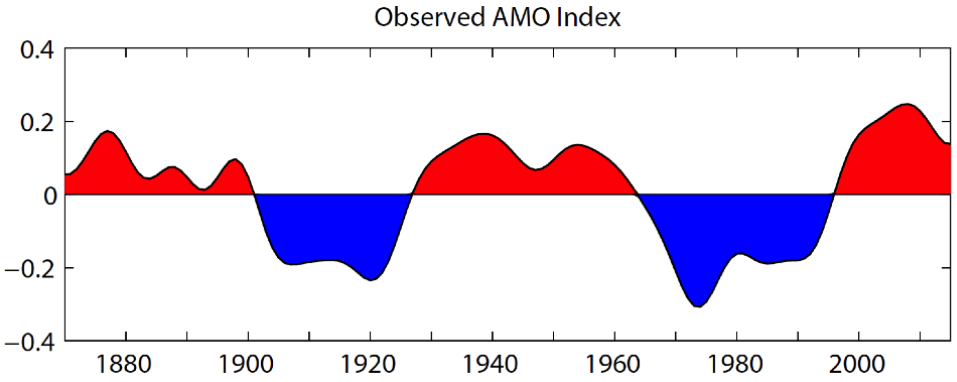

Figure 6 Observed AMO index, defined as detrended 10-year low-pass filtered annual mean area-averaged SST anomalies over the North Atlantic basin (0° – 65° N, 80° W – 0°), for the period 1870 – 2015 (Trenberth *et al*., 2019).

2.5.2.4. Southern Annular Mode – SAM

The Southern Annular Mode, SAM, is the leading mode variability affecting the Southern Hemisphere's atmospheric circulation, responsible for approximately 30 % of the climate variability in the region (Hemer *et al*., 2010; Marshall *et al*., 2018). SAM is calculated based on the zonal pressure difference between 40° S and 65° S. A positive SAM phase is associated with stronger westerlies from 50° S to 70° S, where storm waves are generated, and weaker from 30° S to 50° S. Therefore, during +SAM extreme wave conditions are favored and an increase in Hs and Tp are usually associated.

SAM has been the center of a debate regarding positive trends of Hs, wind speeds and storms in the Southern Hemisphere. According to Marshall (2003) and Hemer *et al*. (2010), these could all be linked to the Southern Ocean storm belt shift which has been observed since the 1970s.

2.5.2.5. Atlantic Meridional Mode – AMM

The Atlantic Meridional Mode (AMM) is the leading mode of coupled ocean-atmosphere variability in the Atlantic Ocean and could be interpreted as the equatorial gradient of SST, along the ITCZ. It affects rainfall in the northeast of Brazil and tropical cyclone development in the North Atlantic, generating storm waves, which hit the north coast of Brazil. Therefore, AMM is linked to climatic conditions that cooperate on the seasonal hurricane activity and can be excited by AMO (Vimont and Kossin, 2007). During +AMM, in which ITCZ is displaced northward, there is an increase of SST and decrease of SLP in the North Atlantic, favoring the tropical cyclone development (Figure 7). This process is associated with a decrease of NE trade winds in North Atlantic and an increase of SE trade winds in the South Atlantic. As a result of increased cyclogenesis in the North Atlantic, wave heights on the northern coast of Brazil are likely to increase.

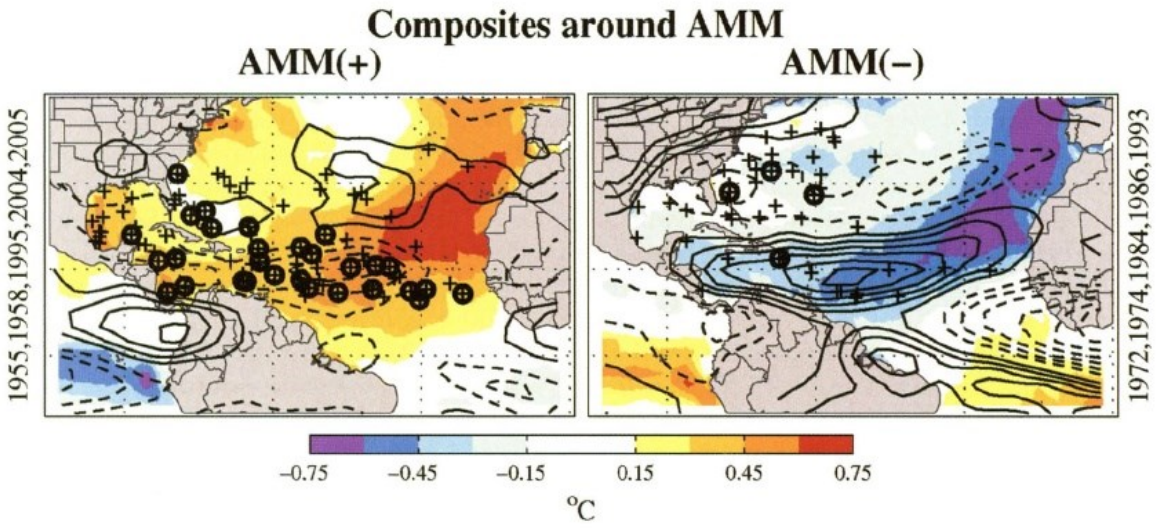

Figure 7 Tropical cyclogenesis points for the five strongest and five weakest AMM years, superimposed on composites of SST (shaded) and shear (contours) anomalies (Kossin and Vimont, 2007).

2.6. Wave Climate in Brazil

The wave climate off the coast of Brazil is determined by the winds originated in the SAO and Southern Ocean, involving three large atmospheric systems: ITCZ, trade winds from the SASA and cold fronts (Figure 8). Given these major mechanisms responsible for wave formation in the Southwest Atlantic Ocean, it can be concluded that the Brazilian coastline is influenced by two main wave systems: east-northeastern and south-southeastern waves (Dominguez, 2013). The importance of these atmospheric and wave systems varies with latitude and coastal orientation.

In addition, the role of the cold fronts over the Brazilian wave climate is important given the fact that the most energetic waves come from the south and are generated by strong winds associated with such systems. As a result, the southern region of Brazil is the most affected and the influence of cold fronts decrease with decreasing latitude (Pianca *et al.*, 2010). Moreover, from the south region to the eastern region of the Brazilian coast, the winter months are the most energetic ones whilst the most energetic period in the north region is from December to March.

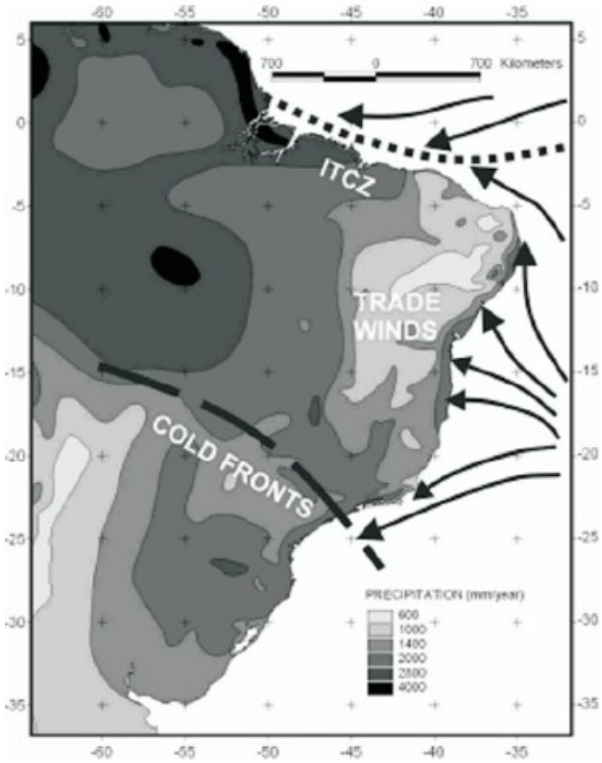

Figure 8 Major elements of climate affecting the Brazilian coastal zone, including the ITCZ, trade winds and cold fronts (Dominguez, 2013).

Given the extent of Brazil and the variability of orientation of the coastal zone, not all atmospheric systems affect all the regions in the same way. Therefore, for a more adequate characterization, a separation into large regions is useful.

The following literature review presents a simplified description of the wave climate along the coast of Brazil, based on studies that have different temporal and spatial coverage, resolution and methodologies.

2.6.1. South and Southeast Regions

The south and southeast regions have a strong seasonality marked by the action of cold fronts during autumn and winter, generating waves from S and SE. This was pointed out by Tessler and Goya (2005) who identified long period waves during winter. These waves ranged from 10 s to 16 s, representing a swell dominated wave climate, and wave heights from 1 m to 4 m. When reconstructing the wave climate in the south and southeast coasts of Brazil, from 1997 to 2005, Alves *et al*. (2009) observed that the swell regime on the Southwest Atlantic Ocean is predominantly from SW. This changes once waves from the fourth quadrant (NW) become dominant. The authors concluded that this is probably due to the atmospheric circulation at the ocean surface being associated to the SASA. On the other hand, Lourenço (2012) examined the interannual wave climate variability in the south and southeast coast of the Brazilian coast from 1997 to 2010 and concluded that waves from S are the most energetic ones. In addition, an interannual pattern was not identified.

Araujo *et al.* (2003) concluded that in Santa Catarina, sea-state derives mainly from E and swell from S. This agrees well with the results found by Lourenço (2012), who described the waves from E and S as the most important ones regarding sediment transport. In Santa Catarina, sea-state has typically an average Hs of 1.25 m and Tp of 8 s, whilst swell waves range from 1.25 m to 2 m with a Tp of 12 s. Although not frequent, Hs higher than 4 m occurred in all seasons in Santa Catarina. In general, swell conditions prevailed during autumn and winter, sea-state during summer while a balance between both conditions could be identified during spring (Araujo *et al*., 2003). Even though Sprovieri (2018) examined hindcast results for Rio Grande do Sul, the author also observed

a seasonality of the wave climate in the south of Brazil with the most energetic waves coming from SE during autumn and winter.

In São Paulo, in the southeast region, waves from S and SW are the most frequent ones (Lourenço, 2012). A 23-yearlong study performed by Cecilio and Dillenburg (2019) revealed a bimodal wave climate along the southern Brazilian shelf with a predominance of SSW and ENE waves.

Moreover, the South and Southeast regions present the most numerous *in situ* information, as well as modelled experiments involving wave climate. For example, by combining observational data with reanalysis product from WWIII, Campos (2009) observed that SW waves with Tp higher than 11 s compose the largest waves to arrive in the Campos Basin. This result was associated to cyclones occurring during autumn and winter and was also observed by Cuchiara *et al*. (2006).

2.6.2. East and Northeast Regions

Due to the lack of wave measurements along the state of Bahia, Bittencourt *et al*. (2000) constructed standard wave refraction diagrams and estimated two main wave patterns which were confirmed by Tessler and Goya (2005). The first pattern is controlled by the trade winds and is composed of wave fronts coming from NE and E, which start interfering with the bottom at approximately 20 m depth. The second pattern represents the winter regime with waves from SE and SSE, which begin their interaction with the bottom at around 35 m. This depth difference indicates that the winter pattern is composed of bigger waves. The waves in the first pattern have periods of 5 s to 10 s and wave heights ranging between 1 m and 2 m. On the other hand, the winter regime was represented by waves with periods of 7 s to 12 s and wave heights of 1 m to 2 m as well.

Moreover, a one-year long study performed in Pernambuco, evidenced the same Tp limit between summer and winter wave regimes, 7 s (Silva *et al*., 2016). By analysing four years of wave measurements, Gomes and Silva (2018) observed that summer waves come from SE in Pernambuco, representing the sea-state regime, while swell energy derives from S and SSE.

Seasonal variability of the wave climate has also been demonstrated by Almeida *et al*. (2015). According to the authors, the most frequent waves in Rio Grande do Norte are from ESE, and although these waves are predominant throughout the year, E waves become dominant from December to February. When analysing the variables altogether, they concluded that the typical wave climate in Rio Grande do Norte is composed of waves with Hs ranging from 1.3 m to 1.7 m, with Tp of around 8 s and waves coming mainly from ESE.

To summarize, it has been shown by several studies that the most frequent waves in this region are from E and ESE, associated to the trade winds variability. Along the Northeast coast, around 95 % of sea-state waves come from 90 ° to 135 ° (Silva *et al*., 2016), while 75 % of the waves in Rio Grande do Norte come from ESE (Almeida *et al*., 2015) and 60 % from SE in Pernambuco (Gomes and Silva, 2018).

2.6.3. North Region

In addition to being located on the Equatorial region, the Northern coast of Brazil has a NW-SE orientation, being exposed to waves coming from the Northern Hemisphere (Beserra *et al*., 2007)(Beserra et al., 2007). When comparing the North region to the rest of the coast, Pianca *et al*. (2010) observed a lower variability regarding the wave parameters, with Hs ranging from 1.5 m to 2 m and Tp from 6 s to 8 s.

According to Tessler and Goya (2005), the wave climate in the north region is dominated by the action of the ITCZ resulting in low periods and waves from E and SE. On the other hand, the authors also discuss the effects of storms in the Northern Hemisphere over the waves in this region, which generate waves with long periods of up to 18 s. This occurs mainly from January to March, due to the Boreal winter (Pianca *et al*., 2010). In contrast, Espindola and Araújo (2017) described the highest Hs during autumn and the lowest during spring.

Moura (2012) observed that, between 2007 and 2008, 75 % of the sea-state presented a period from 6 s to 9 s in Ceará, while Silva *et al*. (2011) concluded that 80 % of the waves in the region have 4 s to 9 s periods. This means that the wave climate along the eastern coast of Ceará is dominated by sea-state. Swell waves were identified from September 2007 to March 2008.

Furthermore, the largest wave heights were recorded from March to May 2007, pointing to a more energetic wave climate during those months.

On the other hand, Vieira *et al*. (2007) identified the swell coming from 20 ° to 45 ° and periods ranging from 10 s to 16 s while sea-state arrived mainly from 75 ° to 120 °, from 1997 to 2001. Silva *et al*. (2011) performed a study with a similar temporal scope and observed that the first half of the year exhibited waves coming from the first quadrant (40 ° to 60 °), while the second semester presented waves from the second quadrant (100 ° to 120 °). Both these studies were also focused on Ceará. Alternatively, by analyzing the dispersive behavior of a swell arrival in Ceará, Farias and Souza (2012) associated the wave climate in the region to storms in the Northern Hemisphere, around 20° N and 50° N.

Located between PNE and PN2, Assunção (2017) observed that Fernando de Noronha Archipelago presents a wave climate similar to the northern region of Brazil. Both sea-state and swell waves come from ENE and NNW, although the latter is concentrated between October and January. The highest Hs values were associated with swells from January to March.

3. Methods

This study describes the wave regime of the Brazilian coast based on the reanalysis results provided by the ECMWF. This data refers to the 20th century (1900-2010) and is part of the ERA-20C as described by Poli *et al*. (2016).

3.1. Data

The ERA-20C results were extracted from the ECMWF website: https://apps.ecmwf.int/datasets/data/era20c-daily/levtype=sfc/type=an/.

As previously mentioned, one of the wave parameters to be analyzed is the significant wave height, which is calculated as four times the square root of the area under the energy spectrum. The peak period is the period correspondent to the maximum peak of energy of the spectrum and the mean wave direction is correspondent to the direction containing the peak period. Based on the literature review, significant wave height is indicated as Hs and is equivalent to H_{m0}, peak period is referred to as Tp and mean wave direction as Dir.

The dataset has a 3 h frequency from 4th of January 1901 to 28th of December 2010 for six selected points, each representative of its own region (Figure 1).

3.2. Data Validation

To assess how well the ERA-20C product represents the reality of the wave climate in the study area, *in situ* data was downloaded and ERA-20C validated against them. Although the observed data is sparse, with short coverage periods in specific areas, it can give an idea of the quality of the model.

Data validation can be performed with different methods. According to WMO (1998) the most common approach is to perform a regression analysis, but other parameters might be computed in order to calculate the magnitude and variation between modeled and observed data. Among these parameters are mean error or bias, root mean square error (RMSE), scatter index and r, a

simple linear correlation coefficient. For example, Bertin *et al.* (2013) computed the root mean square of the difference to compare observed data with ERA40.

Data from Rio Grande buoy, located in the south sector, ranges from April 2009 to January 2010. Data from a buoy located in Cabo Frio, in the southeast sector, refers to the period from June 2009 to June 2010. Both observational buoy datasets are part of the National Buoy Program (*Programa Nacional de Boias* – PNBOIA) and were downloaded from: http://www.goosbrasil.org/pnboia/dados/. The locations of the buoys and their respective ERA-20C points are presented in Figure 9. Coordinates, distance to shore and depths of the buoys used are presented in Table 1.

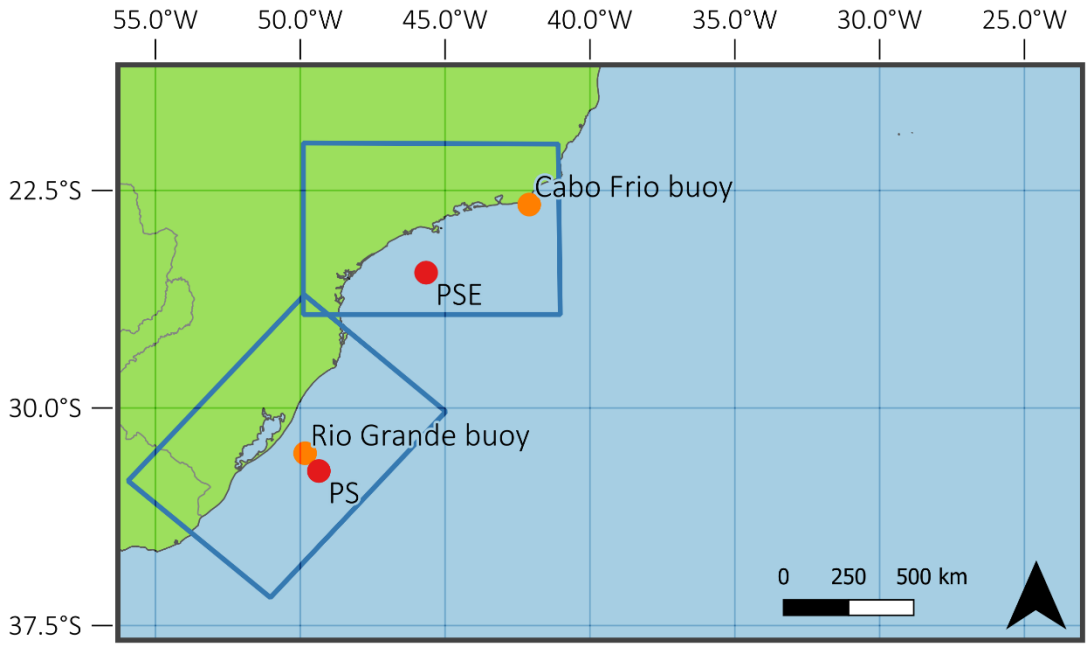

Figure 9 Locations of Rio Grande and Cabo Frio buoys in comparison to the ERA-20C points.

The observational data to be analysed has many gaps within their respective temporal scopes. Accordingly, the time vectors of both buoys and ERA-20C will be compared to validate only the dates occurring in both datasets.

Pearson correlation coefficients will be computed, as well as RMSE and R^2 to examine how similar the datasets are. RMSE shows how closely related the data points are to each other and R^2 represents how close the points are to a linear fit.

Table 1 Location and depth of PNBOIA buoys used in the ERA-20C data validation.

Buoy	Latitude	Longitude	Distance to shore (km)	Depth (m)
Rio Grande	31° 33' 44" S	49° 50' 14" W	100	200
Cabo Frio	22° 58' 80" S	42° 06' 00" W	3	45

3.3. Wave Climate Characterization

Prior to analysing the wave climate variability, it is necessary to characterize the wave climate of each region of the study area for the entire time series. A statistics summary will be calculated for Hs, including mean (Hs-Mean), median (Hs-Median), standard deviation (Hs-Std), variance (Hs-Var) and range (Hs-Range), as well as minimum (Hs-Min) and maximum (Hs-Max) values. The variability of extreme events will also be analyzed by classifying the patterns of exceeded values, highest 10 %, 5 % and 2 % of Hs. These will be referred to as Hs10, Hs5 and Hs2, respectively. Additionally, the interquartile range between the 75 % and 25 % quartiles (Hs-IQR) will be calculated in each sector, indicating where 50 % of the data lies, given that it represents the difference between the first and the third quartiles.

The Tp analysis will follow the same methodology as the one applied in Hs and similar nomenclatures and abbreviations will be applied (Tp-Mean, Tp-Median, Tp-Std, Tp-Var, Tp-IQR, Tp-Range, Tp-Min, Tp-Max, Tp10, Tp5 and Tp2). An additional calculation regarding the percentage of sea-state and swell will indicate the Tp behavior of each sector. The threshold to be used between both patterns will be 10 s.

The statistics summary of Dir will be computed similarly to Hs and Tp. However, given that a mean value would not reproduce the correct Dir, this value will not be calculated. Moreover, Dir will also be analyzed through calculations of the percentages of waves coming from each class of Dir as described in Table 2.

The analysis of unimodality or bimodality will be performed by observation of the wave parameters representations through frequency distribution plots to understand whether a specific region has different patterns in its wave climate. Furthermore, these distributions will also be used to understand whether the data is skewed in the direction of lower or higher values.

A wave direction distribution analysis will also be carried out to better understand the origin of the wave energy. The Hs and Tp frequency distributions and the Dir distribution will be analysed jointly for observation of possible discrepancies, namely because of the direction aggregation by ranges (Table 2).

To better understand how each sector is compared to the others, correlation matrixes will be constructed for each wave parameter analyzed.

Finally, to complement the wave climate characterization, an extreme wave analysis will be carried out. The extreme wave analysis has the objective of investigating the storm waves, those with the highest Hs, for example. This will be done by extracting the exceeded values by 5 % (Hs5; Tp5) of each month, year and decade. Although, it should be pointed out that Tp5 indicates that there are more waves being formed at open ocean reaching the coast but not necessarily storms or high energy, just long swells.

Table 2 Mean wave directions and their respective ranges.

Mean wave direction	Range of Dir (°)
N	337.5 ≥ Dir < 22.5
NE	22.5 ≥ Dir < 67.5
E	67.5 ≥ Dir < 112.5
SE	112.5 ≥ Dir < 157.5
S	157.5 ≥ Dir < 202.5
SW	202.5 ≥ Dir < 247.5
W	247.5 ≥ Dir < 292.5
NW	292.5 ≥ Dir < 337.5

3.3.1. Hs vs Tp Relationship

This analysis aims to investigate the possible relationship between the Tp frequency distribution and Hs through a joint distribution analysis. In order to do so, Hs will be divided into classes of 0.5 m intervals. Tp values will also be grouped in intervals of 0.5 s and the class with the most occurrences of Tp will be considered as the corresponding mode of its respective Hs class. Depending on the amount of values, the Hs interval might be changed to 0.25 m in order to obtain a more precise analysis.

An exponential fit will then be computed, with the equation representing the observed relationship. RMSE values will be calculated to understand how similar the Tp mode values of different Hs classes are. Pearson correlation coefficients will be calculated to assess the goodness of the fit and they will be evaluated based on the confidence interval.

Each sector will have its wave climate divided into groups depending on the Dir analysis performed in Section 4.2 and thus, different Hs vs Tp relationships can be obtained for the same sector, for different wave directions. However, for PN1 and PN2, the division of groups will be based on Tp patterns given that for these regions the dominant difference in wave regimes is a strong Tp bimodality and not changes in wave direction.

If evident that the relationship does not apply to lower Hs values due to a high variability on data, those values will be excluded from the exponential fit. Furthermore, for some sectors of the coast, an additional analysis might be performed based on a Tp threshold.

3.3.2. Wave Climate Variability

Given that the main objective of this study is to analyse possible changes throughout the 20th century, the monthly averages of Hs and Tp will be calculated as well as averages per year and per decade. The latter will be computed by applying a moving average with a window of 29220 points to represent 10 years. This will result in a smoothed version of annual averages which facilitates the identification of patterns and changes in the wave climate throughout the time series, as well as the analysis of peaks and throughs in the data. Although it is not a decadal analysis, by applying a smoothing method through the use of moving average it is possible to observe decadal level variability. In other words, the annual average analysis provides the wave climate variability and the smoothed annual averages analysis gives a more generic evolution of it.

Furthermore, even though parts of the study area (PNE, PN1 and PN2) do not show different seasons throughout the year, the purpose of computing monthly averages and variability is to detect possible seasonality patterns.

3.4. Relationships Between Wave Climate and Climate Indices

Pearson correlation analyses will be performed to identify a possible association between the wave climate and the climate indices. In order to use this method, both time series must have the same time frame and the result will tell if there is a correlation between the variables. Pereira and Klumb-Oliveira (2015) detrended monthly averages of Hs and then calculated a 3-month running average in order to perform a cross-correlation with ONI. By detrending the data set, the climate change signal and any existing trend are removed from the time series. This same method will be applied in the present study to the monthly averages of Hs and Tp. However, a cross-correlation will not be used.

Instead, Pearson correlation coefficients between the wave parameters (Hs and Tp) and climate indices will be calculated and analyzed for both 95 % and 99 % confidence intervals. Ergo, in order to determine its significance, the p-values will be computed as well. A p-value lower than 0.05 represents a 95 % confidence interval and p-value lower than 0.01 a 99 % confidence level.

This analysis will be performed for both mean (Hs; Tp) and extreme wave conditions (Hs5; Tp5).

The climate indices being examined are presented in Table 3.

Table 3 Climate indices used in the correlation analysis and their respective sources.

Climate Index	Source
Oceanic Niño Index (ONI)	https://psl.noaa.gov/gcos_wgsp/Timeseries/Nino34/
Tropical Southern Atlantic Index (TSA)	https://psl.noaa.gov/data/correlation/tsa.data
Atlantic Multidecadal Oscillation (AMO)	https://psl.noaa.gov/data/timeseries/AMO/
Atlantic Meridional Mode (AMM)	https://psl.noaa.gov/data/timeseries/monthly/AMM/ammsst.data
Southern Annular Mode (SAM)	https://legacy.bas.ac.uk/met/gjma/sam.html
Antarctic Oscillation (AAO)	https://psl.noaa.gov/data/correlation/aao.data

3.5. Trend Analysis

To complement, a trend analysis will be performed to understand if there are changes along time and possible future tendencies. This will be accomplished by calculating the linear regression model of both mean and extreme values of Hs and Tp for monthly and annual cases. Linear regression fits are the most direct way of calculating trends and the p-values will indicate whether these trends are significant or not.

In order to understand if the storm waves are getting more or less energetic, their extreme values need to be compared to the mean ones along time. In other words, the trends need to be calculated separately and then compared. This will be important to see if there is an upward trend and whether Hs rates are higher or lower than Hs5 rates, for example.

The trend analysis will be done for the overall period under examination (1901 – 2010) as well as per month. Given the long-term data being used in this study, it is likely that the trends are not constant, so an analysis will be done to understand the trend variation through time by dividing the time series into shorter periods. These are: 1901 – 1939, 1940 – 1969 and 1970 – 2010.

3.6. Wavelet Transform Analysis

The wavelet analysis provides a time-varying spectral estimate, on a time scale that depends on the phenomenon to be described. It is therefore particularly suited for identifying events against a random background (Holthuijsen, 2007). This method recognizes that the processes underlying the spectrum might be changing, and thus the spectrum might vary with time (Talley *et al*., 2011). Wavelet transforms are applied to several fields of study including noise removal, traffic mapping and pattern recognition.

In this study, the wavelet method aims for a better understanding of the 1940s peak of Hs and Tp and the wavelet spectrum will be computed considering the Morlet Wavelet Transform (Torrence and Gilbert, 1998). This method will be applied for ONI, AMO and both Hs and Tp time series of each sector.

4. Results

4.1. Data Validation

The ERA-20C validation showed significant correlation results for both locations examined (Table 4). Besides the Pearson correlation coefficient, RMSE and R^2 were also computed.

Table 4 Error statistics of ERA-20C validation against Florianópolis and Cabo Frio buoys.

ERA-20C Validation	Hs			Tp		
	Corr. Coeff.	RMSE (m)	R^2	Corr. Coeff.	RMSE (s)	R^2
PS vs Rio Grande	0.85	0.29	0.73	0.67	1.45	0.45
PSE vs Cabo Frio	0.62	0.23	0.39	0.73	1.23	0.54

4.1.1. South Region

The south region of the study area, here represented by PS data from ERA-20C, was compared with a buoy located in Rio Grande do Sul state, 100 km offshore from Lagoa dos Patos mouth. The Pearson correlation coefficient for Hs was 0.85 (p-value < 0.01), RMSE was 0.29 m and R^2 was 0.73 (Figure 10; left).

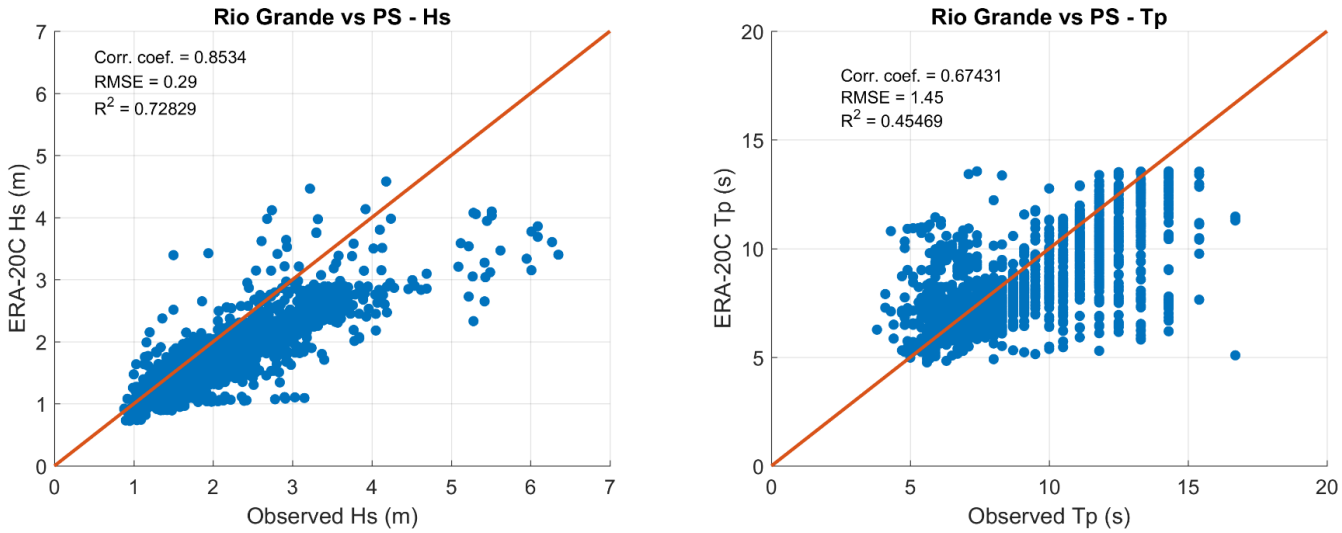

Figure 10 ERA-20C data validation with observed data from Rio Grande buoy for Hs (left) and Tp (right). Orange lines indicate 1:1 relationship.

Even though most of the values are around the 1:1 relationship (orange line), there is a higher number of points below this line indicating an underestimation of Hs by the model, namely for the highest wave heights. Additionally, the maximum observed Hs was 6.4 m while the modelled Hs did not go over 5 m (Figure 10).

Regarding the validation of Tp, the results show that the data does not agree as well as for Hs. For the Rio Grande buoy, Pearson correlation coefficient was 0.67 (p-value < 0.01), RMSE was 1.45 s and R^2 was 0.45. Observed Tp reaches almost 17 s, while the modelled values do not go over 15 s (Figure 10; right).

The trends for an underestimation of both Hs and Tp by ERA-20C are clearer in the time series plots (Figure 11).

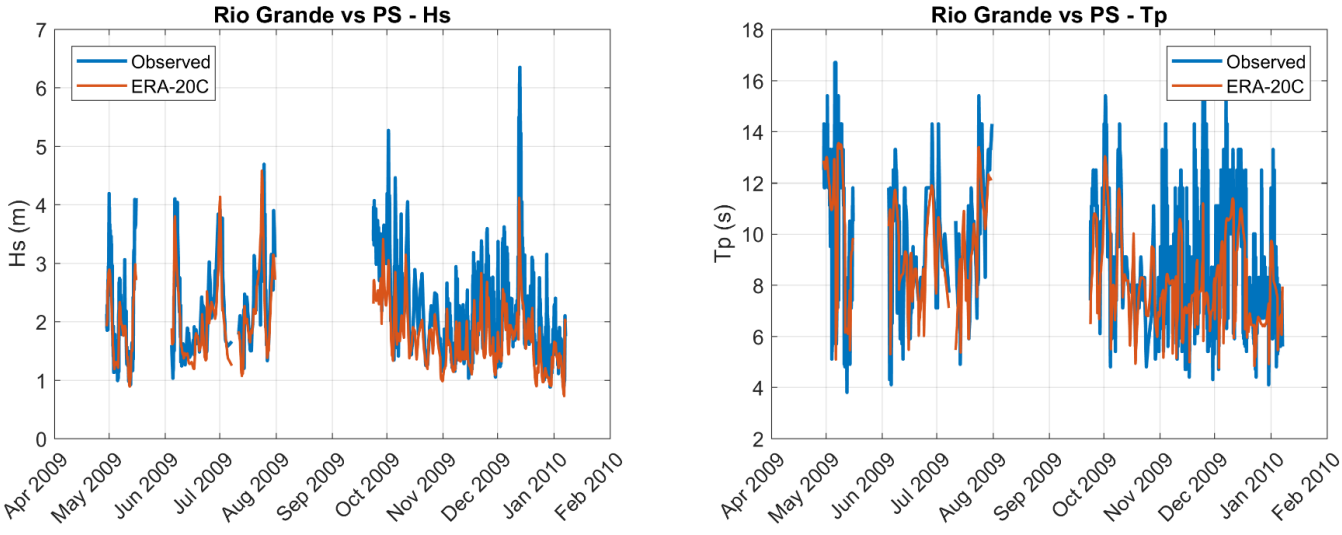

Figure 11 Time series of observed data from Rio Grande buoy and ERA-20C data for PS for Hs (left) and Tp (right).

4.1.2. Southeast Region

Cabo Frio buoy was compared with PSE data and the correlation coefficient for Hs was high, even though the buoy is located close to the shore in shallow waters with 45 m depth. The correlation coefficient was 0.62 (p-value < 0.01), RMSE was 0.23 m and R^2 was 0.39 (Figure 12; left). For the period analyzed, the buoy registered waves with Hs higher than 3 m while ERA-20C did not. By

comparing the scatter points with the linear model, it is possible to observe that ERA-20C underestimates Hs values for PSE throughout most of the period analyzed. However, waves smaller than 1 m are overestimated by the reanalysis product. These differences between the observed and the modelled data are noticeable in the time series plots as well (Figure 13; left).

Unlike the observed for PS, Tp was better reproduced than Hs in PSE. The Pearson correlation coefficient was 0.73 (p-value < 0.01), RMSE 1.23 s and R^2 0.54. Observed Tp reaches 20 s, while the modelled values are never higher than 15 s (Figures 12 and 13; right).

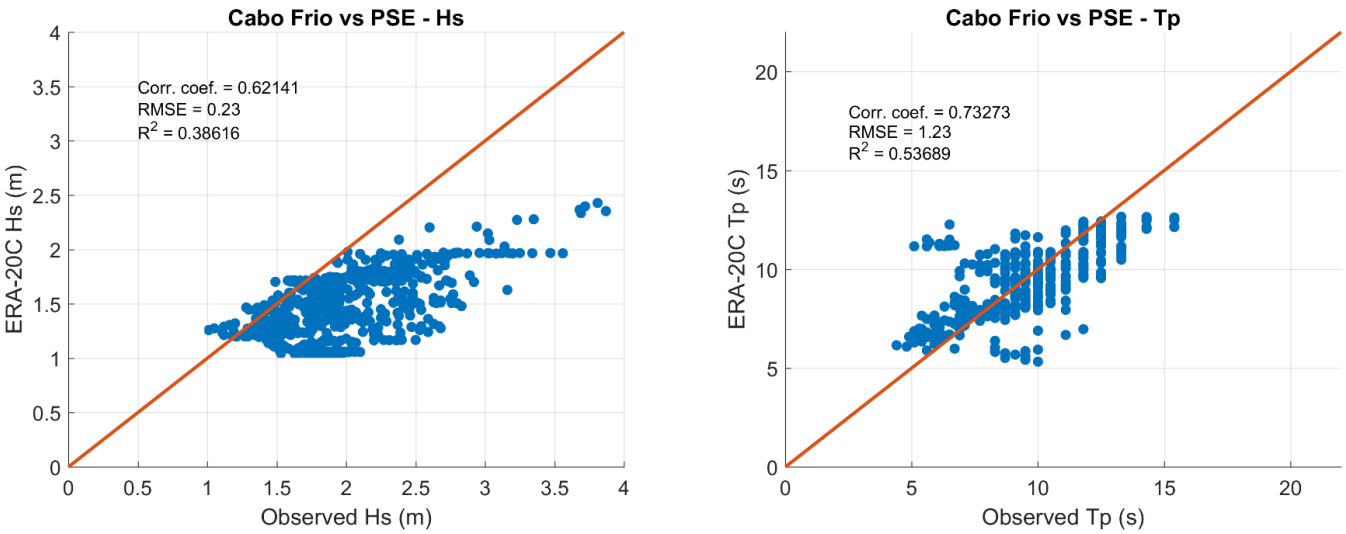

Figure 12 ERA-20C data validation with observed data from Cabo Frio buoy for Hs (left) and Tp (right). ERA-20C data for PS

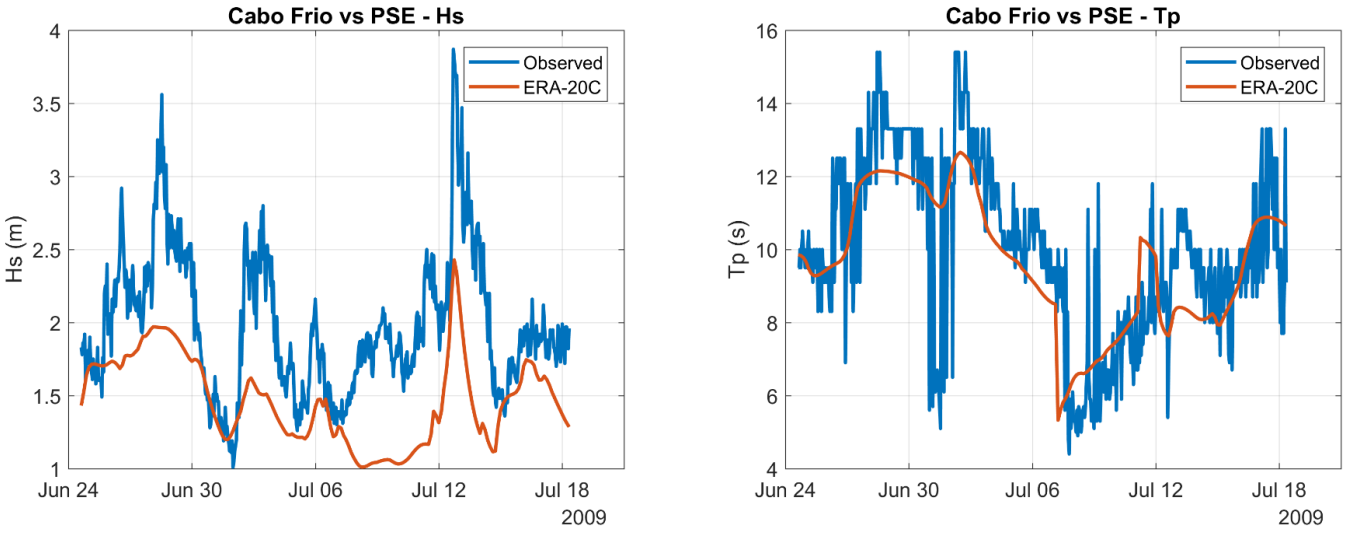

Figure 13 Time series of observed data from Cabo Frio buoy and ERA-20C data for PSE for Hs (left) and Tp (right).

The underestimation of Hs could be associated to extreme wave heights which have been described inaccurately by wave simulations (Campos *et al*., 2018). It must be pointed out that the buoy position could already have refraction and shoaling effects since it is located approximately 3 km from the coast.

4.2. Wave Climate Characterization

4.2.1. Significant Wave Height – Hs

Following the steps described, the mean significant wave height for each sector of the study area was calculated and all Hs averages are between 1.2 m and 1.6 m, showing some uniformity between sectors regarding this parameter (Table 5, Figure 14). The Hs median in PN2 is 1.5 m, being the highest median value. On the other hand, the lowest median is in PSE, 1.1 m. PS, PSE and PNE present median values lower than the mean, indicating a positively skewed distribution. PE, PN1 and PN2 show similar values for both parameters which probably represents a normal distribution. The frequency distribution histograms show that all sectors have a unimodal distribution of Hs (Annex A).

With regard to extreme values, the only sector which presented Hs higher than 5 m was PS, which had the maximum value equal to 8.1 m. This sector also presented the highest extreme values (Hs10, Hs5 and Hs2) while all other sectors showed similar results. Even though PN1 showed the lowest maximum Hs (3.0 m), PSE presented the lowest average (1.2 m). This can be explained by the lower variance, range, and standard deviation, which indicate that PN1 has a narrower distribution of data (Table 5, Figure 14).

By analyzing the dispersion of the Hs values, it is possible to identify PS as the region with the highest dispersion, followed by PSE (Figure 14). The IQR of PS is 0.72 m whilst of PSE it is 0.48 m. All other regions have IQR lower than 0.4 m with PN1 showing the lowest IQR (0.35 m) (Table 5).

The differences in IQR, minimum and maximum visible in Figure 14 alongside the frequency distribution histograms (Annex A) confirms the more spread dataset in PS. Furthermore, the longer

tails of higher values of Hs are notable, which backs-up the previous conclusion of a positively skewed distribution. The same can be observed for PSE and PNE.

Table 5 Significant wave height (m) statistics per sector off the Brazilian coast from 1901 to 2010.

Statistics	PS	PSE	PE	PNE	PN1	PN2
Hs-Mean	1.6	1.2	1.3	1.5	1.4	1.5
Hs-Median	1.5	1.1	1.3	1.4	1.4	1.5
Hs10	3.0	2.0	2.0	2.1	1.9	2.1
Hs5	3.4	2.2	2.2	2.3	2.0	2.2
Hs2	4.0	2.5	2.4	2.5	2.2	2.3
Hs-Std	0.6	0.4	0.3	0.3	0.3	0.3
Hs-Var	0.4	0.1	0.1	0.1	0.1	0.1
Hs-Min	0.4	0.4	0.6	0.8	0.7	0.7
Hs-Max	8.2	4.4	3.8	4.1	3.0	3.2
Hs-IQR	0.7	0.5	0.4	0.4	0.4	0.4
Hs-Range	7.7	4.0	3.2	3.4	2.3	2.4

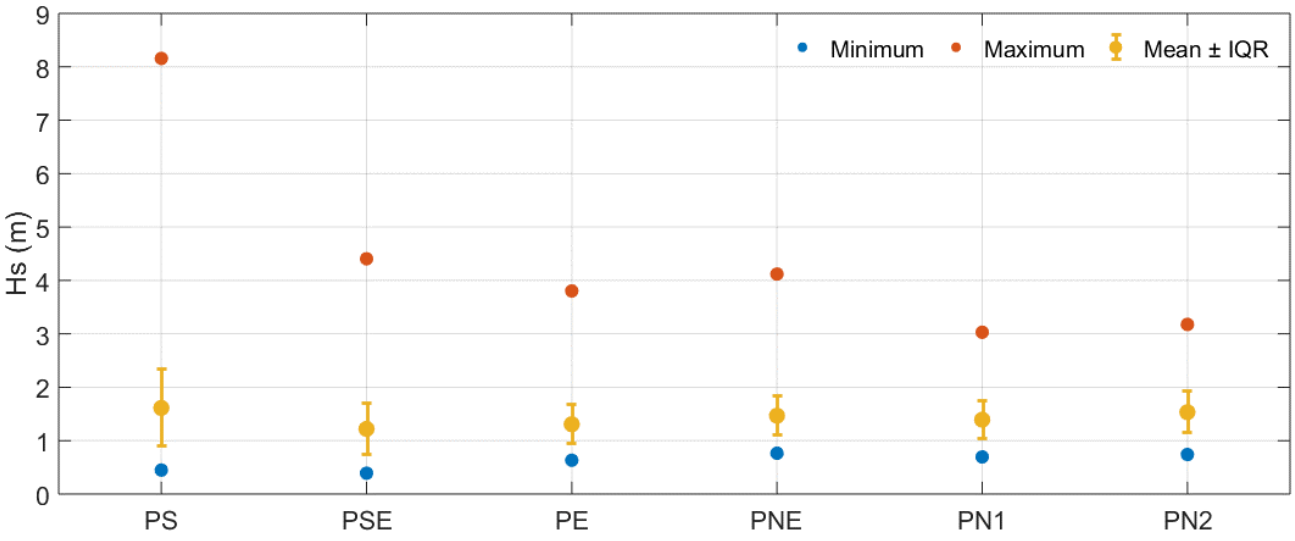

Figure 14 Significant wave height (m) basic statistics per sector from 1901 to 2010.

Even though PS displayed the largest Hs and PSE the smallest, it is noticeable that PS and PSE have a more similar wave climate between themselves, which can be confirmed with the correlation matrix (Annex B). The same applies for PE and PNE and to PN1 and PN2. The highest observed correlation is between PE and PNE, 0.7. PSE can be interpreted as a transition area between the

south and the east coast of Brazil, while PN1 shows negative correlation with all other sectors, except with PN2, indicating a completely distinct wave regime at the north coast of Brazil.

4.2.2. Peak Period – Tp

All sectors of the Brazilian coast show similar Tp mean values, ranging from 8.2 s to 8.9 s (Table 6). PN1 presents the lowest mean, followed by PN2 and PS. On the other hand, PSE presents the highest mean value of Tp. The parameter which differs the most is the variance, with 2.8 s in PE and 4.6 s in PN2. PE also stands out for the lowest standard deviation (1.7 s) and highest range and maximum values (15.5 s and 19.6 s, respectively).

All sectors present a positive skewness distribution with median values of Tp being lower than mean values. The frequency distribution histograms show that only PS and PNE are unimodal regarding their Tp distribution, while all other sectors are bimodal (Annex C).

Regarding the extreme values of Tp (Tp10, Tp5 and Tp2), the largest Tp values are found in PN2 and PN1. This result indicates that swells have longer periods in the north region of Brazil, whereas the smaller extreme Tp are observed in PS and PE.

Table 6 Peak period statistics (s) per sector of the Brazilian coast from 1901 to 2010.

Statistics	PS	PSE	PE	PNE	PN1	PN2
Tp-Mean	8.3	8.9	8.4	8.6	8.2	8.3
Tp-Median	8.1	8.6	7.9	8.0	7.6	7.5
Tp10	11.9	12.3	12.0	12.7	12.8	13.4
Tp5	12.5	12.8	12.5	13.4	13.7	14.3
Tp2	13.2	13.5	13.2	14.4	14.8	15.3
Tp-Std	1.9	1.8	1.7	1.8	1.8	2.2
Tp-Var	3.5	3.1	2.8	3.3	3.3	4.6
Tp-Min	3.1	3.1	4.1	4.5	4.8	4.3
Tp-Max	16.4	18.3	19.6	19.6	19.5	19.3
Tp-IQR	2.6	2.6	1.9	2.0	1.1	1.6
Tp-Range	13.3	15.2	15.5	15.2	14.7	14.9

The difference between range and IQR shows how concentrated or dispersed the data is (Figure 15). For example, PS has the lowest range (13.3 s) but one of the highest IQR (2.6 s) (Table 6).

Meanwhile, PN1 has the lowest IQR (1.1 s). The positive skewness can be interpreted with the IQR as well. This is represented when the upper half of the IQR representation is larger than the bottom half, which shows to be true for all sectors.

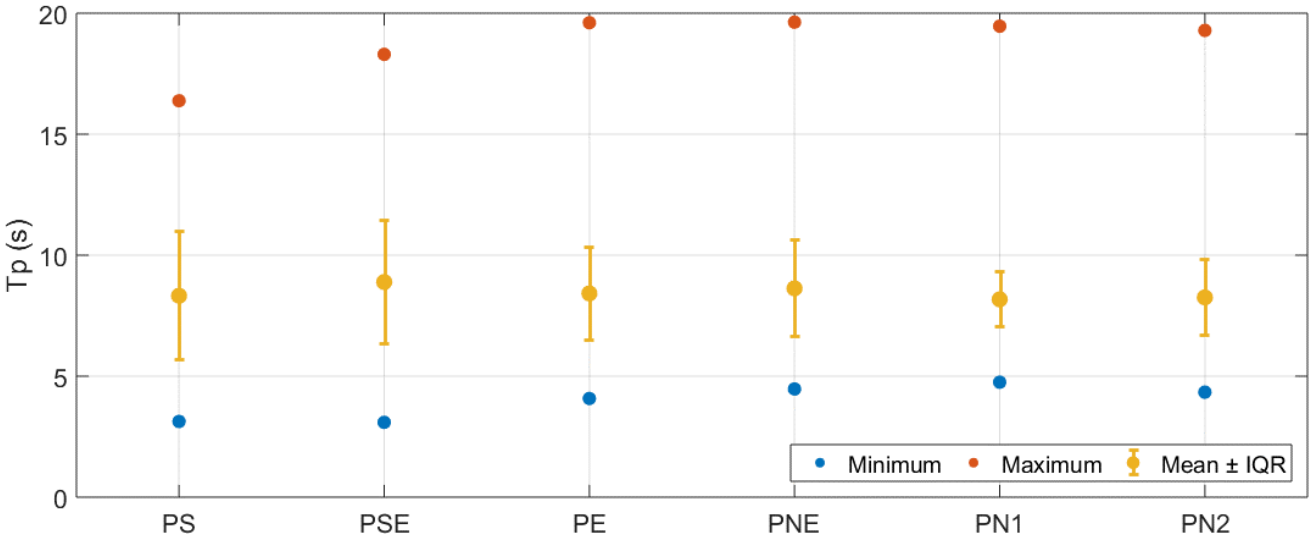

Figure 15 Peak period (s) basic statistics per region from 1901 to 2010.

The same groups could be identified in the Tp analysis even though PSE and PE seem more similar for Tp than observed for Hs. Additionally, PN1 and PN2 also show higher correlation coefficients for Tp compared to the Hs analysis. These sectors present negative or zero correlations for Tp with all other sectors indicating their Tp behavior is more unique than their Hs. This can be explained by the dominance of sea-state and the lower variability of Tp in the north region (Annex B).

Considering swell regime as being composed of waves with Tp equal or higher than 10 s and sea-state composed of Tp lower than 10 s, the wave climate of each sector was examined through their respective proportions. PSE presents the highest percentage of swell (27.4 %) while PN1 presents the lowest (13.1 %) (Table 7).

Table 7 Swell and sea-state percentages within the wave climate of each sector of the Brazilian coast.

Sector	Swell (%)	Sea-state (%)
PS	20.2	79.8
PSE	27.4	72.6
PE	17.9	82.1
PNE	20.9	79.1
PN1	13.1	86.9
PN2	17.4	82.6

4.2.3. Mean Wave Direction – Dir

Most of the study area shows median values of Dir in the second quadrant, 90 ° to 180 ° (PS, PSE, PE and PNE) while the north region's Dir is mainly from the first quadrant (Figure 16) as a result of the different wave generating areas within the study area (see Section 2.6). For some regions, Dir has a bimodal distribution indicating that there might be two climatic systems responsible for generating waves. This is the case for PN1 and PN2, according to the frequency distribution histograms (Annex D).

The dispersion of Dir varies along the coast. PS has the most spread distribution with waves coming from all directions while almost all the waves in PNE come from the second quadrant, being the least dispersed of all the sectors. In fact, PNE has a range of only 165 ° and IQR of 27 ° while all other sectors present waves from all four quadrants and IQR ranging from 37 ° in PE and 93 ° in PS (Figure 16).

Although the sectors remain grouped in the same way, a different relationship could be found for Dir analysis with PS and PSE presenting lower correlation coefficient between them, indicating the existence of different positions on the wave generation sources for these sectors. On the other hand, the correlation coefficient between PE and PNE is the same as the one between PN1 and PN2 (Annex B).

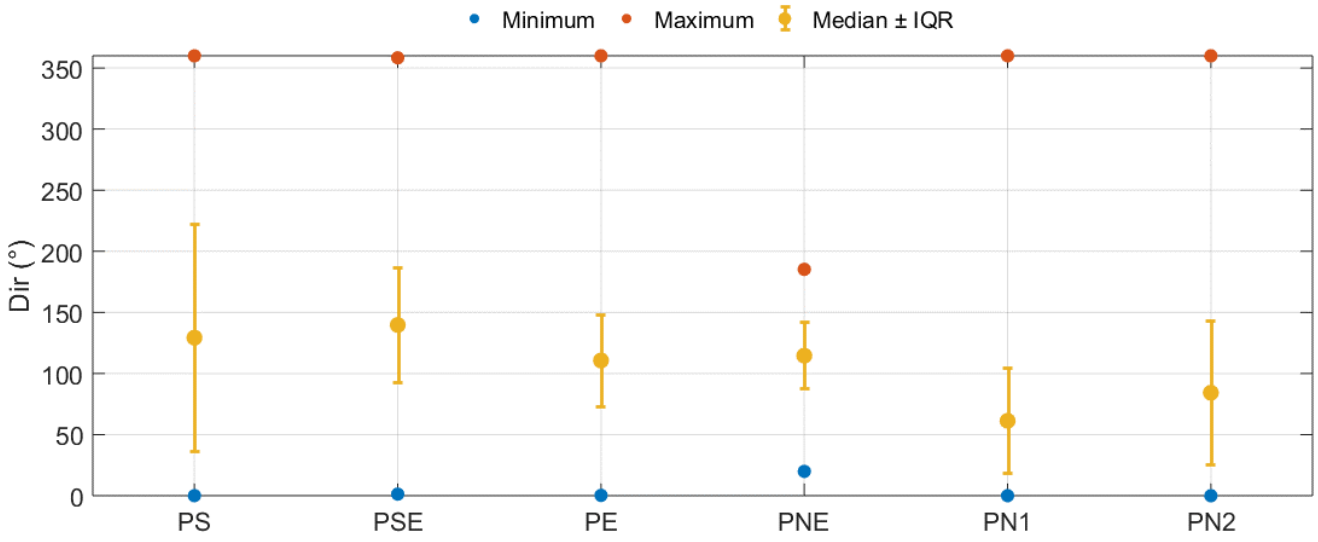

Figure 16 Mean wave direction (°) basic statistics per region from 1901 to 2010.

4.2.4. Wave Climate per Region

The characterization of the wave climate of each sector of the study area was analyzed through the relationship between parameters (Dir/Hs and Dir/Tp) from 1901 to 2010 through the construction of wave roses and 2D histograms. Wave roses are used to characterize the interaction between Dir and Hs or Tp. The relationship between Hs and Tp will be studied in Section 4.2.5.

4.2.4.1. South Sector

The South sector of the study area has the most unique and diverse wave climate with Hs around 1.6 ± 0.6 m and Tp equal to 8.3 ± 1.9 s. The dispersion analysis showed that 50 % of the waves in PS range from 1.2 m to 1.9 m and 7 s and 9.6 s and Dir indicated that waves come from all quadrants, but mainly ranging from 15 ° to 195 ° (Figures 17 and 18). Moreover, 79.8 % composes of sea-state and 20.2 %, can be considered as swell. All variables present a unimodal distribution in PS but with a high dispersion of values (Annexes A, C and D).

As mentioned, PS is the only sector which presents waves coming from all directions, although the percentage of waves from W and N is low (1.1 % and 1 %, respectively). Additionally, 23.5 % of waves come from E, 24 % from SE and 25.3 % from S, representing the highest percentage (Figure 17). It should be noted that waves from W do not occur in the region due to the location of the continent. However, in the models there is a possibility that swells shift from south to north through the west due to the influence of atmospheric systems.

The percentage of small waves (Hs < 1 m, dark blue) decreases as the percentage of higher waves (Hs > 2 m, warm colors) increases from NE to SW. In general, the higher waves with Hs > 2.5 m (red colors), are predominantly from SW and the smaller ones from E and SE (Figure 17; left).

Although the yellow representation in the wave roses correspond to a mix of sea-state and swell making it difficult to interpret it, the ratio of sea-state and swell waves arriving in PS changes between the first and third quadrant. While for sea-state (blue colors) the dominant waves are in the first quadrant (NE waves), for swell (orange colors) the dominant waves are on the third quadrant. Ergo, swells come mainly from S whilst sea-state come mainly from NE (Figure 17; right).

Although waves with heights larger than 3 m from NE are also present, their Tp indicate these are composed mainly of sea-state (dark blue circles, Figure 18). Thus, there is an indication of waves with greater intensity from NE and the smaller Hs come from the E quadrant. In addition, SW waves present larger Tp values confirming the swell coming from SW, as indicated by the orange and yellow circles on Figure 18. Waves with a direction close to 250 ° to 300 ° have a behavior where the Hs/Tp ratio is almost linear, whereas for the other Dir there is a huge dispersion.

To summarize, the wave regime in PS is composed mainly of small sea-state waves from NE and higher swells from S.

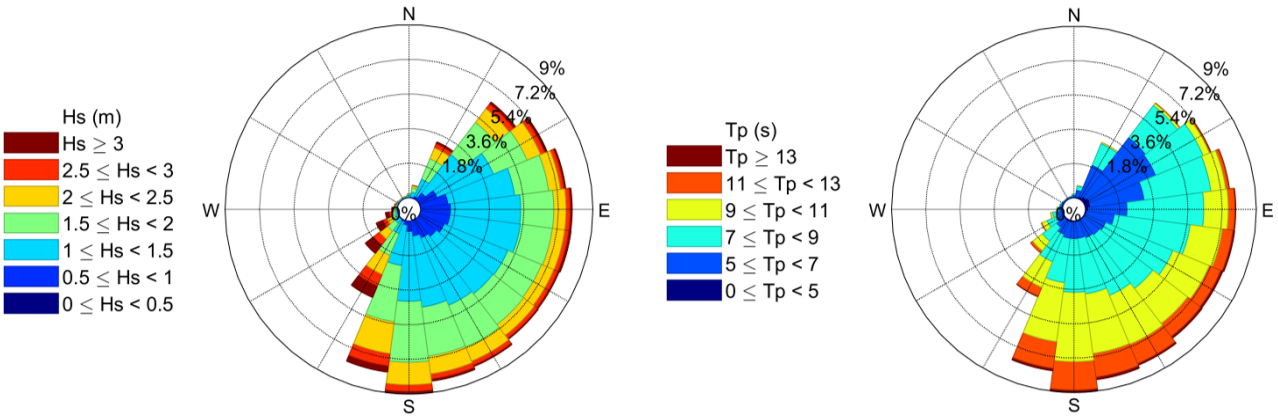

Figure 17 Wave roses of mean wave direction against Hs (left) and Tp (right) for the South region for data from 1901 to 2010. The percentages indicate how often the waves come from each direction.

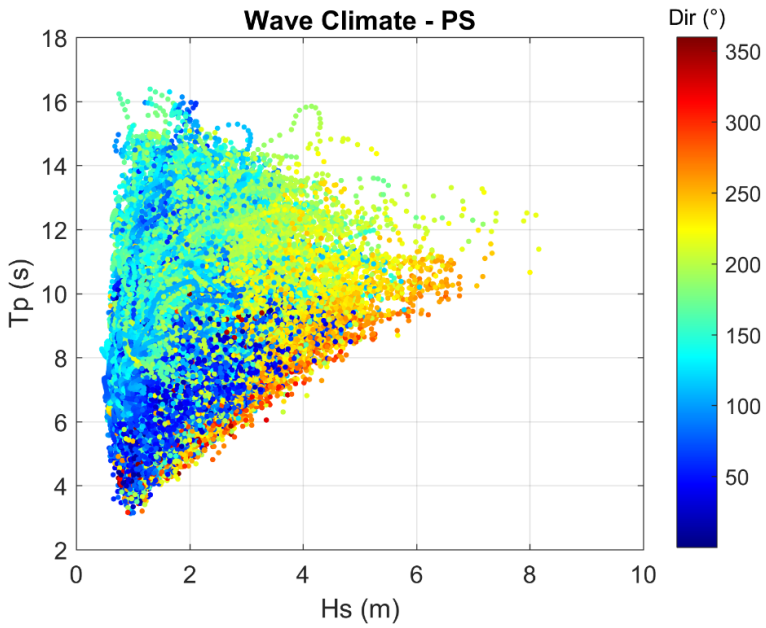

Figure 18 Interrelationships between Hs, Tp and Dir for the South region from 1901 to 2010.

4.2.4.2. Southeast Sector

The southeast sector of the Brazilian coast presents Hs values smaller than those in PS and higher Tp values. Hs has an average of 1.2 ± 0.4 m and Tp of 8.9 ± 1.8 s. The dispersion analysis showed that 50 % of the waves in PSE range from 0.9 m to 1.4 m and 7.6 s to 10.1 s. Even though PSE has a unimodal distribution of Hs and Dir, it shows a bimodal distribution of Tp indicating two well established wave patterns. The first one represents a sea-state regime with a Tp mode of 7.9 s and the second represents the swell regime with a Tp mode of 10.2 s (Annexes A, C and D). Moreover, 72.6 % composes of sea-state and 27.4 %, can be considered as swell.

Unlike PS, PSE has a narrow Dir distribution in which most of the waves come from the second quadrant (Figures 19 and 20). Almost half of the waves in PSE come from SE (47.4 %) and waves from E and S represent 22 % and 29.9 %, respectively. The remaining waves come from NE and SW.

Waves smaller than 1 m (dark blue) come mainly from SE while waves higher than 2 m (orange colors) are predominantly from SSW (Figure 19; left). Given the Hs5 of 2.2. m in PSE, it is possible to affirm that a large amount of storm waves come from SSW in this sector.

Additionally, sea-state waves come from E and swell waves are mostly from SE. The small percentage of yellow color coming from E indicates the well-established sea-state regime from E (Figure 19; right).

Even though the larger Hs comes from the S, the larger Tp comes from SE, which also coincides with the highest percentage of waves smaller than 1 m (Figure 19). Swell waves come mainly from S and SSE, while sea-state comes from ESE. As a result, the most energetic waves in PSE are from S with Hs higher than 2.5 m.

The concentration of waves from the third quadrant becomes clearer in Figure 20. The lighter the blue, the more southern the waves are, which is the case for most of the waves in this region. The combination of waves with Hs higher than 2.5 m and Tp ranging from 10 s to 14 s, indicates the swell waves coming from S, depicted in green color. Moreover, these also represent storm waves. Lourenço (2012) had already stated that the most energetic waves in this region are the S ones.

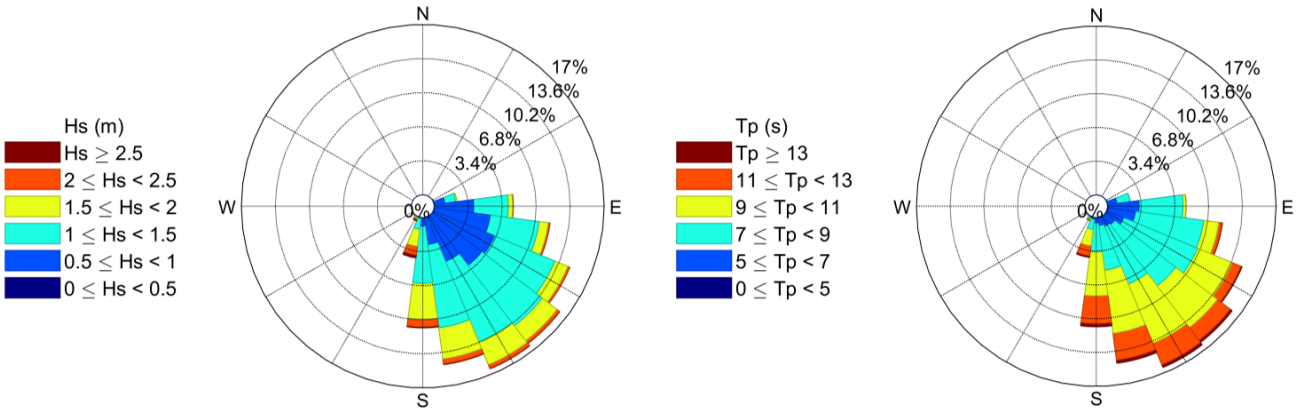

Figure 19 Wave roses of mean wave direction against Hs (left) and Tp (right) for the Southeast region from 1901 to 2010. The percentages indicate how often the waves come from each direction.

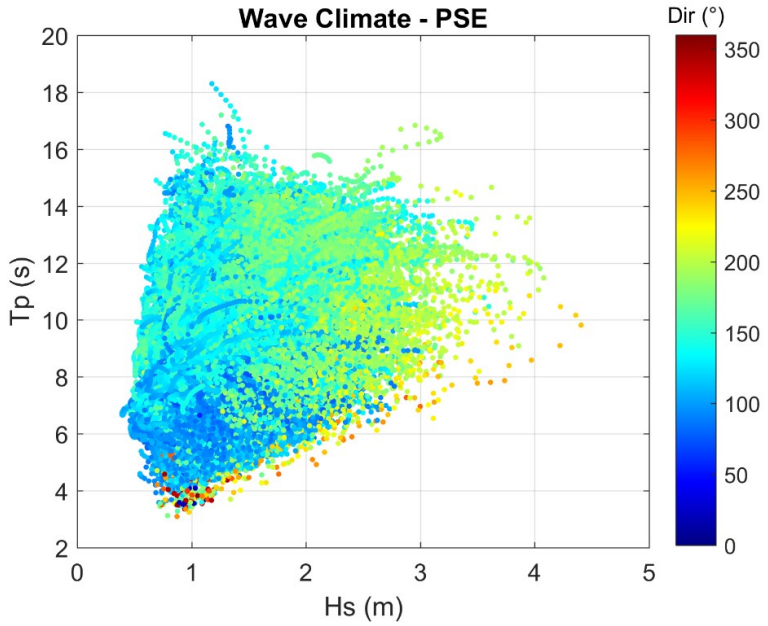

Figure 20 Interrelationships between Hs, Tp and Dir for the Southeast region from 1901 to 2010.

4.2.4.3. East Sector

The east sector of the Brazilian coast presents a wave climate with Hs around 1.3 ± 0.3 m and Tp is 8.4 ± 1.7 s and a wave climate which is not as dispersed as it is in the previous two sectors. The dispersion analysis showed that 50 % of the waves in PE range from 1.1 m to 1.5 m and 7.3 s to 9.2 s. Both Hs and Dir present a unimodal distribution in PE (Annexes A and D) as observed in PSE.

On the other hand, Tp is bimodal evidencing two well established wave patterns in which one represents sea-state (8 s mode) and the other swell (12 s mode) (Annex C). Moreover, 82.1 % composes of sea-state and 17.9 % can be considered swell.

The dominant wave direction in PE is E (45.4 %), followed by SE waves (42.4 %). Waves from NE compose 6.9 % of the waves, 5 % are S waves and 0.3 % N waves. There are no waves arriving from SW to NW quadrants.

Small waves (Hs < 1.5 m, blue colors) in PE come mainly from E and higher waves (Hs > 2 m, orange colors) from SSE (Figure 21; left). Meanwhile, sea-state (Tp < 9 s, blue colors) is predominantly from E and ESE and the swell (Tp > 11 s, orange colors) from SE (Figure 21; right).

Even though mean wave direction ranges from NE to SE, almost 23 % of the waves in PE come from ESE (~ 100 °). These waves represent a small sea-state regime given that they are mostly composed of waves with Hs lower than 1.5 m and Tp lower than 9 s, although there is a considerable amount of mixed sea-state and swell waves, represented by yellow color. As Dir increases, both Hs and Tp increase as observed in the southern sectors of the coast. Hence, the most energetic waves (highest Hs and Tp) come from SE (Figure 21).

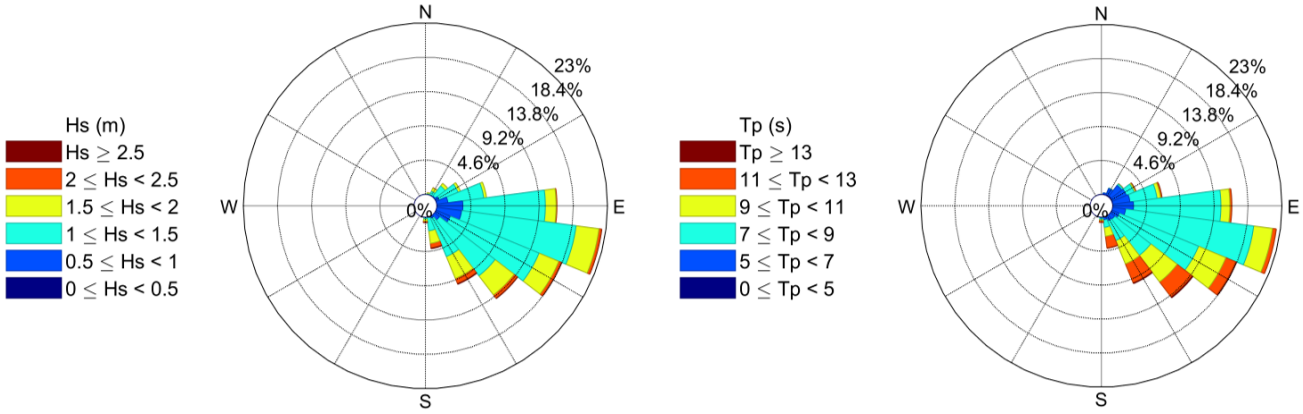

Figure 21 Wave roses of mean wave direction against Hs (left) and Tp (right) for the East region from 1901 to 2010. The percentages indicate how often the waves come from each direction.

Moreover, the previously mentioned small waves coming from N and NE are more visible in Figure 22. In addition, there is a substantial number of large waves with small Tp coming from S which

indicates that not all storm waves form a swell pattern in this sector. The predominant Dir from SE in PE is once again confirmed as indicated by green and yellow colors.

In general, PE follows the same pattern observed in PS and PSE. From the first to the second quadrant, waves become higher with longer Tp. Consequently, waves with higher Hs and Tp come from SE. Sea-state waves, with Tp lower than 10 s, come mainly from E and ENE.

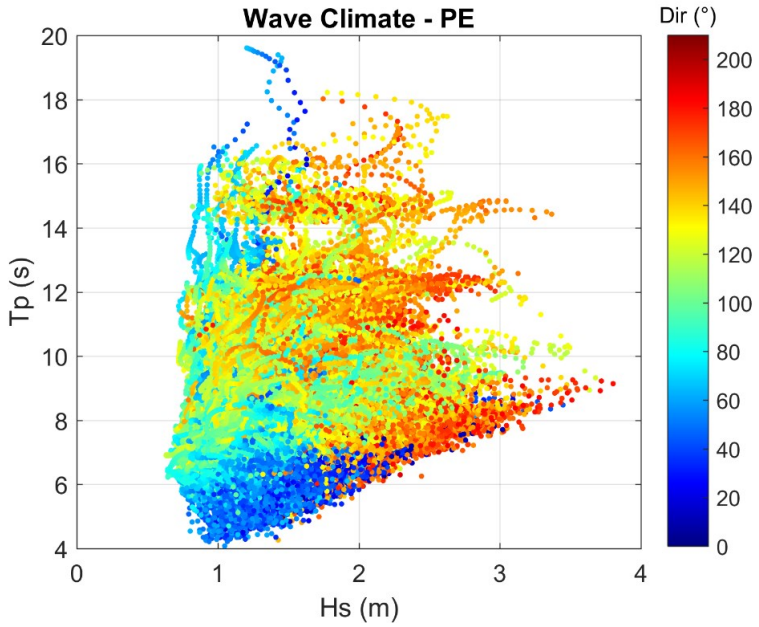

Figure 22 Interrelationships between Hs, Tp and Dir for the East region from 1901 to 2010.

4.2.4.4. Northeast Sector

The northeast sector of the Brazilian coast presents a wave climate with Hs around 1.5 ± 0.3 m and Tp that equals to 8.6 ± 1.8 s. The dispersion analysis showed that 50 % of the waves in PNE range from 1.3 m to 1.6 m and 7.4 to 9.4 s. All variables present a unimodal distribution in PNE (Annexes A, C and D). Moreover, 79.1 % composes of sea-state and 20.9 % can be considered as swell.

The wave climate in PNE presents the least dispersed (narrowest) distribution of Dir with almost all the waves coming from the second quadrant. Over half of the waves arriving in PNE are from SE (52.4 %). Waves from E are also significant in this region, representing 43.7 % of the waves. The remaining waves come from S and NE (2 % and 1.9 %, respectively).

Small waves (Hs < 1.5 m, blue colors) in PNE come mainly from ESE and higher waves (Hs > 2 m, orange colors) from SE (Figure 23; left). Meanwhile, sea-state (Tp < 9 s, blue colors) is predominantly from ESE and swell (Tp > 11 s, orange colors) from SE (Figure 23; right). While they represent a small percentage, waves from S and SSE are predominantly higher than 1.5 m with Tp higher than 11 s. These waves could then represent a swell regime, as well as storm waves given the extreme values and the Hs5 of 2.3 m previously calculated. On the other hand, small sea-state waves with Hs lower than 1.5 m and Tp lower than 9 s come mainly from E and ESE (Figure 23).

Although the percentage of sea-state is much higher than swell waves in this region as concluded by Moura (2012), waves with higher Hs come from ESE and SE while the larger Tp come from SE, as well. This indicates that there might be some storm waves which do not compose a swell, but rather a sea-state pattern. Additionally, the amount of sea-state from E is also notable.

The waves in PNE come only from the first and second quadrants confirming the less disperse wave directions regime, given that the colorbar scale does not go over 180 degrees in Figure 24. The warmer colors are also represented by larger values of Hs meaning the larger waves come from S as well as SE.

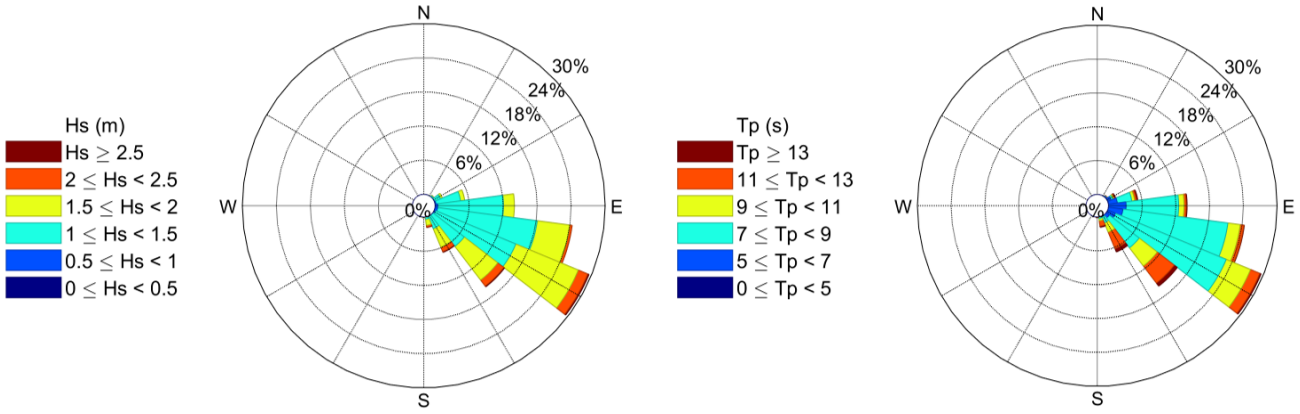

Figure 23 Wave roses of mean wave direction against Hs (left) and Tp (right) for the Northeast region from 1901 to 2010. The percentages indicate how often the waves come from each direction.

As a result, the wave climate in PNE is composed of two patterns. Although they represent a small percentage, waves from S and SSE are predominantly higher (Hs > 2 m) with longer Tp (Tp > 11 s).

These waves could then represent a swell regime as well as extreme values. On the other hand, small sea-state waves (Hs < 1.5 m and Tp < 9 s) come mainly from E and ESE.

According to Bittencourt *et al*. (2000) and Tessler and Goya (2005) the wave pattern observed in this study represents the winter regime for the Northeast region. Wave climate variability and seasonality will be discussed later as there seem to be two different patterns of Hs/Tp but they are not separated by Dir.

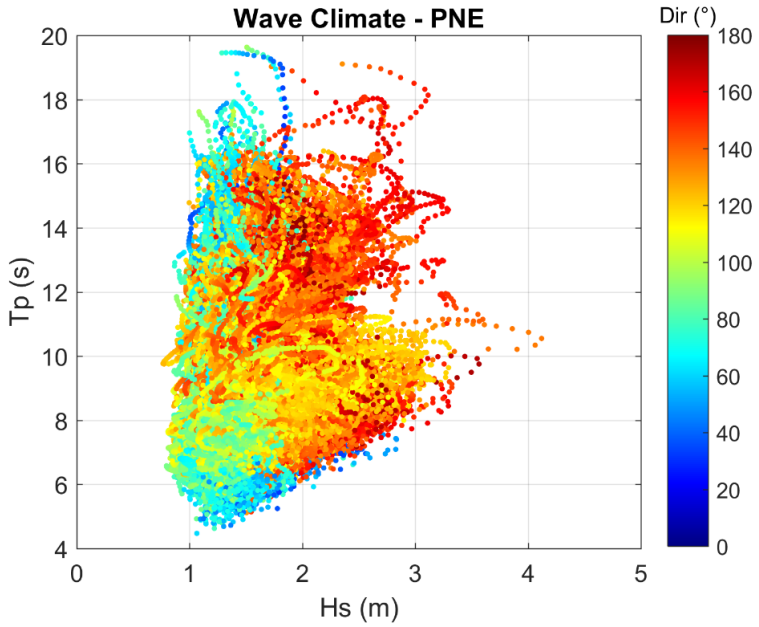

Figure 24 Interrelationships between Hs, Tp and Dir for the Northeast region from 1901 to 2010.

4.2.4.5. North 1 Sector

The north 1 sector of the Brazilian coast presents a wave climate with Hs around 1.4 ± 0.3 m with Tp that equals to 8.2 ± 1.8 s. The dispersion analysis showed that 50 % of the waves in PN1 range from 1.2 m to 1.6 m and 7.2 s to 8.3 s. By presenting the lowest IQR for both Hs and Tp, the wave climate in PN1 appears to vary the least along the coast of Brazil. Additionally, PN1 also shows a bimodal distribution of Tp with a mode value of 7.7 s representing sea-state and 12.3 s for swell (Annex C). Moreover, 86.9 % composes of sea-state and 13.1 % can be considered swell. This is the sector with the lowest percentage of swell waves.

PN1 is the northernmost region in the study area and as such, it receives the most influence from the Northern Hemisphere. Over half of the waves arriving in PN1 are from NE (52.8 %). Waves from E are also substantial in this region, representing 44.4 % of the waves. The remaining waves arrive from N and represent 2.8 %. Unlike the sectors examined previously, PN1 presents a clear bimodality of Dir with E (45 ° mode) and NE (81 ° mode) waves (Annex D). Consequently, waves arrive mainly from the first quadrant.

Small waves (Hs < 1.5 m, blue colors) in PN1 come mainly from NE and E and higher waves (Hs > 2 m, orange colors) from NE (Figure 25; left). The Tp direction follows the same pattern with sea-state (Tp < 9 s, blue colors) coming from NE and E and swell (Tp > 11 s, orange colors) from NE (Figure 25; right). In addition, all waves from E represent sea-state, even those with Hs ranging from 1.5 m to 2 m.

There is also a small number of waves coming from N, which appears to have high values of both Tp and Hs, indicating storm and swell waves generated in the Northern Hemisphere (Figure 26). The light blue colors show the small Tp coming from ESE, confirming the influence of northern storms in this region represented by sea-state waves with higher Hs from E. Meanwhile, the warm colors symbolize the small Hs sea-state regime from SE.

It is important to point out that waves with Dir ranging from 292.5 ° and 360 °, which represent N waves, were plotted as Dir = 4 ° for wave climate representation purposes in Figure 26.

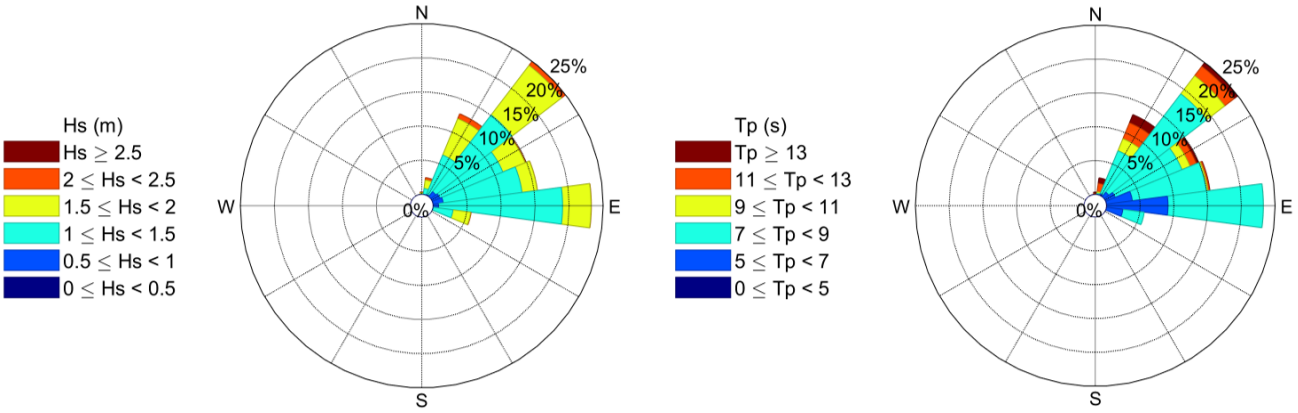

Figure 25 Wave roses of mean wave direction against Hs (left) and Tp (right) for the North 1 region from 1901 to 2010. The percentages indicate how often the waves come from each direction.

To summarize, swell waves come from NE while sea-state come from E and the small percentage of waves from N are probably composed of storm waves given their high values of Hs and Tp.

The bimodality seen at PNE is probably also present here in the Hs/Tp ratio, but would only be confirmed by separating the regimes by mode values, allowing the observation of possible different Hs/Tp associations as a function of Dir.

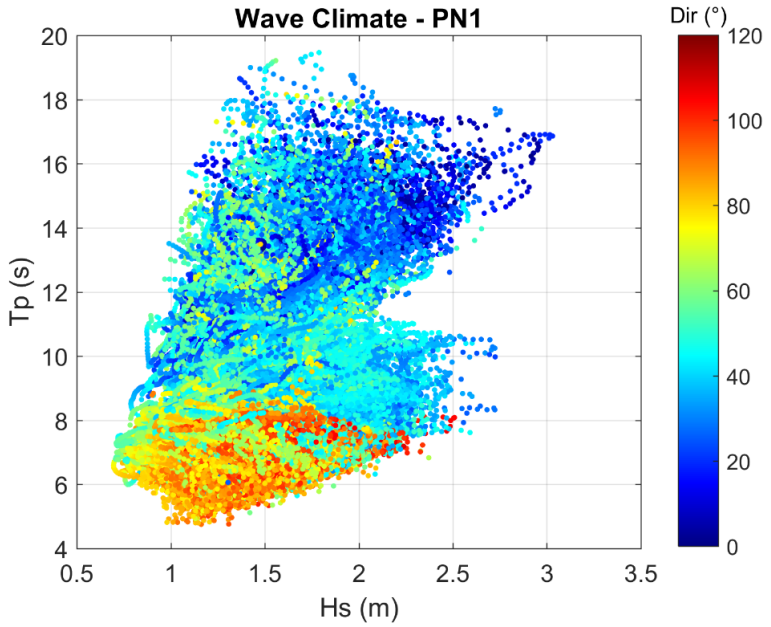

Figure 26 Interrelationships between Hs, Tp and Dir for the North 1 region from 1901 to 2010.

4.2.4.6. North 2 Sector

The north 2 sector of the Brazilian coast presents a wave climate with Hs around 1.5 ± 0.3 m, Tp equals to 8.3 ± 2.2 s. The dispersion analysis showed that 50 % of the waves in PN2 range from 1.3 m to 1.7 m and 6.9 s to 8.5 s. The same distribution behavior observed in PN1 is notable here. PN2 has a unimodal Hs distribution but bimodal Dir and Tp distributions (Annexes A, C and D). Moreover, 82.6 % composes of sea-state and 17.4 % can be considered swell.

Almost half of the waves arriving in PN2 are from E (49.3 %). Waves from NE are also substantial in this region representing 32.1 % of the waves. The remaining waves come from SE (11.5 %) and N (7.1 %). In addition, Dir presented a bimodal distribution in PN2. The first mode value is 45 ° (NE) and the second 99 ° (E).

Small waves (Hs < 1.5 m, blue colors) in PN2 come mainly from NE and E and higher waves (Hs > 2 m, orange colors) from ESE (Figure 27; left). Meanwhile, sea-state (Tp < 9 s, blue colors) comes from E and ESE and swell (Tp > 11 s, orange colors) from N and NE (Figure 27; right). In fact, there does not seem to be swell waves arriving from the second quadrant.

This leads to the assumption that these two distinct patterns of waves in PN2 are based on swell and sea-state directions (Figure 27). Swell waves come from the first quadrant, whilst sea-state comes from the second. These two patterns are not so clear when analyzing Hs. As the wave directions shift to N, high values of Tp become more present. On the other hand, the percentage of high Hs increases with waves from SE.

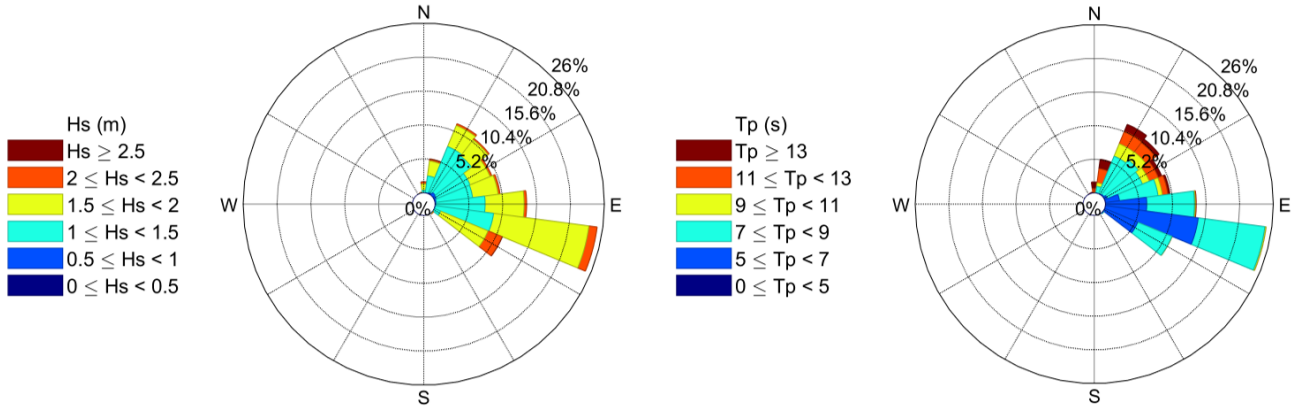

Figure 27 Wave roses of mean wave direction against Hs (left) and Tp (right) for the North 2 region from 1901 to 2010. The percentages indicate how often the waves come from each direction.

The two regimes become more clear in Figure 28, represented by the warm and cold colors, respectively. Most of the N waves have Tp higher than 14 s, indicating N swells depicted in cold colors and the waves with Tp lower than 8 s coming from SSE are illustrated in warm colors. Both patterns are composed of 2.5 m waves. As a result, swell waves come from the first quadrant while sea-state comes from the second and the small percentage of waves from N are probably composed of storm waves given their high values of Hs and Tp. As the wave directions shift to N, high values of Tp become more present. On the other hand, the percentage of high Hs increases with S waves.

Same as the method applied in PN1, waves with Dir ranging from 292.5 ° and 360 ° which represent N waves, were considered as plotted as Dir equals to 4 ° in order to improve the wave climate representation in Figure 28.

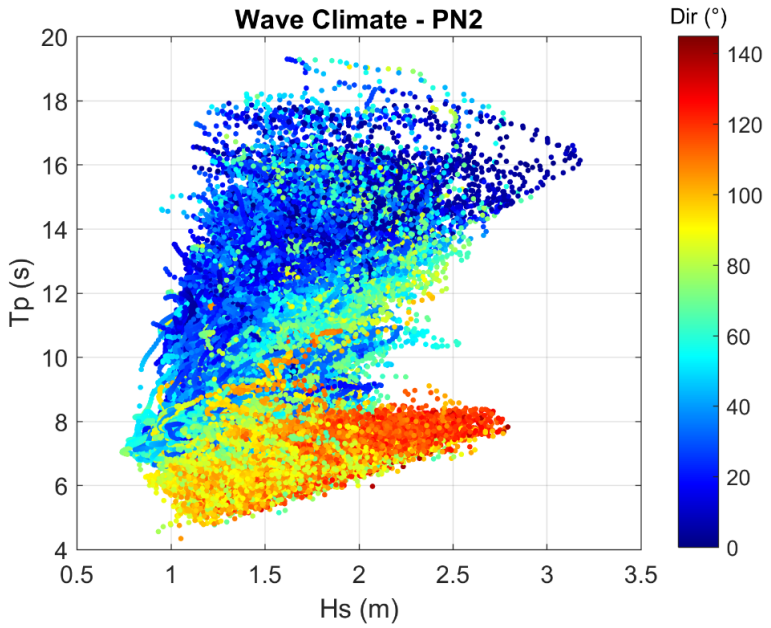

Figure 28 Interrelationships between Hs, Tp and Dir for the North 2 region from 1901 to 2010.

4.2.5. Hs vs Tp Relationship

Based on the wave climate characterization described in Section 4.2.4 and the literature review, each sector had its wave climate divided into two groups depending on the possible Dir bimodality established or different wave regimes based on Tp. Therefore, the wave climate was divided into two regimes based on Dir or Tp depending on the sector (Table 8). The southern (PS and PSE) and central sectors (PE and PNE) had their wave climate divided into waves coming from NW to E (292.5 ° to 112.5 °) and from SE to W (112.5 ° to 292.5 °). The northern sectors (PN1 and PN2) were divided according to low and high Tp, although the values used as limits were different between PN1 (10 s) and PN2 (8.5 s).

Regarding Hs, all sectors presented the highest mean for the wave regime coming from SE – W or with the highest Tp (Table 8).

Table 8 Mean values of Hs (m) and Tp (m) for each wave regime of each sector based on a Dir or a Tp threshold.

Sector	Groups	Mean Hs (m)	Mean Tp (s)
PS	NW – E	1.5	7.5
	SE – W	1.7	9.0
PSE	NW – E	1.1	7.6
	SE – W	1.3	9.3
PE	NW – E	1.2	7.7
	SE – W	1.4	9.2
PNE	NW – E	1.3	8.0
	SE – W	1.6	9.2
PN1	Tp < 10 s	1.4	7.6
	Tp > 10 s	1.6	12.3
PN2	Tp < 8.5 s	1.5	7.2
	Tp > 8.5 s	1.6	11.4

4.2.5.1. South Sector

Based on the previously described wave climate of PS and the literature review, waves were divided into groups according to the Dir regime, given that these were established depending on atmospheric systems. In PS, the wave climate was divided into NE and E represented mostly by sea-state and SE to SW, mainly composed of swell. Both groups present similar wave height characteristics except for the maximum values of Hs which are 5.3 m and 8.2 m, respectively.

The first analysis used all Hs as inputs for the exponential model and it was clear that the fit is better towards higher waves due to a smaller dispersion (Annex E). Moreover, in order to obtain a better understanding of how well Hs and Tp are related, waves from NW to E were once again analyzed but now the fit was only calculated for Hs higher than 1.5 m. On the other hand, waves from SE to W were repeatedly analyzed for Hs higher than 2.5 m.

Waves with higher Hs also have higher Tp for both Dir groups in PS (Figure 29). The RMSE values indicate that waves from NW to E are more similar between themselves (RMSE = 0.29 s) than waves from SE to W (RMSE = 0.50 s).

Given the different RMSE values and the behavior observed in the graphs, Tp mode values for waves < 1.5 m can be considered as 7.25 s. On the other hand, in the case of waves with Hs > 1.5 m, the adjustment formulas must be used for waves with Dir ranging from NW to E. Moreover,

the Tp of waves from SE to W with Hs lower than 2.5 m range from 7.25 s to 10.25 s and the lower RMSE (0.50 s) and higher correlation coefficient (0.92) indicate the fit is better when the first Hs values are eliminated (Figure 29).

The exponential fit describes waves with Dir from NW to E (correlation coefficient = 0.98) better than waves from SE to W (correlation coefficient = 0.92).

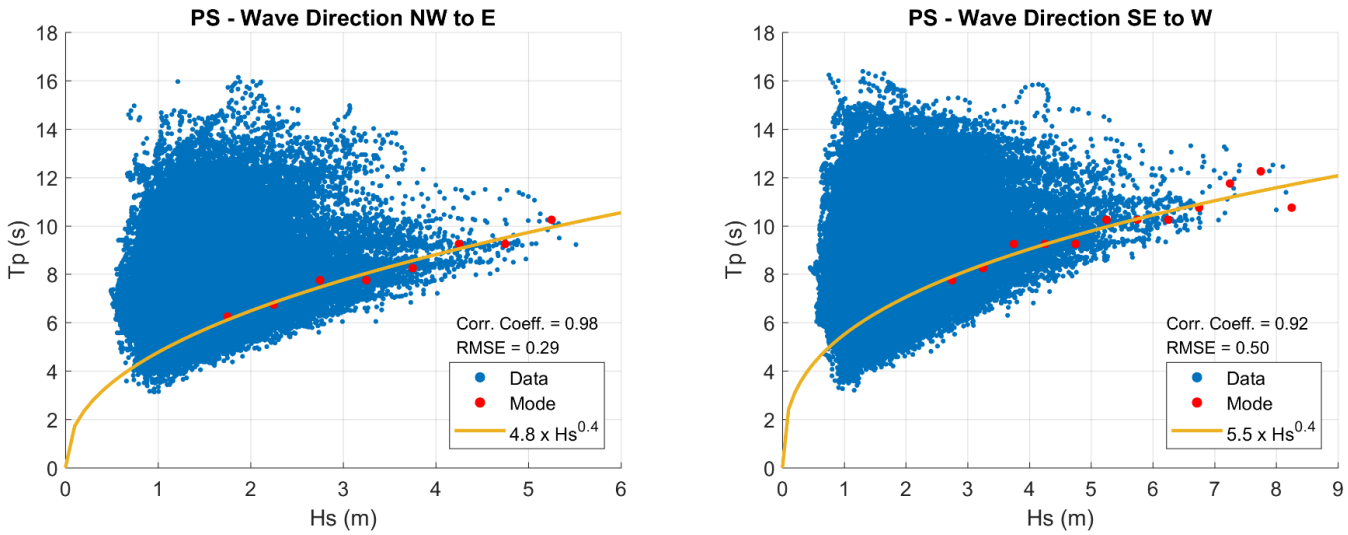

Figure 29 Exponential fits between Hs higher than 1.5 m and Tp for waves with Dir from NW to E (left) and SE to W (right) in PS, including RMSE values and significant correlation coefficients (99 % confidence level).

4.2.5.2. Southeast Sector

The Dir limit chosen between the two groups in PSE was the same as for PS in order to separate the main storm generated waves from the rest. Although the minimum and maximum values of Tp are similar, the second group (Dir ranging from SE to W) is composed of waves with Hs up to 4.4 m while the maximum Hs for waves from NW to E is 3 m.

The differences between the two groups of waves based on Dir is clearer in PSE than in PS. The first group of waves in PSE presents all Tp mode values below 9 s and RMSE equal to 0.40 s. On the other hand, waves from SE to W present only three Tp mode values below 9 s and all waves higher than 1.5 m present Tp mode values higher than 10 s, representing the dominance of the swell regime of this region (Figure 30). Given the correlation coefficient values (0.92) the exponential fit reproduces well the Tp mode values for waves with Dir ranging from NW to E, as opposed to the

SE to W waves (correlation coefficient = 0.75). Additionally, the RMSE of 1.21 s indicates the points are very disperse in waves from SE to W and the exponential fit might not be the best way to represent the Hs vs Tp relationship in this case.

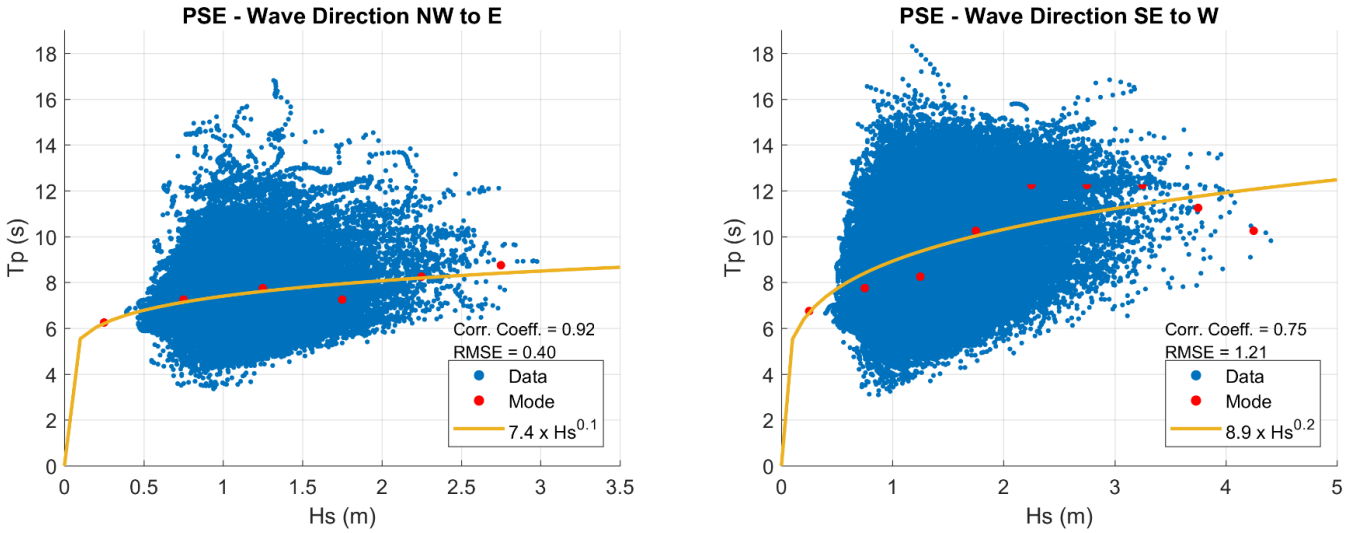

Figure 30 Exponential fits between Hs and Tp for waves with Dir from NW to E (left) and E to SW (right) in PSE, including RMSE values and significant correlation coefficients (95 % confidence level).

4.2.5.3. East Sector

The Dir limit chosen between the two groups in PSE was 112.5 °. This value was chosen for the same reasons as described for PS and PSE. Waves from SE to W present higher value of maximum Hs, 3.8 m, as opposed to 3.5 m for NW to E waves. However, Tp mode values do not follow the same pattern.

Both exponential fits have a similar slope but different RMSE values, 0.57 s and 1.86 s, respectively. Additionally, even though waves from SE to W presented a considerable amount of Tp around 15 s, the mode values are all below 10 s, except for Hs ranging from 1.5 m to 2 m (Tp mode = 12.25 s) (Figure 31). Given these two observations, the exponential fit was also computed excluding the Tp value corresponding to the Hs range of 1.5 m to 2 m from SE to W. Consequently, the curve turned into a better fit with a similar RMSE to the one for waves from NW to E (0.48 s) and a significant correlation coefficient (0.85), which was not true for the previous case (Figure 32; left).

As previously mentioned, waves ranging from SE to W presented a high number of waves with Tp around 15 s. The analysis was repeated considering only waves with Tp equal or higher than 14 s coming from all directions. With this new analysis, the mean Hs showed to be 1.6 m and 53 % of the waves are from SE while 29 % are from S. Furthermore, when computing the exponential fit only for those waves, it was possible to observe that most waves present Tp between 14 s and 15 s and all Tp mode values calculated are from 14.25 to 14.75 s (Figure 32; right).

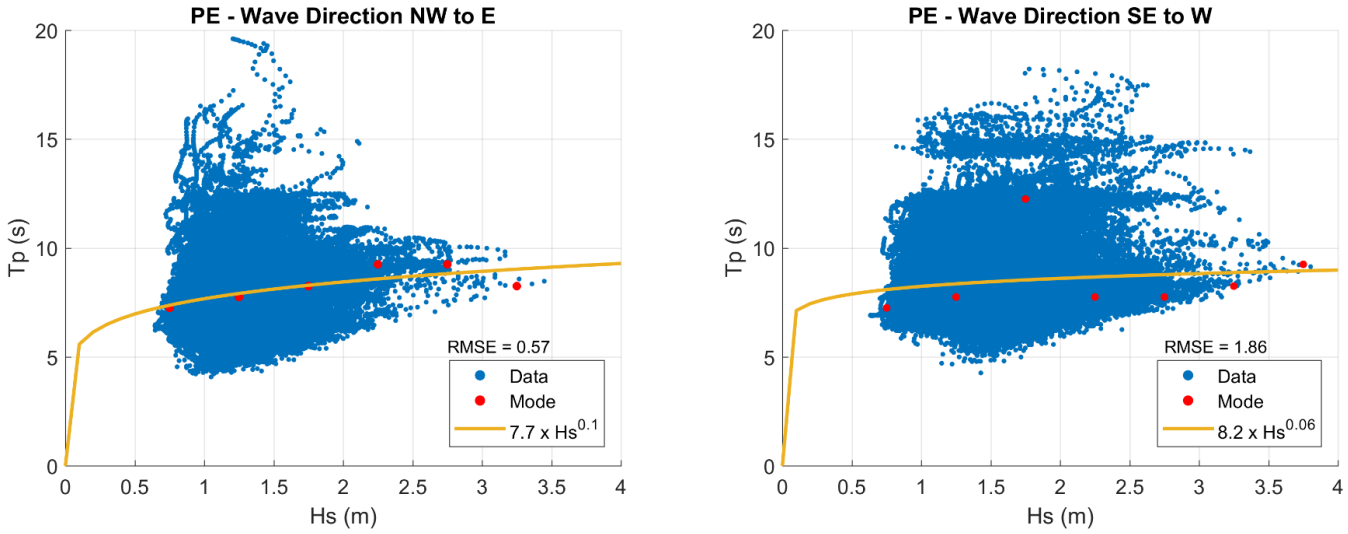

Figure 31 Exponential fits between Hs and Tp for waves with Dir from NW to E (left) and E to SW (right) in PE, including RMSE values. There correlations are not significant for a 95% confidence level.

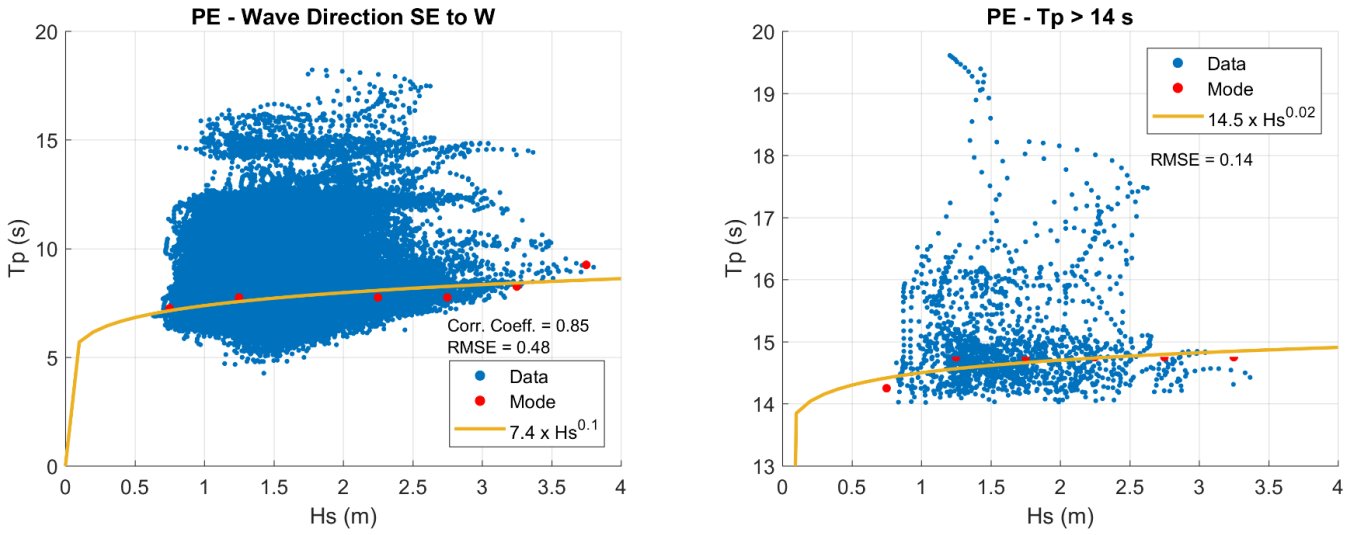

Figure 32 Exponential fits between Hs and Tp for waves with Dir from NW to E excluding outlier values (left) and waves with Tp equal or higher than 14 s (right) in PE, including RMSE values and significant correlation coefficient (left: 95 % confidence level; right: confidence level < 95%).

Even though in all four cases the Tp mode points seemed to lie close to the exponential curve, there was only one correlation coefficient which was significant at a 95 % confidence level.

4.2.5.4. Northeast Sector

The Dir limit chosen between the two groups in PNE was also 112.5 ° in agreement with the literature review findings. The typical swell in this region comes from S and SSE, while sea-state varies from E to SE. When comparing both wave regimes, the largest difference is in the maximum Hs which is 3 m for waves from NW to E and 4.1 m from SE to W.

Given the equal correlation coefficient for both groups of waves (0.94) it can be concluded that both exponential fits represent well their own groups. However, the different RMSE values indicate that waves from NW to E are more similar between themselves (RMSE = 0.39 s) than waves from SE to W (RMSE = 0.68 s) (Figure 33). Nevertheless, regarding waves from SE to W, the exponential model is a good fit but the presence of two wave patterns based on Tp in which the threshold can be interpreted as approximately 12 s is noticeable.

Furthermore, when examining all waves with Tp equal or higher than 12 s in PNE separate from the other waves, the mean Hs is 1.7 m and 70 % of the waves come from S.

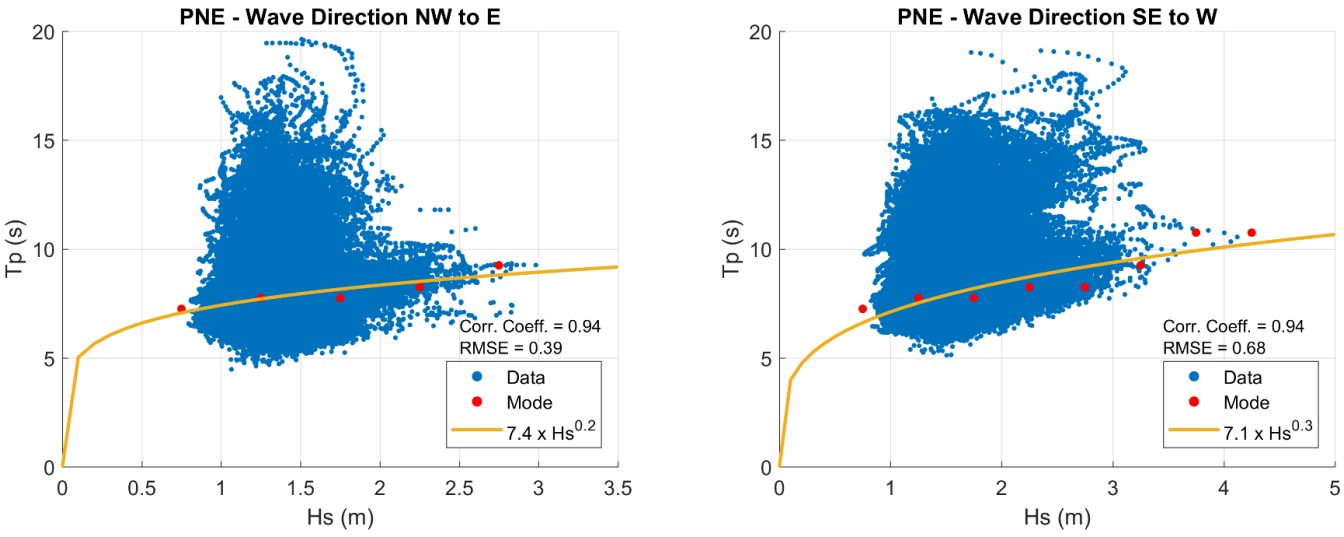

Figure 33 Exponential fits between Hs and Tp for waves with Dir from NW to E (left) and E to SW (right) in PNE, including RMSE values and significant correlation coefficients (left: 95 % confidence level; right: 99 % confidence level).

4.2.5.5. North 1 Sector

In PN1 a simple adjustment based on Dir is much weaker because there is a mix of sea-state and swell or two different conditions. In other words, there are local conditions and offshore conditions mixed together. Thus, given the Tp bimodality of this region, the groups were divided according to Tp, splitting between Tp lower and higher than 10 s. Waves with longer periods are slightly higher with maximum Hs of 3 m compared to a maximum of 2.7 m Hs of the ones with lower period (mostly sea-state).

The exponential fits describe the Hs/Tp relationship better for swell regimes since this was the only case with a significant correlation coefficient (0.99). With regard to the case of swell, it can be considered that waves smaller than 1.5 m have Tp lower than 12 s while sea-state waves present Tp mode values ranging from 7.25 s to 8.25 s (Figure 34). However, the RMSE values indicate that swell waves have a more disperse Tp values than sea-state since their RMSE values are 0.79 s and 0.37 s, respectively.

To conclude, the Hs vs Tp relationship analysis showed that sea-state regime (Tp < 10 s) in PN1 is composed of Hs around 1.4 m and Tp of 7.7 s, with 51 % of the waves arriving from E and 49 % from NE. On the other hand, swell regime (Tp > 10 s) comes from NE and N (77 % and 20 %, respectively). Furthermore, swell waves with Hs lower than 1.5 m present Tp lower than 12 s.

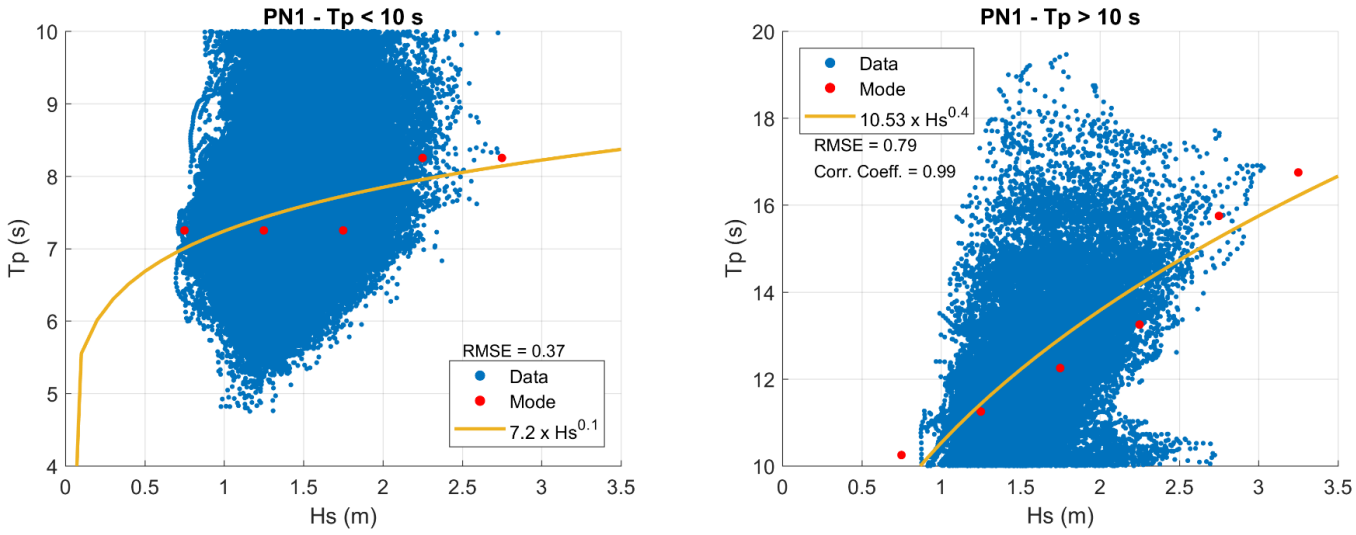

Figure 34 Exponential fits between Hs and Tp for sea-state waves with Tp < 10 s (left) and swell waves with Tp > 10 s (right) in PN1, including RMSE values and significant correlation coefficients (left: confidence level < 95 %; right: 99 % confidence level).

4.2.5.6. North 2 Sector

As for the previous sector, waves in PN2 were divided according to Tp, although the limit here was 8.5 s. Waves with longer periods are slightly higher with maximum Hs of 2.8 m compared to a maximum of 3.2 m Hs of the ones with lower period.

In regard to the exponential fits, waves with higher Tp (Tp >= 8.5 s) show a better fit given the significant correlation coefficient (0.97), even though the Tp mode values are more disperse which is indicated by the RMSE equal to 0.84 s as opposed to the lower RMSE for waves with low Tp (0.37 s) (Figure 35).

Overall, in PN2 waves smaller than 1.5 m can be considered as sea-state composed by Tp lower than 10 s while higher waves lie closer to the exponential curve calculated for high values of Tp. In contrast, waves with Tp lower than 8.5 s are not well represented by the exponential fit since none of the Tp values lie on the curve and the correlation coefficient is non-significant (Figure 35).

To summarize, the Hs vs Tp relationship analysis showed that waves with Tp < 8.5 s in PN2 are composed of Hs around 1.5 m and Tp of 7.2 s with 61 % of the waves arriving from E. On the other hand, waves with Tp > 8.5 s come from NE and N (62 % and 25 %, respectively). Furthermore, waves with Hs lower than 1.5 m inserted in the long period group present Tp lower than 10 s.

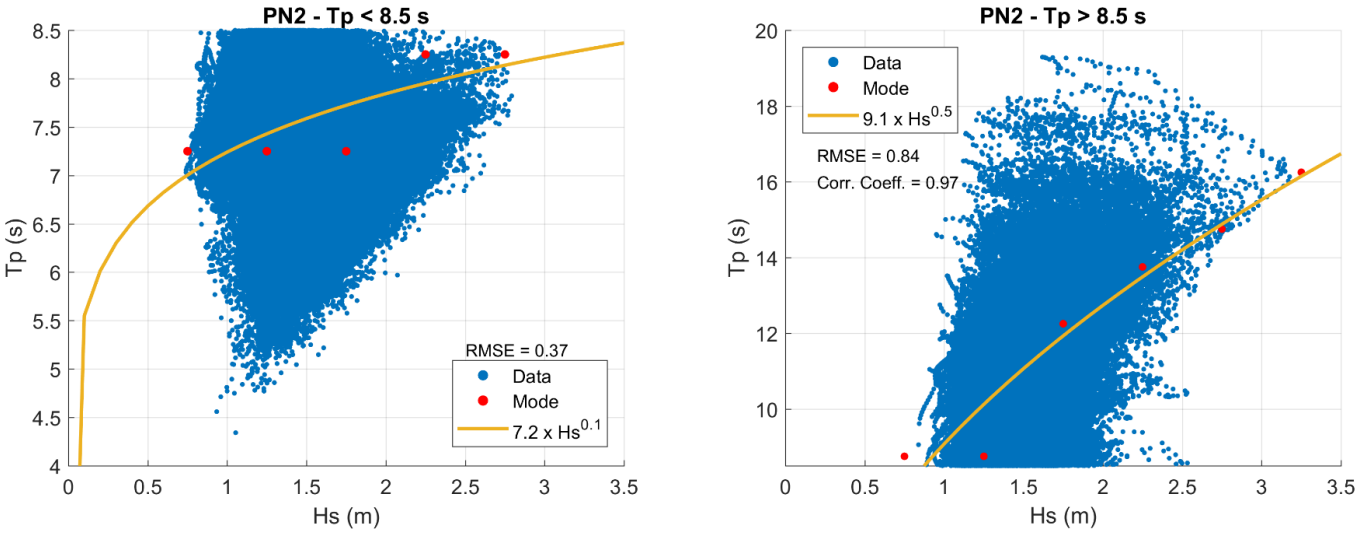

Figure 35 Exponential fits between Hs and Tp for waves with Tp < 8.5 s (left) and with Tp > 8.5 s (right) in PN2, including RMSE values and significant correlation coefficients (left: confidence level < 95 %; right: 99 % confidence level).

4.3. Wave Climate Variability

4.3.1. Monthly Variability

In general, the north region of Brazil (PN1 and PN2) shows a different seasonality pattern than the rest of the coast for both Hs and Tp (Figure 36).

The highest waves occur in February in PN2 while the other sections of the coast have the highest waves from July to September, including PN1 which is also in the north region. PSE shows two distinct peaks of Hs, although its first peak of the year in May is lower than the second one, which is in September. On the other hand, both PN1 and PN2 presented their smallest waves in May and April, respectively. The rest of Brazil have the smallest waves in January and February.

Although PSE and PE show lower values of Hs throughout the year, the entire coast has a similar range of Hs when comparing their monthly averages (approximately 0.4 m) (Figure 36; left).

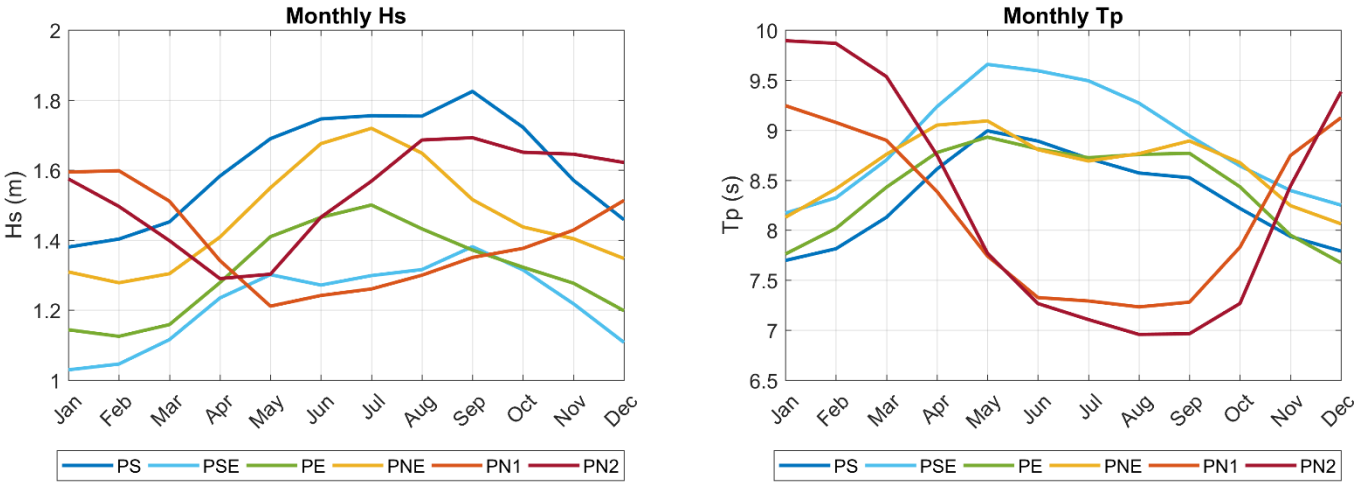

Figure 36 Monthly averages of significant wave height (m) (left) and peak period (s) (right) per region of the Brazilian coast from 1901 to 2010.

The monthly variability of Tp along the coast of Brazil shows a high contrast between the north region of Brazil (PN1 and PN2) and the rest of the coast (Figure 36; right). While the longest Tp occur in January for the north region, in other regions of Brazil the highest values of Tp occur in May. On the other hand, the north region's lowest Tp values occur in August whilst the rest of the

regions present their lowest Tp in December and January. Furthermore, when looking more closely, it is noticeable that PE and PNE present two peaks during the year, in May and September. Although, the September peak in PE is not as abrupt as in PNE.

Not only the monthly averages of Tp make the north region stand out but their ranges as well. When comparing the highest peaks of Tp with the lowest troughs, PN1 and PN2 present a difference of 2 s and 2.9 s, respectively, while the other sectors have ranges varying between 1 s and 1.5 s (Figure 36; right).

4.3.2. Annual Variability

The interannual variability analysis helps to identify if there are any (abrupt or smooth) changes in the wave climate of the study area.

There seems to be two clear peaks of Hs in the time series in all sectors of the coast. The first one occurred in the late 1910s and the second in the early 1940s. Although the Hs oscillations complicate a precise conclusion, a positive trend is evident on the second half of the time series leading to a currently higher Hs when compared to the beginning of the time series. However, depending on the region, the 1940s peak presents higher values than the end of the time series (Figure 37; left).

When comparing the sectors, PSE stands out for having the lowest values of Hs throughout the 110 years analyzed, followed by PE. On the other hand, PS has the highest Hs annual mean, especially since the 1970s.

The interannual variability of Tp is not as clear as the Hs. The peak in the 1940s is still visible in some sectors but not the 1910s. In addition, there seems to be a decrease in Tp from 1940s to 1970s. This decrease could simply be due to the accuracy of the model which improves with time or it might reflect the start of the positive trend the data shows (Figure 37; right).

Moreover, all mean values of Tp are between 7.5 s and 9.5 s which is lower than the 10 s swell classification. This could indicate more frequent sea-state conditions along the entire coast.

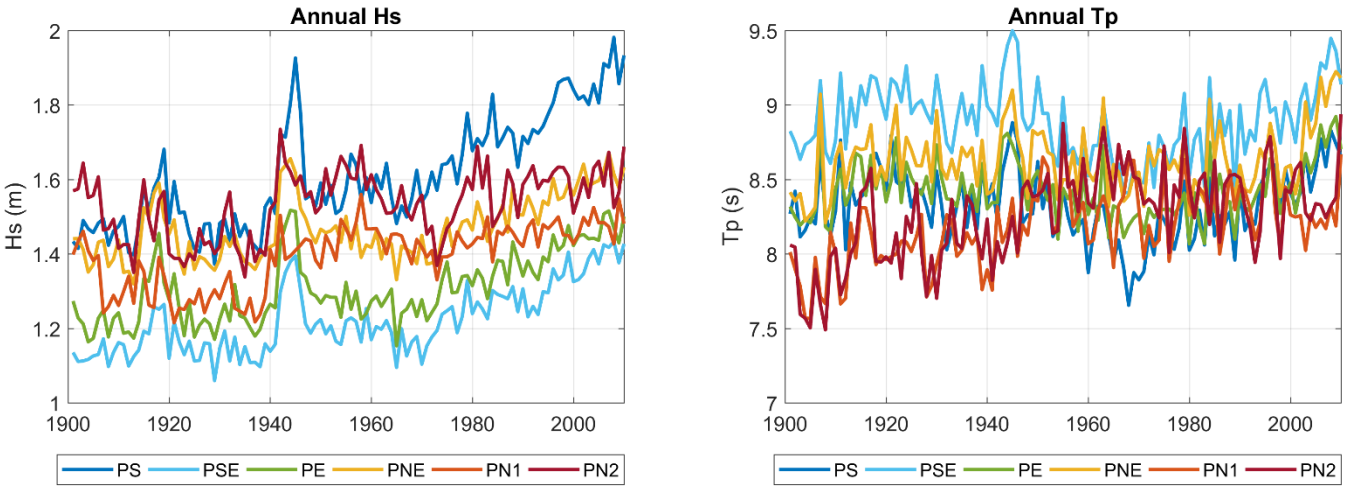

Figure 37 Annual averages of significant wave height (m) (left) and peak period (s) (right) per region of the Brazilian coast from 1901 to 2010.

4.3.3. Decadal Variability

The decadal analysis clarifies some aspects identified in the previously presented annual analysis. All sectors present the same pattern throughout the whole time series, with some small differences between the north region and the rest of the coast (Figure 38).

In general, there appears to be a stabilization of Hs from 1901 to 1970, with prominent peaks around the 1910s and the 1940s, followed by an accelerated rise after the 1970s. This positive trend starting around 1970, previously observed in the annual results, is clearer in the decadal analysis. This indicates that in the last 40 years of the temporal scope of this study, Hs has been increasing even though the rates have changed both temporally and spatially, with lower trends in the north region (Figure 38; left).

The 1910s and 1940s Hs peaks and positive Hs trend present for PS, PSE, PE and PNE will be further investigated in the Discussion and the 1970s positive trend in the Section 4.6.

Regarding the development of Tp from 1901 to 2010, each region of the coast presents a different pattern without a clear oscillation (Figure 38; right). However, all sectors start with a positive trend up until 1910, followed by a decrease in Tp. In fact, most of the coast seems to show negative trends until 1960.

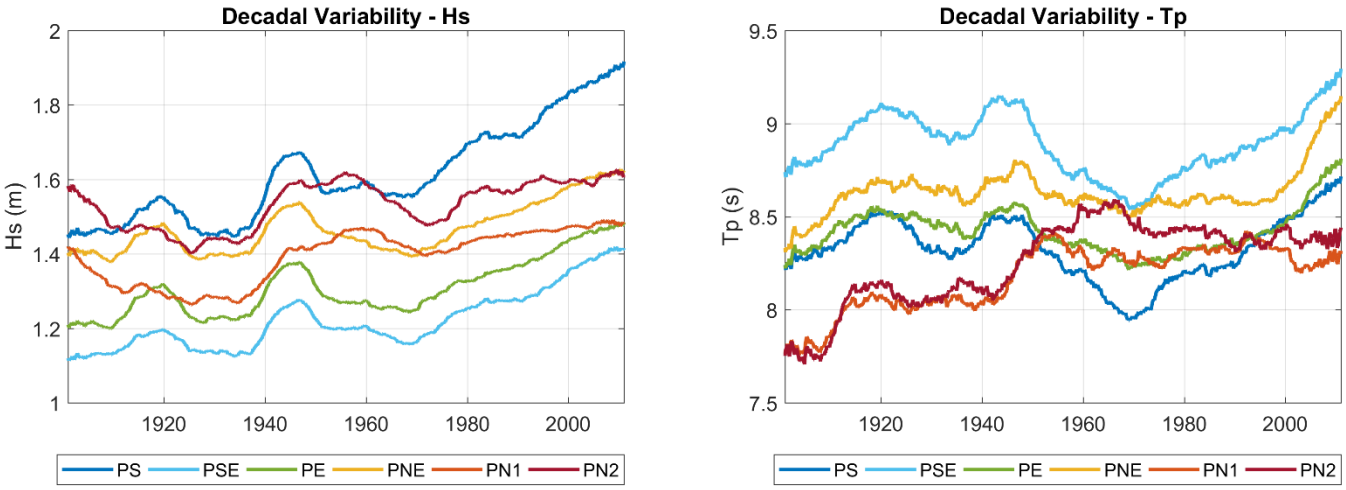

Figure 38 Decadal results for significant wave height (m) (left) and peak period (s) (right) per region of the Brazilian coast from 1901 to 2010.

Despite the fact that they are less attenuated and also as a result of the performed data smoothing, the peaks in the 1910s and 1940s are also visible when analyzing Tp (Figure 38; right). Moreover, even though the rates oscillate, the same positive trend in Hs starting in the 1970s is also observed in Tp for the southern (PS and PSE) and central (PE and PNE) sectors.

The north region also shows different oscillations and peaks of Tp when compared to the rest of the study area. For example, the 1910s and 1940s peaks are not visible in these sectors. However, there is an increase in both Hs and Tp in the 1940s and the values remain higher for the next two decades (Figure 38).

4.4. Extreme Wave Analysis

The extreme wave analysis allows the understanding of storm events as these represent the most energetic waves, reflecting the behavior of the storm generating areas in the Atlantic Ocean. Monthly, annual and smoothed annual values were examined.

4.4.1. Monthly Extreme Wave Variability

Monthly analyses were also performed for extreme wave conditions (Hs5 and Tp5). The sector to stand out the most regarding monthly values of Hs5 was PS and for Tp5 were the northern sectors (Figure 39).

Regarding Hs5, PS presents the highest values for every month, always remaining above 2.5 m. In fact, only PE and PNE present values above the threshold of 2.5 m for the months of July and August. Looking more carefully at the monthly results for Hs5 it is possible to observe a range of less than 1 m for most of the coast. PS shows the highest range (approximately 1.4 m) between its lowest value in January and the highest in June (Figure 39; left).

Concerning Tp5, although the values are slightly higher between May and August, the southern and central sectors do not show any type of seasonality as opposed to the Tp monthly analysis in which all sectors displayed clear seasonality patterns. In these sectors, the values range approximately from 12 s to 14 s. Meanwhile the northern sectors present a range of almost 8 s between their highest values (November to March) and their lowest values (June to September) (Figure 39; right).

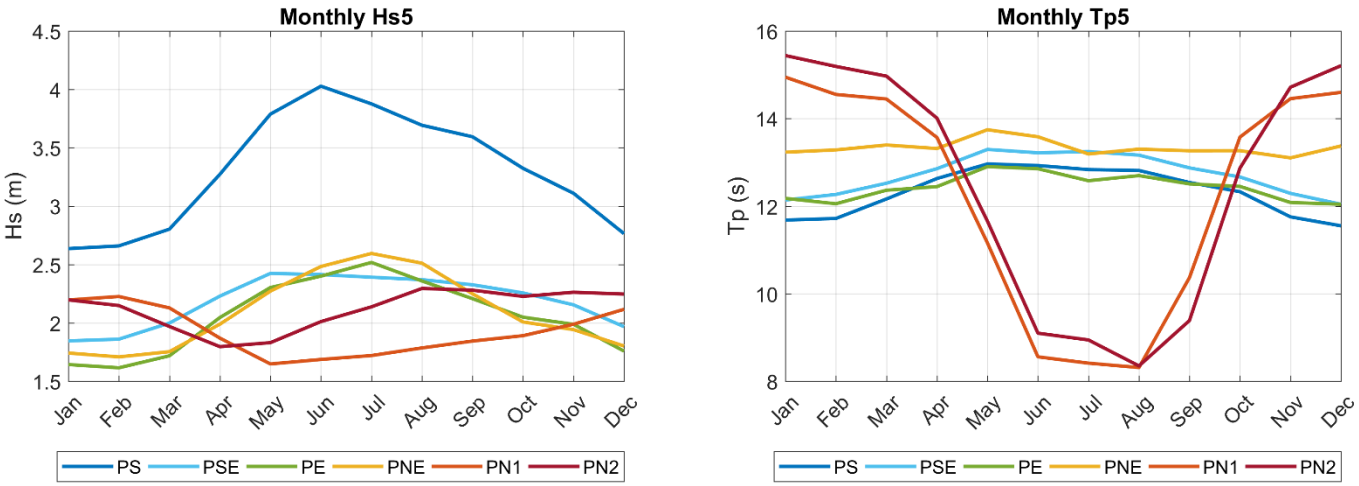

Figure 39 Extreme wave analysis, calculated per month for exceeded by 5% of Hs (left) and exceeded by 5% of Tp (right) for each sector of the Brazilian coast.

4.4.2. Annual Extreme Wave Variability

Regarding extreme Hs, PS presents the highest values with most results being above 3 m while the other sectors' are below 2.5 m for the entire time series. Additionally, the oscillations observed in PS have a larger magnitude than the other sectors (Figures 40 and 41). From 1970s PS values for Hs5 are above 3.5 m and seem to be increasing. This positive trend in the last four decades is also visible for the other sectors but not as abrupt. In fact, all sectors present their lowest Hs5 values in the first three decades of the time series and their highest values in the last two decades. In general terms, it seems that there is no variation in the maximum values of Hs5 until 1940/50.

When analyzing the extreme values per year, the trends tend to be the same as the smoothed annual values, but it allows to see if there were periods of stability or acceleration. For example, the upwards Hs5 trend is confirmed for the last four decades analyzed (Figure 40; left). It is also possible to observe that the decades of higher Hs5 values are a reflex of a specific period within that decade. The first half of the 1940s decade presents a peak of Hs5 for all sectors except PN1. In addition, PNE shows a prominent peak in 1988 which is not visible in the smoothed analysis.

Just as observed for mean Hs, there are two peaks of Hs5 values (1910s and 1940s) with the north region being an exception. However, given their magnitudes and the results shown in Section 4.3.2, only the second peak calls for attention.

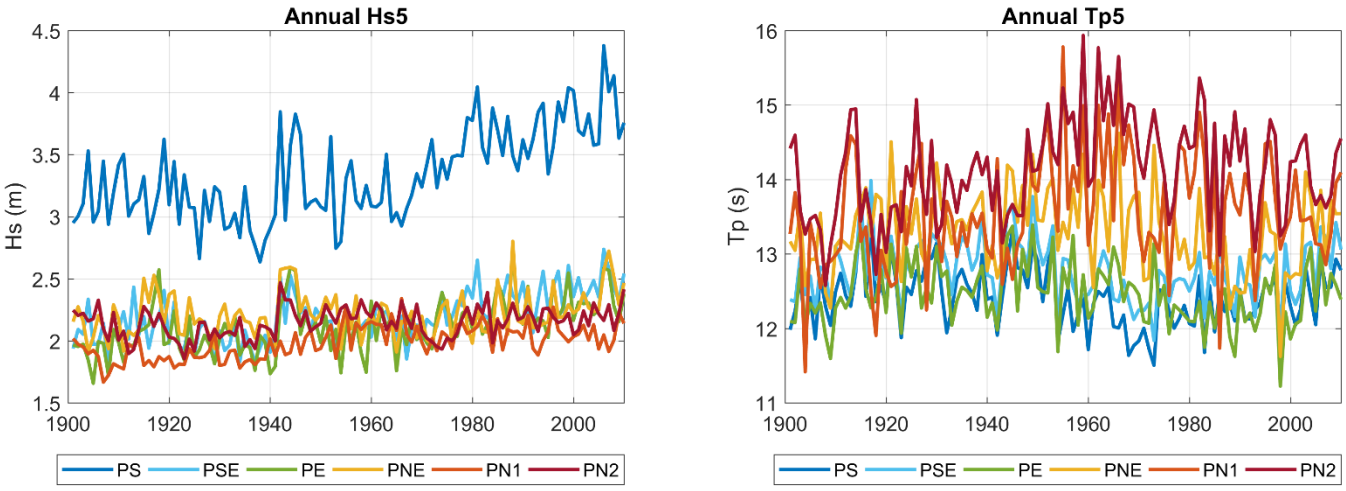

Figure 40 Extreme wave analysis, calculated per year for exceeded by 5% of Hs (left) and exceeded by 5% of Tp (right) for each sector of the Brazilian coast.

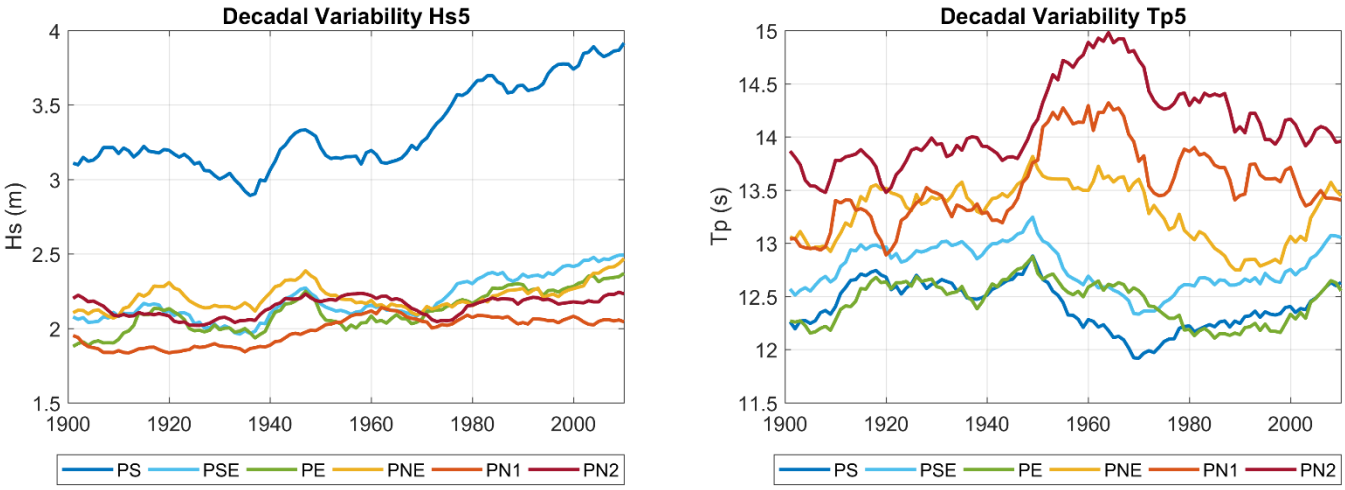

Figure 41 Extreme wave analysis, calculated per decade for exceeded by 5% of Hs (left) and exceeded by 5% of Tp (right) for each sector of the Brazilian coast.

The results for annual Tp5 values show high variability and oscillations or trends which are not clear. In general, Tp5 ranges from 12 s to 15 s for the entire study area throughout most of the 110 years analyzed (Figures 40 and 41).

The coast of Brazil can be divided into two groups based on the Tp5 analysis (Figure 41). The first group is composed of PNE, PN1 and PN2 with the highest values which remain almost always above 13 s. The second group, composed of PS, PSE and PE, presents Tp5 mostly below 13 s. Besides the Tp5 values, the peaks are also different between these two grouped regions. While the northern group exhibits a peak between 1950s and 1960s, the southern one shows a decrease in Tp5. Moreover, from 1970s and 1980s there is a positive trend of values for the southern group while the northern one oscillates and decreases.

The southern and central sectors present the highest Tp5 in around 1950 and the northern sectors between 1950 and 1970. On the other hand, the north region presents its lowest values in the first three decades of the time series, the central sectors around the 1990s and the southern around 1970s. In general, a trend for Tp5 is not evident and it is not clear whether there is an increase, except in PN1 and PN2 (Figure 41; right).

4.5. Correlations with Climate Indices

Considering the correlation analysis described in the Methods, the Pearson correlation coefficients between wave parameters and climate indices were calculated for each sector of the study area.

In order to understand the analysis of correlation with climate indices it is important to consider that a positive correlation indicates an increase of the wave parameter being analyzed during the positive phase of a certain index. The negative correlation indicates a decrease in wave parameter during a positive phase.

Despite all correlation coefficients being low (< 0.30) they are mostly significant (Table 9). For example, the ONI/Hs and ONI/Tp relationships are significant in most sectors of the coast with a 95 % confidence level (8 out of 12) and even 99 % confidence level (6 out of 12).

Regarding the ONI/Hs correlations, the relationship in PN1 is positive and in the remaining significant areas (PSE, PE, PNE) it is negative. This indicates that the north region shows an increase in Hs during El Niño while the central and southern regions present a decrease in Hs during these events. The opposite behavior occurs for La Niña events. The highest correlations for ONI/Hs are found in PE and PN1, -0.12 and 0.12, respectively, representing the regions where Hs is most influenced by ENSO. Concerning the ONI/Tp correlation, the north region presents non-significant correlations. All other regions show a negative correlation meaning that Tp decreases during El Niño. PS is the most influenced region with a correlation coefficient of -0.1 (Table 9).

Other climate indices such as TSA, AMO, SAM and AMM were also examined. The AAO was analyzed as well but the results were non-significant for all sectors (Annex F).

All significant correlation coefficients computed for TSA/Hs and TSA/Tp were higher than the ones for ONI analysis (Table 9). Regarding Hs, only the north region presented negative correlations with TSA although only PN2 presented a significant result. PS, PSE, PE and PNE presented positive significant correlations (99 % significance level). The northern sectors did not have a significant correlation for TSA/Tp, while the other sectors presented positive relationships. PS and PSE presented the highest levels of correlation with TSA for Hs while Tp in PNE is the most influenced by TSA.

Table 9 Pearson correlation coefficients between Hs and Tp and climate indices for each sector of the coast. Significant results for 95 % confidence interval are underlined and for 99 % are in bold.

Index	Parameter	PS	PSE	PE	PNE	PN1	PN2
ONI	Hs	-0.04	**-0.09**	**-0.12**	**-0.09**	**0.12**	0.05
	Tp	**-0.10**	-0.07	-0.07	**-0.09**	-0.01	0.04
TSA	Hs	**0.28**	**0.28**	**0.23**	**0.17**	-0.03	**-0.15**
	Tp	**0.15**	**0.16**	**0.20**	**0.25**	0.01	0.06
AMO	Hs	**0.20**	**0.23**	**0.23**	**0.24**	0.03	**0.22**
	Tp	**0.13**	**0.14**	**0.14**	**0.13**	0.00	-0.02
SAM	Hs	**0.14**	**0.13**	**0.11**	0.08	-0.03	0.01
	Tp	0.07	0.02	0.05	0.03	-0.05	-0.08
AMM	Hs	-0.01	0.02	0.04	0.06	0.02	**0.19**
	Tp	0.05	0.04	0.00	0.02	**0.12**	0.09

As for the previous analysis, PN1 does not have any significant results regarding its correlation with AMO (Table 9). All other sectors of the Brazilian coast show a positive and significant result (to a 99 % level) between AMO/Hs. PNE presents the highest correlation (0.24), followed by PSE (0.23) and PE (0.23), PN2 (0.22) and PS (0.20). On the other hand, only the southern and central sectors presented significant results for AMO/Tp, with all correlation coefficients indicating positive and significant correlations (> 99 % level).

Regarding SAM, only the southern and central sections presented significant results for SAM/Hs (Table 9). The correlation coefficients decrease from PS (0.14 for a 99 % confidence level) to PNE (0.08 for a 95 % confidence level) and all of them indicate positive relationships. On the other hand, AMO/Tp did not show any significant correlation values.

While SAM only indicated significant correlation for the southern and central sectors, AMM only presented significant results for the northern sectors which indicated positive relationships (Table 9). However, only PN2 showed significant correlation for AMM/Hs (0.19 for a 99 % confidence interval) and both sectors presented significant positive relationships for AMM/Tp.

In summary, the correlations between ONI/Hs and ONI/Tp presented the lowest coefficients when compared to other indices, indicating a lower level of significance for this indicator. TSA and AMO are the indices with better correlations and significance for the southern and central areas,

although their correlations are better with AMO. The northern sectors correlate well with AMM. Additionally, SAM showed to be an important index to Hs in the southern and central sectors but not to Tp. There is not one single index that is significant to a high level, suggesting the interaction of several meteorological conditions on the definition of wave conditions variability in the area.

4.6. Trend Analysis

Trend analyses were performed in order to understand if the wave climate has been affected by climate change. Ergo, this section aims to determine the possible existence of Hs and Tp trends. Results will be shown for the entire time series, monthly, and trends of specific time periods.

4.6.1. Hs Trends

All sectors have significant positive Hs and Hs5 trends from 1901 to 2010, indicating waves are getting higher along the coast of Brazil (Table 10, Figure 42). Most of the coast presents a higher trend in the extreme events (Hs5) than the mean Hs, except for PNE and PN2. All trends are significant for a 99 % level, except for the Hs5 trend in PNE that is significant for a 95 % level.

Even though PN2 starts the time series with the highest value, PS quickly surpasses it becoming the sector with the highest Hs rate with 3.7 mm/yr. While PSE presents the lowest values of Hs through the studied period, it presents the second highest rate with 2.1 mm/yr. All other sectors show Hs rates lower than 2 mm/yr with PN2 displaying the lowest rate, 1.3 mm/yr (Table 10, Figure 42; left).

Table 10 Hs linear regression trends for each sector of the Brazilian coast from 1901 to 2010, including mean annual (Hs) and extreme (Hs5) wave height values. Significant values for a 99 % confidence level are in bold and for 95 % confidence level is underlined.

Sectors	Hs Trend (mm/yr)	Hs5 Trend (mm/yr)
PS	**3.7**	**7.4**
PSE	**2.1**	**3.9**
PE	**1.9**	**3.5**
PNE	**1.5**	<u>1.3</u>
PN1	**1.8**	**2.5**
PN2	**1.3**	**1.0**

Hs5 values were also examined and almost all sectors (with the exception of PS) present rates between 1 mm/yr and 4 mm/yr (Table 10, Figure 42 right). PN1 presents the lowest Hs5 values for the entire time series and once again, PS presents the highest values and highest rate, 7.4 mm/ yr.

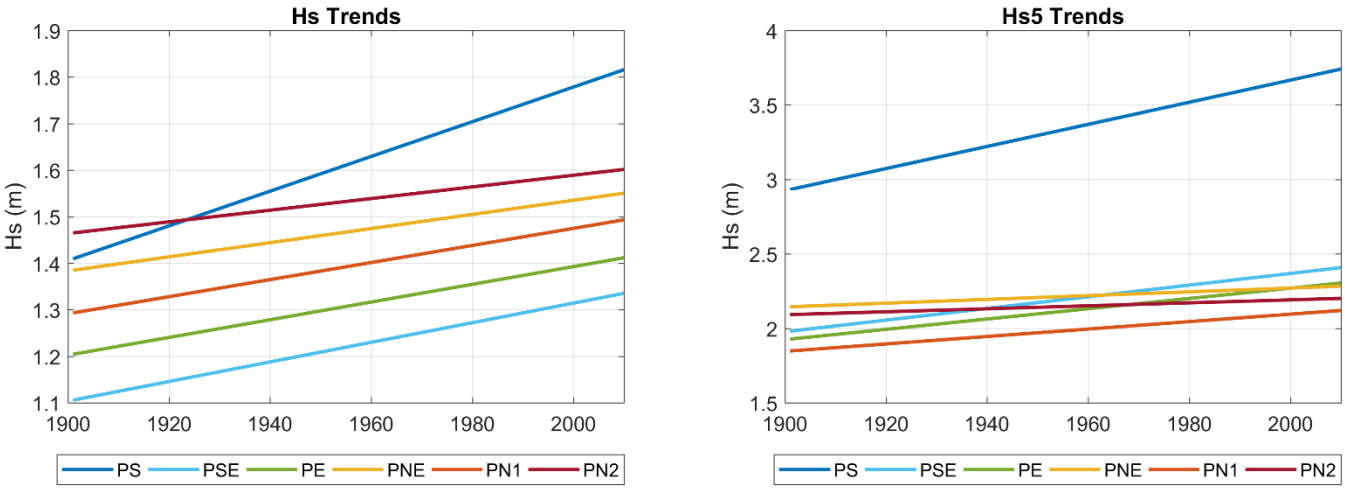

Figure 42 Linear trends, calculated for the entire time series of mean Hs (left) and annual Hs5 (right) values, for each sector of the Brazilian coast.

4.6.1.1. Hs Monthly Trends

In addition to temporal variability, it is important to analyze in which month(s) the waves are changing. If the trend is higher in a summer month (lower wave energy), there might not be enough impact on the coast to justify coastal management actions towards erosion for example, but increasing the ones related with beach safety given the possible increase in rip currents.

From the southern sectors to the northern, the number of significant trends decrease for both Hs and Hs5. For Hs trends, 61 values out of 72 were significant at a 99 % confidence level and 65 for 95 %. On the other hand, for Hs5 trends, 48 values were significant for 99 % confidence level and 51 for 95 % (Table 11). PNE and PN2 were the only sectors to present negative monthly trends, in May for PNE and from June to August in PN2, although these rates were not significant. When comparing Hs and Hs5 trends, PS, PSE and PE showed higher rates for Hs5 in all months.

Out of all sectors, PS presents the highest Hs rates throughout the entire time series for all the months except for Hs5 trends in August. Regarding Hs, the values are the highest for the months

of September and November, except for PN1 that has its highest rate in January. Concerning Hs5 trends, the months with the highest rates vary depending on the sector (Figure 43). PS and PSE share the same monthly behaviour and oscillations of both Hs and Hs5 trends, and the same happens for PE and PNE. The monthly variability is not as well marked for the northern sectors.

Table 11 Hs linear regression trends for each sector of the Brazilian coast per month from 1901 to 2010, including mean (Hs) and extreme (Hs5) wave height values. Significant values for a 99 % confidence level are in bold and for 95 % confidence level are underlined.

Months	Hs / Hs5 Monthly Rates (mm/yr)					
	PS	PSE	PE	PNE	PN1	PN2
Jan	**3.5** / **6.1**	**1.7** / **3.9**	**1.8** / **2.3**	**1.6** / **1.5**	**2.9** / **3.1**	**1.9** / 1.3
Feb	**3.1** / **6.5**	**1.6** / **3.4**	**1.6** / **1.7**	**1.6** / **2.1**	**2.6** / **3.1**	**2.0** / 1.7
Mar	**3.5** / **5.8**	**1.8** / **3.2**	**1.8** / **2.6**	**1.8** / **1.8**	**2.5** / **3.0**	**1.8** / **2.5**
Apr	**3.8** / **8.8**	**2.2** / **5.1**	**1.5** / 2.2	**1.4** / 1.0	**2.7** / **3.4**	**2.1** / **2.6**
May	**3.8** / **7.9**	**2.6** / **4.4**	**1.3** / 1.6	0.4 / -0.8	**2.6** / **3.2**	1.1 / 0.9
Jun	**4.6** / **11.9**	**2.7** / **6.3**	**2.1** / **3.8**	1.1 / 0.7	**1.5** / 1.2	-0.1 / -0.8
Jul	**4.3** / **8.3**	**2.4** / **4.1**	**2.4** / **4.6**	1.2 / 1.9	0.7 / 0.8	-0.7 / -1.0
Aug	**2.8** / 2.6	**1.6** / **2.9**	**2.2** / **3.7**	**1.4** / 1.3	0.5 / 0.7	0.0 / -0.3
Sep	**4.8** / **8.7**	**2.8** / **4.3**	**2.7** / **4.6**	**2.4** / **3.2**	0.4 / 0.5	1.0 / 0.8
Oct	**2.6** / 1.7	**1.2** / 0.9	**1.4** / 0.9	**1.5** / 0.9	**1.2** / **1.5**	**1.5** / 0.8
Nov	**4.9** / **8.6**	**2.8** / **3.8**	**2.3** / **2.9**	**2.3** / **2.3**	**2.0** / **2.4**	**2.3** / **2.6**
Dec	**3.1** / **4.2**	**1.9** / **3.1**	**1.8** / **2.6**	**1.7** / **1.5**	**2.5** / **3.3**	**2.2** / **3.2**

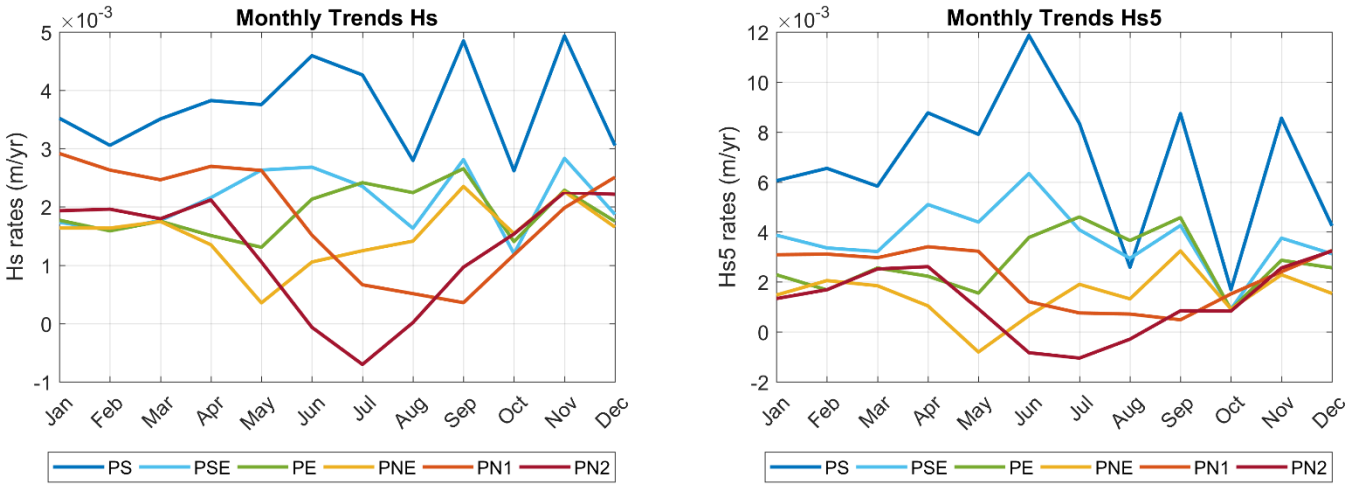

Figure 43 Linear trend slopes, calculated per month for mean values of Hs (left) and monthly Hs5 (right), for each sector of the Brazilian coast.

4.6.1.2. Hs Trends Variability through Time

When analysing a 110-year time series, as it is the case of the present study, the use of a single equation for the entire period might not be the best way to describe the trends. By dividing the time series into different periods, according to different observable trends, it is possible to perceive that the wave climate goes through periods of clear increase and/or decrease in Hs and Hs5. Hence, based on the wave climate variability results, three time periods were chosen to better describe the existing different trends: 1901 to 1939, 1940 to 1969 and 1970 to 2010.

With the graphical representations of the Hs and Hs5 trends variability the differences between each period analysed as well as the similarities between the southern, central and northern ones become clearer. It is also notable the impact the 1940s peak caused in the negative trends observed in most of the sectors during the second period (Figure 44).

From the first period analysed to the last, the amount of significant Hs and Hs5 rates increases and When comparing trends in Hs between the first and third periods, an increase of over 100 % in the southern and central sectors is observed (Table 12).

The first period (1901 – 1939) presents a negative trend of Hs for all sectors, except for PE which shows no trend. However, only PNE, PN1 and PN2 show significant results (99 % confidence level) and the values increase from -0.6 mm/yr in PNE to -3.9 mm/yr in PN2. On the other hand, only PS and PN2 present significant rates of Hs5 for this same period, with a 95 % confidence level. Additionally, PN2 shows the highest Hs trend (-3.9 mm/yr with a 99 % confidence level) and PS the highest Hs5 trend (-8.1 mm/yr with 95 % confidence level) (Table 12).

All Hs rates during the second period (1940 – 1969) are significant for a 99 % confidence level and only PN1 shows a positive trend. Meanwhile, for Hs5 PNE presents a rate of -8.6 mm/yr (95 % confidence interval) and PN1 displays a rate of 7.4 mm/yr (99 % confidence level). The other sectors do not show significant Hs5 trends for this period. Moreover, PN1 is the only sector to show different trends for Hs and Hs5, being positive for the former and negative for the latter. The highest rates for both Hs and Hs5 are found in PNE, -5.9 mm/yr (99 % confidence level) and -8.6 mm/yr (95 % confidence level), respectively (Table 12).

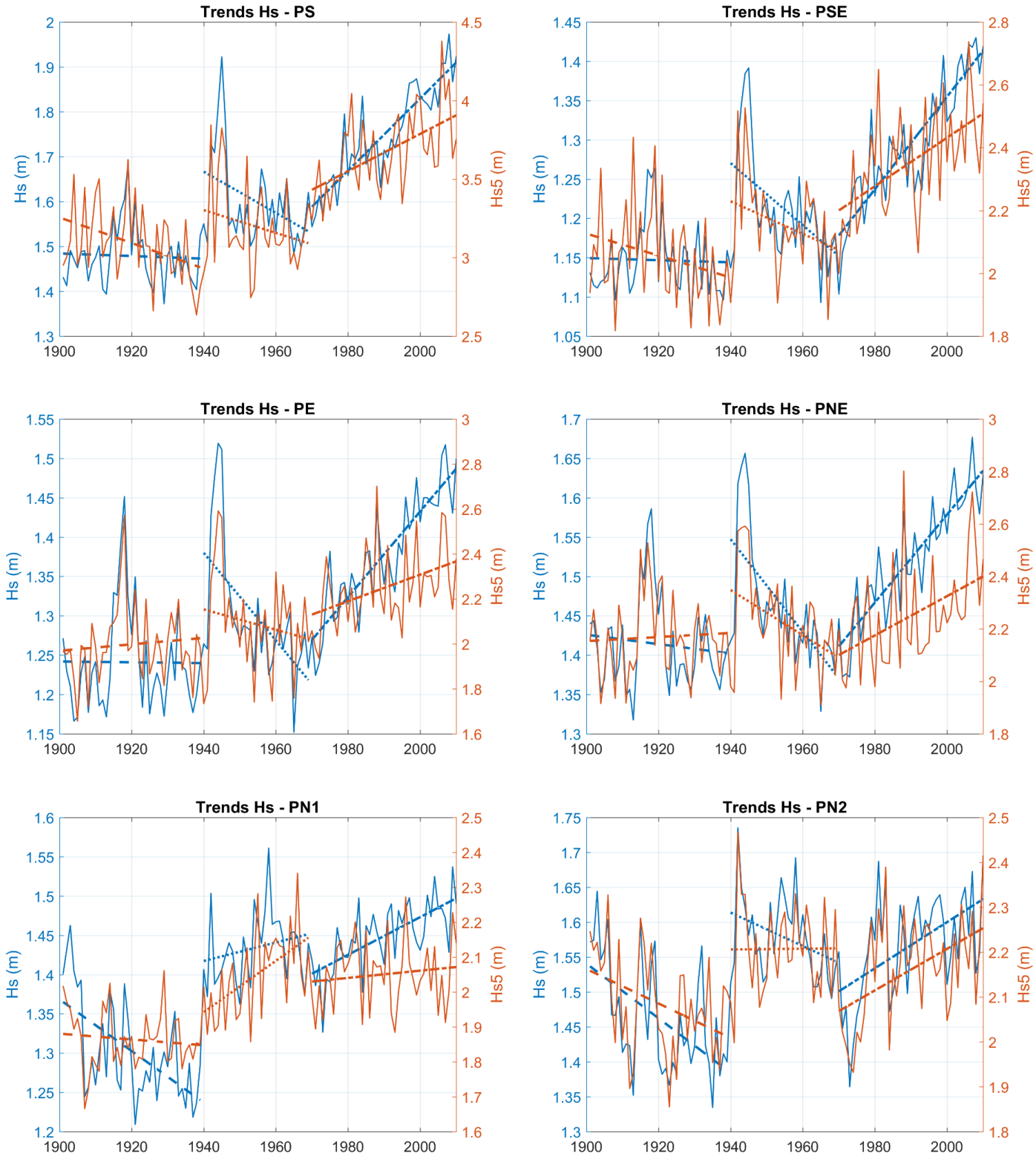

Figure 44 Linear trends, calculated for the periods of 1901 to 1939, 1940 to 1969 and 1970 to 2010 for Hs and Hs5 for each sector of the coast.

Lastly, the third period (1970 to 2010) confirms the strong increasing trend suggested in the wave climate variability results. Except for the Hs5 rate in PN1, all results for this period are significant at a 99 % confidence level and all sectors show higher Hs5 rates than Hs (Table 12). PS shows the highest rates for both Hs and Hs5, 8 mm/yr and 11.9 mm/yr, respectively.

Table 12 Hs and Hs5 trends (mm/yr) based on linear regressions for the periods of 1901 to 1939, 1940 to 1969 and 1970 to 2010 for each sector of the coast. Significant values for a 99 % confidence level are in bold and for 95 % confidence level are underlined.

Sectors	Hs / Hs5 Trends (mm/yr)		
	1901 - 1939	1940 - 1969	1970 - 2010
PS	-0.3 / -8.1	**-4.6** / -7.3	**8.0** / **11.9**
PSE	-0.1 / -3.5	**-4.0** / -5.2	**5.9** / **7.7**
PE	0.0 / 1.4	**-5.6** / -4.5	**5.4** / **5.9**
PNE	**-0.6** / 0.8	**-5.9** / -8.6	**5.6** / **7.5**
PN1	**-3.3** / -0.8	**1.2** / **7.4**	**2.4** / 1.0
PN2	**-3.9** / -3.8	**-2.4** / 0.1	**3.3** / **4.6**

4.6.2. Tp Trends

The same comparison was performed for Tp, given that extreme Tp indicates the swell intensity. By understanding if swells are becoming more intense or not, it is possible to estimate whether a certain region is being more or less affected by open ocean climatic conditions.

Unlike Hs, not all sectors present an increase in Tp. Tp rates increase with decreasing latitudes and only PS and PSE present negative rates, although the values are non-significant. In fact, only PNE, PN1 and PN2 present significant Tp trends (Table 13, Figure 45).

PNE has a positive trend of mean Tp and a negative trend of Tp5, although only mean Tp trend is significant (95 % confidence level) (Table 13, Figure 45).

Even though both PN1 and PN2 start the time series with the lowest values of Tp amongst all sectors (< 8 s), the situation changes towards the last four decades. Moreover, only the north region presents positive and significant trends of Tp5, 0.0054 s/yr in PN1 and 0.0057 s/yr in PN2. PN2 shows the same rate for both Tp and Tp5 (significant for a 99 % confidence level), meaning the region is not under any changes regarding storms intensity or frequency (Table 13, Figure 45).

In general, regardless of being positive or negative, the rates at which Tp5 change from 1901 to 2010 are either the same or higher than mean Tp. The oscillations of annual Tp are greater than the trends and this may be associated with variations in climatic indices, as this depends on the positioning of atmospheric depressions in the Atlantic Ocean. In any case, only the northern regions present effective trends, indicating that Tp is stable all over and increasing in the north which will increase wave power. Moreover, the increase in Tp5 in PN1 and PN2 may indicate a greater wind intensity or a larger fetch area.

Table 13 Tp linear regression trends for each sector of the Brazilian coast for the entire temporal scope of the study, including mean annual (Tp) and extreme (Tp5) peak period values. Significant values for a 99 % confidence level are in bold and for 95 % confidence level are underlined.

Sectors	Mean Tp Trend (s/yr)	Tp5 Trend (s/yr)
PS	-0.0001	-0.0024
PSE	-0.0003	-0.0015
PE	0.0003	-0.0017
PNE	<u>0.0017</u>	-0.0020
PN1	**0.0045**	<u>0.0054</u>
PN2	**0.0057**	**0.0057**

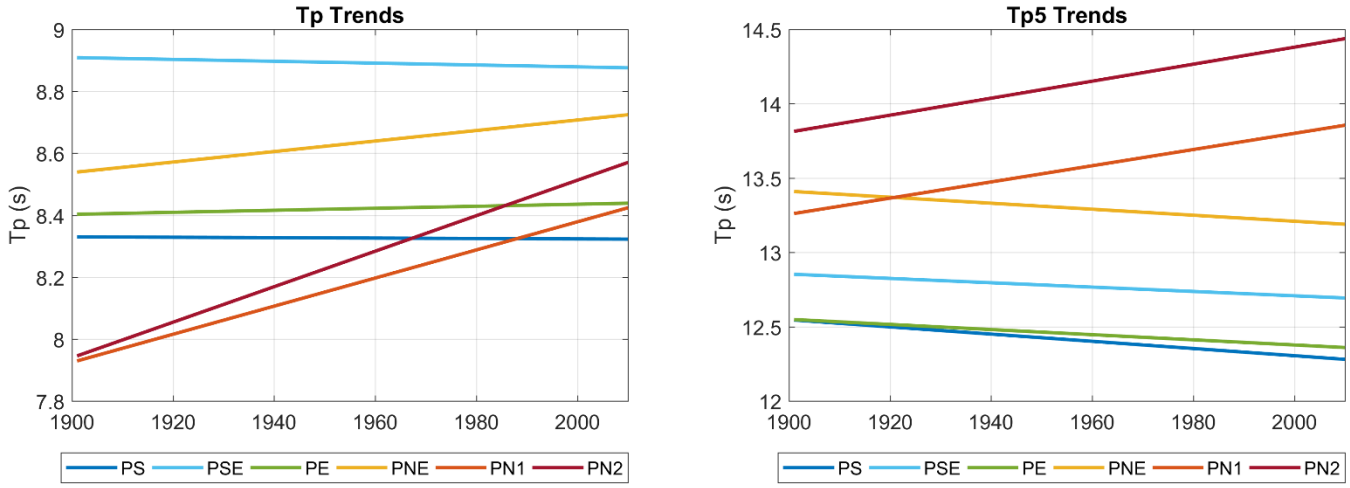

Figure 45 Linear trends, calculated for mean Tp (left) and annual Tp5 (right) values, for each sector of the coast.

4.6.2.1. Tp Monthly Trends

Monthly trends of Tp were also examined. The southern and central sectors display similar monthly variability while the northern sectors behave in a similar manner (Figure 46). The monthly trend plots also show more clearly that Tp5 rates are one order of magnitude larger than Tp rates. While most of the rates in the southern and central sectors remain close to zero or even negative, the values for the northern sectors are higher for most months for both Tp and Tp5.

Unlike the observed for Hs and Hs5 trends, the northern sectors present the largest numbers of significant Tp and Tp5 trends. For Tp trends, 18 rates out of 72 are significant at a 99 % confidence level and 25 for 95 %. On the other hand, for Tp5 trends, 8 values are significant for 99 % confidence level and 13 for 95 % (Table 14).

The highest significant results in PS, PSE and PE indicate a decrease in Tp in October. PNE does not present any significant rates for Tp, and PSE and PE do not show significant results for Tp5 rates (Table 14). Consequently, a comparison between Tp and Tp5 results could only be performed for PN1 and PN2, which showed that all Tp5 rates are higher than Tp. Additionally, the highest Tp rates are observed in October for PN1 and December for PN2 while both sectors display the highest Tp5 rates in October.

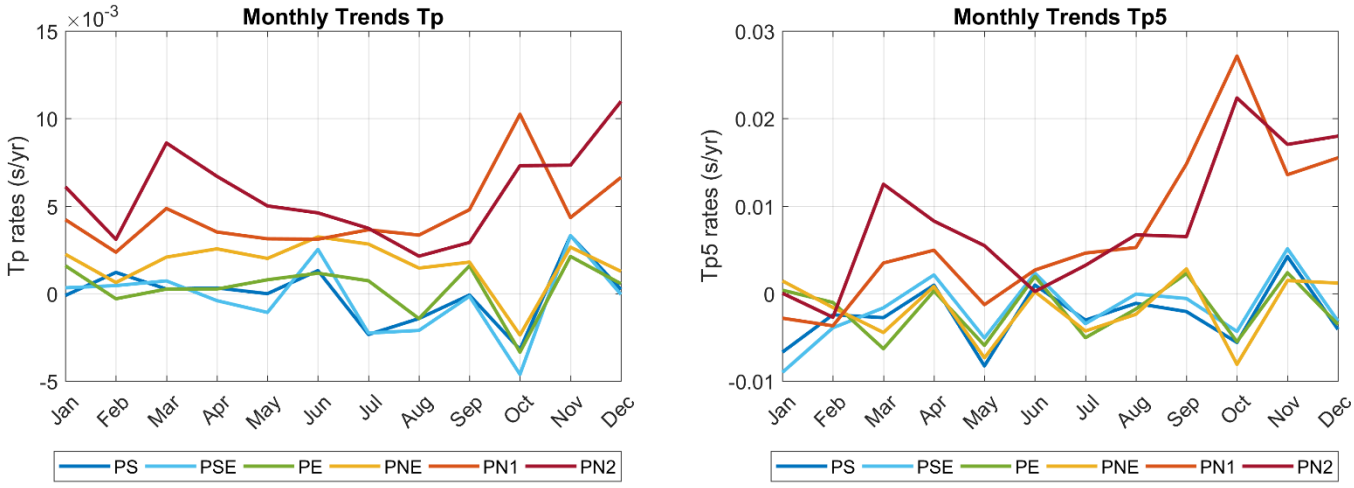

Figure 46 Linear trends, calculated per month for mean values mean Hs (left) and annual Hs5 (right) values, for each sector of the Brazilian coast.

Table 14 Tp linear regression trends for each sector of the Brazilian coast per month from 1901 to 2010, including mean (Tp) and extreme (Tp5) wave height values. Significant values for a 99 % confidence level are in bold and for 95 % confidence level are underlined.

Months	Tp / Tp5 Monthly Trends (s/yr)					
	PS	PSE	PE	PNE	PN1	PN2
Jan	-0.0001 / -0.0067	0.0003 / -0.0090	0.0016 / 0.0004	0.0022 / 0.0014	0.0042 / -0.0028	0.0061 / 0.0000
Feb	0.0012 / -0.0024	0.0005 / -0.0039	-0.0003 / -0.0010	0.0006 / -0.0016	0.0024 / -0.0037	0.0031 / -0.0027
Mar	0.0003 / -0.0028	0.0007 / -0.0016	0.0003 / -00063	0.0021 / -0.0045	0.0049 / 0.0035	**0.0086** / 0.0125
Apr	0.0003 / 0.0010	-0.0004 / 0.0021	0.0003 / 0.0003	0.0026 / 0.0008	0.0035 / 0.0050	**0.0067** / 0.0083
May	0.0000 / **-0.0083**	-0.0011 / -0.0051	0.0008 / -0.0059	0.0020 / -0.0073	**0.0031** / -0.0013	**0.0050** / 0.0055
Jun	0.0013 / 0.0010	0.0025 / 0.0023	0.0012 / 0.0020	0.0032 / 0.0002	**0.0031** / 0.0027	**0.0046** / 0.0002
Jul	-0.0023 / -0.0030	-0.0023 / -0.0034	0.0007 / -0.0050	0.0028 / -0.0043	**0.0036** / **0.0046**	**0.0037** / 0.0032
Aug	-0.0014 / -0.0011	-0.0021 / -0.0001	-0.0014 / -0.0018	0.0015 / -0.0024	**0.0033** / 0.0053	**0.0021** / **0.0067**
Sep	-0.0001 / -0.0021	-0.0002 / -0.0006	0.0016 / 0.0023	0.0018 / 0.0028	**0.0048** / 0.0148	**0.0029** / 0.0065
Oct	-0.0032 / -0.0056	**-0.0046** / -0.0043	-0.0033 / -0.0055	-0.0024 / -0.0081	**0.0102** / **0.0272**	**0.0073** / **0.0224**
Nov	0.0033 / 0.0042	0.0033 / 0.0051	0.0021 / 0.0024	0.0027 / 0.0015	0.0043 / 0.0136	**0.0073** / **0.0170**
Dec	0.0002 / -0.0041	-0.0001 / -0.0031	0.0006 / -0.0035	0.0013 / 0.0012	**0.0066** / **0.0155**	**0.0110** / **0.0180**

4.6.2.2. Tp Trends Variability through Time

Even though the trends are low for Tp, it is possible to observe some significant changes throughout the time series (Figure 47). Most Tp and Tp5 rates are significant and the period with less significant rates is 1970 to 2010 (Table 15).

The first period (1901 – 1939) presents an upward trend of Tp in all sectors, the second period (1940 – 1969) shows a decrease in the southern and central sectors and increase in the northern ones and the third period (1970 – 2010) presents an increase in all sectors, except for PN2 (Figure 47; Table 15).

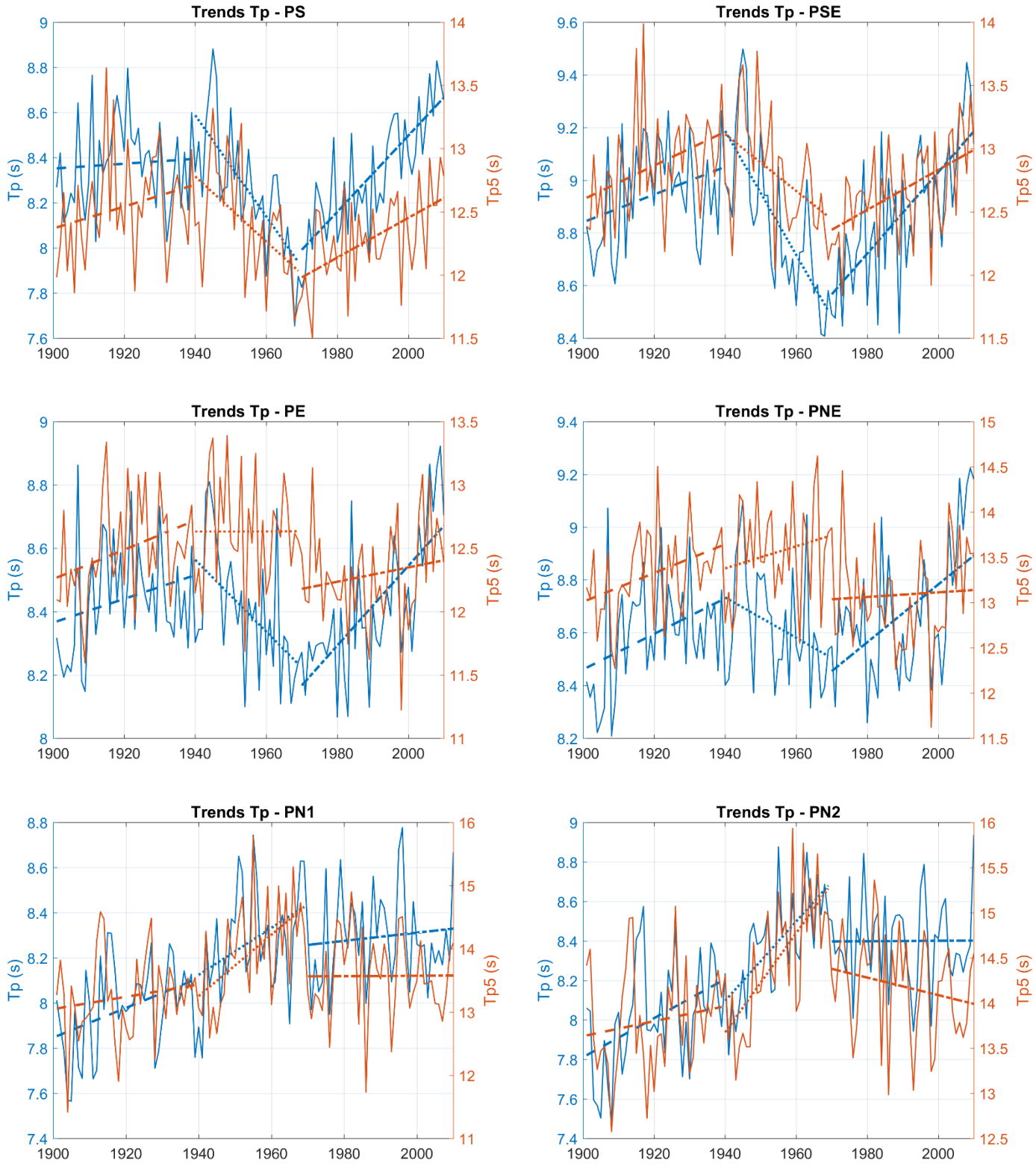

Figure 47 Linear trends, calculated for the periods of 1901 to 1939, 1940 to 1969 and 1970 to 2010 for Tp and Tp5 for each sector of the coast.

Apart from PSE in the second period and PS and PSE in the third period, all Tp rates are lower than Tp5 rates. Additionally, the highest significant rates of Tp are detected in PN2 in the first period, PSE in the second period and PS in the third period. Concerning Tp5, the highest rates are observed in PNE during the first period, PN2 in the second and PS in the final period analyzed (Table 15).

Unlike the rest of the study area, the north region does not present a steep slope during the period of 1970 to 2010. In fact, the rates are nearly zero, which could indicate that Tp has been stable in the last decades of the time series or that the model is more stable for this period in these regions.

The overall trend analysis (Section 4.6.2) showed Tp increase in the northern regions but when divided by periods here, the last period presents no trend or a decrease in the north and increase in the south. Thus, it seems that Tp in the northern regions increased until 1969 and then stabilized while it was stable or decreasing in the southern and central regions until 1969 and then started to rise. Nevertheless, this states how important it is to split the periods of analysis instead of analyzing the entire time series at once.

Table 15 Tp and Tp5 trends (s/yr) based on linear regressions for the periods of 1901 to 1939, 1940 to 1969 and 1970 to 2010 for each sector of the coast. Significant values for a 99 % confidence level are in bold and for values 95 % confidence level are underlined.

	Tp / Tp5 Trends (s/yr)		
Sectors	1901 - 1939	1940 - 1969	1970 - 2010
PS	0.001 / 0.009	**-0.022** / **-0.026**	**0.017** / **0.016**
PSE	**0.005** / 0.013	**-0.024** / -0.022	**0.015** / **0.016**
PE	**0.004** / 0.012	**-0.011** / 0.000	**0.013** / 0.006
PNE	**0.007** / 0.016	**-0.008** / 0.012	**0.011** / 0.003
PN1	**0.007** / 0.010	**0.010** / **0.049**	**0.002** / 0.000
PN2	**0.010** / 0.008	**0.020** / **0.055**	0.000 / **-0.010**

4.7. Wavelet Transform Analysis

The wavelet transform analysis is a different way of representing a time series based on existing periodicity within the dataset.

Given the warm patches surrounded by the 95 % confidence interval white lines, it can be assumed that both ONI and AMO displayed significant events from the 1930s to the 1950s period coinciding the 1940s peaks observed in the wave climate of Brazil (Figure 48).

Even though the Hs wavelets do not show significant results, except for PE, strong and large warm patches can be observed in most of the sectors between the band of 8 – 16 yr-period (Figure 49). These results agree with the timing of the 1940s peak as well as the observations made about the ONI and AMO wavelets indicating that these climate modes might have played a role in such peak.

Additionally, the Tp wavelets do not show as high and significant results as the Hs wavelets. A warm patch can be observed in PS, PSE, PE and PNE in the 1940s in the band of 4 – 8 yr-period. Both PN1 and PN2 present no warm patches as well as no significant Pearson correlations with neither ONI nor AMO (Figure 50). These results agree well with the Tp decadal variability analysis since the north region did not present a peak in the 1940s and the peaks observed in the other sectors were not as strong as the Hs peaks.

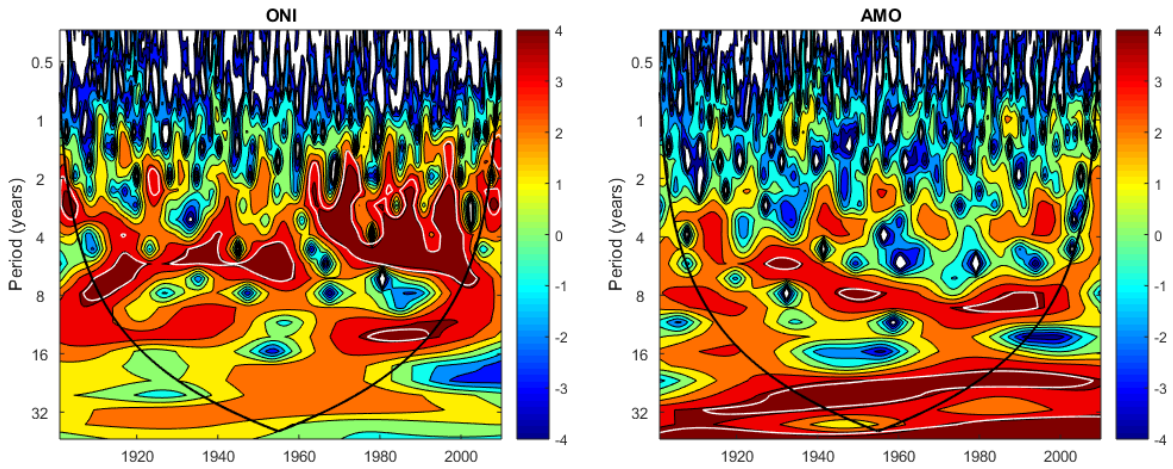

Figure 48 Wavelet transform of ONI (left) and AMO (right). The cone of influence is delimited by the thick black line. The white lines indicate the 95 % confidence interval of the results, or 5 % significance level. Warmer colors represent a higher significance.

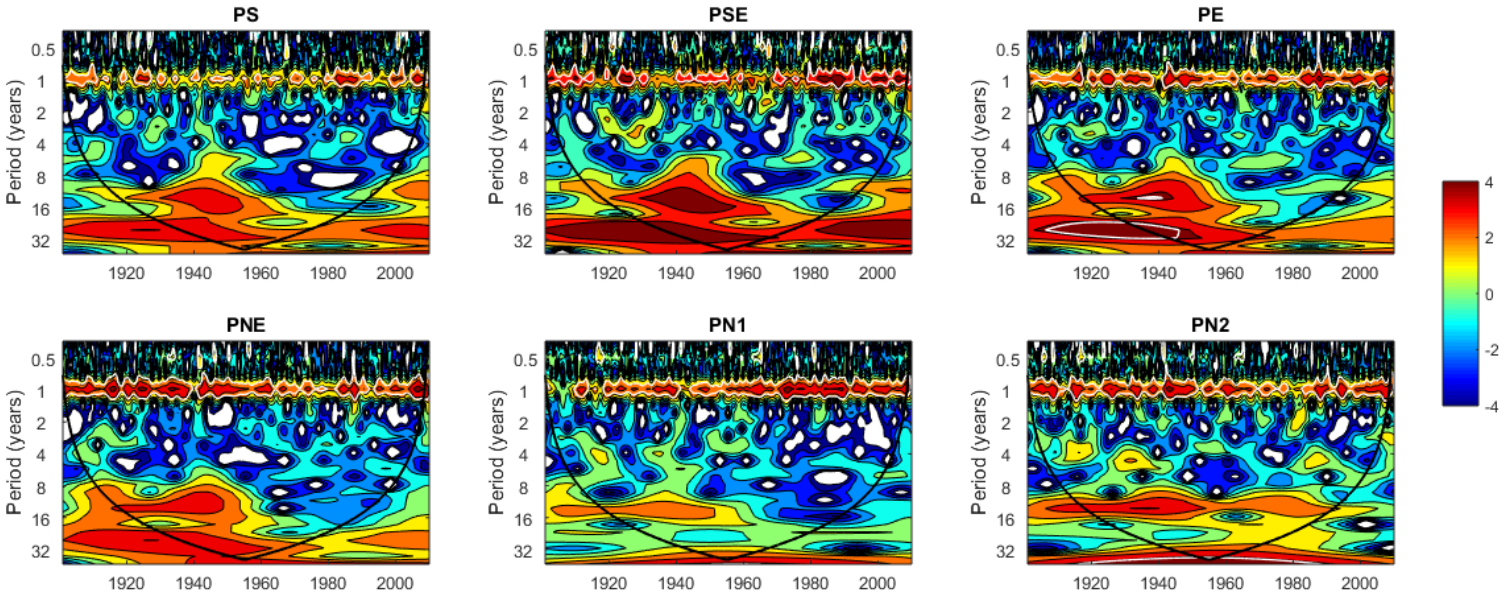

Figure 49 Hs wavelet transform for each sector of the Brazilian coast. The cone of influence is delimited by the thick black line. The white lines indicate the 95 % confidence interval of the results, or 5 % significance level. Warmer colors represent a higher significance.

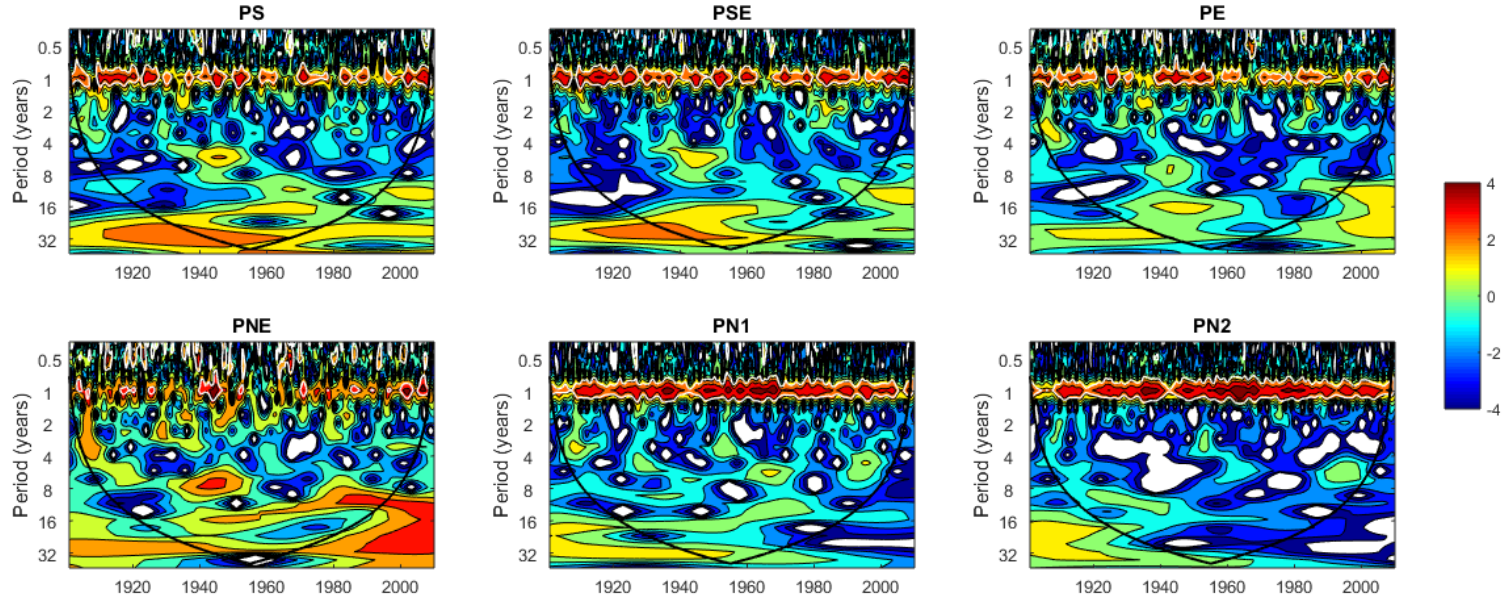

Figure 50 Tp wavelet transform for each sector of the Brazilian coast. The cone of influence is delimited by the thick black line. The white lines indicate the 95 % confidence interval of the results, or 5 % significance level. Warmer colors represent a higher significance.

5. Discussion

The wave climate along the coast of Brazil presents both spatial and temporal variability, as well as trends and relationships between variables. Those will be analyzed in this chapter jointly with their main drivers which are meteorological forcing and climate indices.

5.1. Data Validation

ERA-20C was validated for the south and southeast coasts of Brazil. The Pearson correlation coefficients indicate that Hs is better represented in the south than in the southeast region and the opposite was true for Tp (Table 4). The modelled values are underestimated for Hs and Tp.

Overall, the validation for the Cabo Frio location was not good and this is mostly due to the different positions of the buoy and the ERA-20C point used. However, the variability presented was the same between both datasets and the correlation was significant indicating that despite differences between wave parameters, ERA-20C represents the region well in terms of variability.

Although the validation of ERA-20C in PSE showed higher correlation for Tp, the better representation of Hs usually identified by hindcast models could be due to the resolution of wind data assimilated in these models. Consequently, the models might not reproduce well the bimodality conditions of ocean waves observed in Tp dividing the wave climate into sea-state and swell (Oliveira *et al*., 2019).

Thus far, ERA-20C had not been validated along the coast of Brazil but other models have been. For example, WWIII has been validated by several studies in the study area. Alves *et al*. (2009) compared it to radar and buoys located along the coast of Santa Catarina, Pereira and Klumb-Oliveira (2015) validated it against observed data from the Cabo Frio buoy, Oliveira *et al*. (2019) validated it to three different locations along Santa Catarina and Rio Grande do Sul and Cecilio and Dillenburg (2020) compared the model to two buoys located in the Southern Brazilian Shelf, Tramandaí and Rio Grande. All the studies mentioned detected an overestimation by the model, contrarily to what has been observed in this study.

The overestimation of WWIII was not detected by Silva *et al*. (2015) when validating the Downscaled Ocean Waves model in Santa Catarina. Instead, the authors observed an underestimation of Tp. They associated this with the low spatial and temporal resolution of the wind data assimilated by the model which resulted in the poorly representation of extreme events such as extra tropical cyclones.

Finally, it should be considered that the two buoys validated here present different settings and this as well can lead to different results. The Cabo Frio buoy is closer to the shore while the Rio Grande buoy is near the continental shelf break. Alves *et al*. (2009) and Cecilio and Dillenburg (2020) observed that coastal validation shows a deterioration of Hs results when compared to offshore, with an overestimation of Hs values. The opposite was stated by both studies for Tp with the correlation coefficients being higher for coastal validation than that for offshore. Their findings agree with what was found for ERA-20C. Differences in behaviors of Hs and Tp in models could be due to the spatial resolution of the model and to the difference in location between the extracted points and the used buoys (namely for Cabo Frio – southeast coast).

5.2. Wave Climate Spatial Variability

The wave climate characterization was described for each sector of the Brazilian coast concerning Hs, Tp and Dir. This was achieved by performing simple statistics calculation, temporal variability, and trend analyses which were executed for both mean and extreme wave conditions.

Overall, the minimum values indicate that the model is not successful at describing the state of calm sea as there is no record under 0.4 m. When comparing the southern sectors with the northern ones, it is possible to observe that the wave climate in PN1 and PN2 is relatively constant (low standard deviation and variance) while the southern sectors show the most heterogeneous wave climate, with Hs ranges of 7.7 m and 4.0 m, for PS and PSE, respectively.

Pianca *et al*. (2010) also observed a lower variability of Hs for the North region, although they reached the same conclusion for Tp, which was not identified in the present study. In fact, PN2

displayed the highest standard deviation and variance for Tp, denoting different wave formation regimes and fetches.

The lowest range of Tp in PS could indicate similar wave generation conditions and similar fetch conditions. Moreover, the bimodality of Tp found in some of the sectors (PSE, PE, PN1 and PN2), indicates two well-established wave patterns divided into sea-state and swell bands responsible for wave generation off these sectors. According to Tessler and Goya (2005) these wave patterns are due to the differences in summer and winter climate in the regions of PSE and PE.

To summarize, for all wave parameters analyzed, three behavioral groups could be established and a conclusion made that the closer the sectors are from each other, the higher the correlation coefficient is between them. Ergo, the overall wave conditions off Brazil are split into three dominant areas (South – PS and PSE; Central – PE and PNE; North – PN1 and PN2). The northern sectors are the most distinct ones regarding Tp and the southern sectors are the most distinct regarding Dir. Moreover, these groups were also detected regarding the monthly, interannual and decadal variabilities of Hs and Tp.

Overall, a strong seasonality of waves in each sector of the coast was observed and, in some cases, a bimodal pattern was detected which could be a result of exposure to two distinct wave generation areas or climatic regions. The most energetic waves occurred during the Austral winter, with exception of the north region, which showed its most energetic waves in the Austral summer.

The differences in wave climate along the coast of Brazil are due to the fact that the southern sectors are under the influence of polar front systems and seasonal oscillations of the intensity and position of the SASA. The same can be concluded in the central sectors but for a smaller extent than the southern ones. Meanwhile the wave climate of the northern region is influenced mainly by the ITCZ (Tessler and Goya, 2005).

The variation in monthly values showed a slight delay of the pattern regarding the north region of Brazil. This is because when moving from the south until the northeast region the influence of polar fronts on the wave climate decreases, becoming practically null in the north region.

Thus, the lack of seasonality in the most equatorial regions of Brazil (PNE, PN1 and PN2) is probably due to the climate being driven mainly by the ITCZ. As the ITCZ moves southward in the Austral

summer, waves from the Northern Hemisphere can reach the north coast of Brazil as a result of the northeasterly trade winds (Castro *et al.*, 2006). This explains the unique seasonality patterns in this region. On the other hand, cold fronts are more frequent during winter, as described by Dominguez (2013), and could explain the most energetic waves during Austral winter in the southern regions. In contrast, the northern region presents its extreme wave conditions driven by Northern Hemisphere conditions and generation (Tessler and Goya, 2005; Beserra *et al.*, 2007).

5.3. Hs vs Tp Relationship

The relationship between Hs and Tp (modal) was examined and exponential fits were computed for specific cases and wave regimes in each sector. Dir and Tp were the variables that varied the most between groups of the same sector. This indicates that for each sector there are different dominant directions, each of them having different wave formation and generation mechanisms and different fetch. It was verified for PS, PSE, PE and PNE that waves from E to SW clearly represent the dominant swell regime with waves of greater Tp. On the other hand, waves from NW to E are composed of lower Tp. For PN1 and PN2 the higher Tp waves come from N.

The forecasts presented were for the modal Tp and it was not possible to include the observed variability, namely for the largest Tp, which seemed to happen for waves mainly between 1 m and 3 m high. Even though the best fit was the exponential curve, the correlation coefficients were generally significant but not in all sectors. The Hs vs Tp relationships in PS, PSE and PNE were better represented than in the other sectors. Perhaps the lower significance of the results in PE, PN1 and PN2 are related to the Tp bimodality present in these sectors. However, while PE showed significant correlation for Tp < 14 s, PN1 and PN2 displayed significant correlations only for Tp higher than 10 s and 8.5 s, respectively. Overall, these forecasts can be helpful as a first estimate of Tp based on Hs (or vice-versa) for the analyzed regions.

A similar study was performed in Norway, concluding that a consistent curve representing the Hs vs Tp relationship can easily be established when the joint distribution of both variables is known (Haver, 1985). Unlike what was observed in the northern sectors of the present study, Haver (1985) observed the fit was good for Tp < 12 s and questionable for higher Tp. Moreover, Ferreira

and Guedes Soares (2002) constructed a regression curve for Hs and Tp and assessed the goodness of the fit with the Kolmogorov-Smirnov test in Portugal. Nevertheless, the authors concluded that although the fit was reasonable enough, the lack of symmetry in the Hs dispersion indicated a poor fit of the model.

However, further analysis should be undertaken in order to fully understand how the relationship between these variables change with different meteorological forces for each region. Hs vs Tp ratios can be analyzed for different wave directions and modal Tp at the same time, in other words, dividing the Hs vs Tp ratios in each region according to the wave generating mechanism.

5.4. Wave Climate Temporal Variability

5.4.1. Associations to Climate Indices

5.4.1.1. Oceanic Niño Index – ONI

The highest correlation coefficient regarding the ONI/Hs analysis was noted in PE and the highest ONI/Tp correlation value was observed in PS with both results indicating negative correlations.

The first result could be explained by the intensification of the SASA and the colder temperatures in the Atlantic Ocean which typically occur during El Niño years, leading to a decrease in wind speed and energy being transferred to the ocean in the form of waves, ultimately leading to a decrease of Hs (Mentaschi *et al.*, 2017). The reason for the highest negative correlation in PE could be the fact that this sector is the one most influenced by SASA as described in the literature review.

Furthermore, the highest correlation for ONI/Tp in PS could be related to the decreased occurrences of cold fronts as a result of increased subtropical jets, which would then lead to a decreased amount of storms being generated in the Southern Ocean and less swell waves reaching the coast of Brazil (Pereira and Klumb-Oliveira, 2015). As PS is the sector most influenced by cold fronts, the highest negative ONI/Tp correlation indicates the decrease in Tp during El Niño, agreeing with the literature.

However, the lack of significant correlation between wave parameters and ONI in the PN2 are in dispute with the results found by Araújo Junior *et al*. (2014). The authors observed positive relationship between wind speeds in Ceará and ENSO, indicating an increase in energy during El Niño while the present study did not find significant ONI/Hs relationship in PN2 where Ceará is inserted.

5.4.1.2. Tropical South Atlantic Index – TSA

The highest correlations for TSA/Hs were observed in PS and PSE, while PE and PNE presented the highest correlation coefficients for TSA/Tp. All these associations were positively correlated indicating an increase in the wave parameters (Hs and Tp) when there is a decrease in surface pressure associated with an increase in SST in the South Atlantic. Moreover, the significant negative correlation observed in PN2 for TSA/Hs indicates a decrease of wave height as a result of the intensification of easterly disturbances during +TSA.

The correlations found between TSA and Hs can be explained by the fact that wind waves respond directly to wind regime. Hence during +TSA, with the increased SE trade winds in SAO, the increased Hs in the southern and central sectors and decreased Hs in the northern ones agree well with the literature (Hounsou-Gbo *et al*., 2019; Utida *et al*., 2019). Moreover, given the possible interaction between climate modes and the correlation analysis results, Hs response might be intensified when different phases of TSA and ONI occur at the same time.

5.4.1.3. Atlantic Multidecadal Oscillation – AMO

The highest correlation coefficients for AMO/Hs were found in PSE, PE, PNE and PN2, two of which are the most exposed to the North Atlantic. All significant correlations representing AMO/Hs indicate a positive relationship. Moreover, with the exception of the north region, all other sectors presented similar positive correlation coefficients for AMO/Tp. These results agree well with Reguero *et al*. (2019), which stated that the AMO index is correlated with larger wave power in the Southern Hemisphere.

The correlation values were significant and indicated an increase (decrease) of wave parameters during positive (negative) phases of AMO. In addition to the 1940s peak (Section 5.4.2) and its possible association to AMO, there is a clear trend of decrease in AMO from 1950 to 1970 (Figure 6), which is in agreement with the decrease in most wave parameters for those dates. Additionally, there has been an increase in AMO since the early 1970s until 2005 that can be associated with the increasing trend of Hs and Tp (Section 5.5).

5.4.1.4. Southern Annular Mode – SAM

A +SAM is associated with an increase in Hs in PS, PSE, PE and PNE given the significant positive correlation results, which decrease towards the Equator. This result indicates that SAM influences the southern sector the most. Additionally, this result could be linked to the storms generated in the Southern Ocean, which result in higher Hs and are directly linked to SAM (Hemer *et al*., 2010).

In addition, a study by Hemer *et al*. (2010) focused on the Southern Ocean showed that SAM is the main climate mode influencing Hs variability and trends in the Southern Hemisphere by shifting the location and intensification of storms. However, out of all the sections of the Southern Ocean, the South Atlantic was the one with the least variability indicating less influence from SAM. The authors attributed this result to the shadowing effect of the South American continent over the local wave climate, which reduces the swell propagation from the Southern Ocean storms. Nevertheless, the present study indicates that SAM has some influence over Hs in the SAO. This relationship will be further discussed in the Section 5.5.

5.4.1.5. Atlantic Meridional Mode – AMM

While SAM only correlated with the southern and central sectors, AMM only correlated positively with the north region, indicating an increase in Hs in PN2 and Tp in both PN1 and PN2 during +AMM. Given the AMM relationship to storms in the Northern Hemisphere (Vimont and Kossin, 2007), and the Dir percentages calculated for the north region indicating the amount of swell and storm waves coming from N and NE, the correlation analysis agrees well with the literature. When

put together, these results represent the relationship between storms generated in the Northern Hemisphere and the wave climate of northern Brazil. This relationship will also be further discussed in the Section 5.5.

5.4.1. 1910s Peak

The first peak of the time series is clearer for mean Hs in PS, PSE, PE and PNE while PN1 and PN2 showed peaks of mean Tp during the same time. Regarding extreme values, all sectors presented a peak of Tp5 between 1910s and 1920s, and PE and PNE were the only sectors to present peaks of Hs5. Thus, this could be linked to TSA since PE and PNE presented the highest correlation coefficients between TSA/Hs. However, this could not be tested in the present study given the shorter TSA time series available (starting in 1948).

Moreover, NOAA (2019) determined the occurrence of two strong La Niña events in the 1910s decade which could have aided the peak of Hs and Tp in most of the coast of Brazil. Such events happened right at the start of the decade (1910-11) and towards the end (1917-18). In fact, the latter was stated by Poli *et al*. (2016) as one of the top three strongest La Niña events from 1901 to 2010. The previously presented ONI wavelet confirmed this intense ENSO activity in the 1910s with a significant warm patch with a period of 5 to 8 years right before the 1920s. However, none of the wavelets for Hs or Tp showed a similar result suggesting that ENSO might not be the responsible for this peak.

The literature has also highlighted the period between 1910s and 1920s. Baines and Folland (2007) identified peaks of certain parameters during this time such as south Greenland coastal temperatures, SST over the south Caribbean Sea and intense hurricane activity over the North Atlantic Ocean.

Regarding wave behaviour, when performing a change point analysis focused on the variance variability of Hs from 1900 to 2005, Killick *et al*. (2010) observed a maximum variance shortly before 1920 in the Gulf of Mexico, which could be compared to the north region of the present study. The authors also noticed an upward trend of storm peak Hs before 1920.

However, the 1910s peaks may not be real because the model loses quality at the beginning of the century due to the lack of measured and validated wind field data. Consequently, wave hindcasts' accuracy has been known to degrade prior to mid-1940s due to less satisfactory meteorological data (Seymour *et al*., 1984; Poli *et al*., 2016). According to Killick *et al*. (2010), the questioning behind the veracity of pre-1950 data is because of observations being performed mainly through land-crossing methods and occasional ship reports.

5.4.2. 1940s Peak

Several studies have reported the decade of 1940s as an anomalous period around the globe. A peak of both SLP and SST was identified in the SAO during the 1940s (Venegas *et al*., 1998; Baines and Folland, 2007). Global and Atlantic warming was registered (Kerr, 2000) along with several heat waves in the Himalayan Chain during the same time (Zampieri *et al*., 2016).

The wave climate analyzed showed peaks of Hs and Tp in PS, PSE, PE and PNE in the 1940s. Extreme values displayed the same pattern, although the peak was not so abrupt for Tp5. In fact, the north region showed a different behaviour regarding this period. In the early 1940s there was an intense increase in Hs, but unlike the other regions of Brazil the values of Hs remained higher throughout the next three decades in this region which is why the 1940s peak was not so clear for the northern sectors. This could be associated with the differences or changes in the model prediction.

As a context, it is important to point out that an El Niño event from 1940 to 1942 followed by a La Niña event in 1943 characterized the 1940s decade (NOAA, 2019). This decade was inserted in a positive AMO phase, indicating that SST was higher than usual in the North Atlantic Ocean.

Given that the present study showed negative correlations between PS, PSE, PE and PNE and ONI, a decrease in wave parameters during El Niño phases is implied in these sectors. The opposite would happen during La Niña phases. Depending on the intensity of the 1943 La Niña, the event could have contributed to the Hs and Tp peaks observed in the aforementioned sectors.

In addition, the correlation between the sectors that showed peaks in the 1940s and AMO was positive. This would indicate an increase in Hs and Tp during +AMO, which was the case for the

1940s decade. Even though Baines and Folland (2007) stated that AMO alone cannot explain warming in the North Atlantic, it could contribute to that warming and the same could be said for the Hs and Tp peaks observed in this study.

In other words, the combination of a La Niña event and +AMO could explain the 1940s Hs and Tp peaks observed in most of the study area. These events could also explain the lack of a peak in the north region given the positive correlation with ONI and the negative correlation with AMO observed in PN1 and PN2, respectively.

Finally, based on the climatic conditions described in the literature for the 1940s, the wave climate variability analysis, the Pearson correlation analysis and the wavelet transforms, it could be assumed that the Hs and Tp peaks observed in the 1940s are associated with both ONI and AMO and their respective impacts on the wave climate of Brazil.

5.5. Recent Trends (1970s – 2010)

Variations in Hs trends throughout the 20th century have been observed by several studies and Gulev and Grigorieva (2004) cut the time series in 1950 in order to have a better understanding of global changes in the recent decades. Moreover, the increase in Hs during the second half of the 20th century observed in the present study was also noted in the North Atlantic (Dodet *et al.*, 2010; Wang *et al.*, 2012) and a shift from negative to positive Hs trend in the 1990s was detected in Italy (Martucci *et al.*, 2010).

Bertin *et al.* (2013) proposed several reasons for the increase in Hs in the North Atlantic Ocean throughout the 20th century. Among them are interannual and inter-decadal variabilities, long-term trends driven by global change, storm activities and greenhouse gas concentrations. Besides, several studies discuss the possibility of the upward trend from mid-1960s and 1970s being associated with the improvement of aerial observations and the beginning of the satellite era around the same period (Killick *et al.*, 2010; Dee *et al.*, 2014). Hence, this discussion will focus on the significant trend results for the period of 1970 to 2010, given the higher values and the fact that these are more reliable and correct than rates for the start (and mid) of the 20th century.

The present study confirmed positive Hs trends for the overall temporal scope in all sectors examined with different rates depending on latitude. The southern sectors showed higher rates than the sector closer to the Equator (PN1), while the ones most exposed to the North Atlantic and ITCZ (PNE and PN2) presented the lowest rates. This latitudinal variation of Hs rates was also shown in other locations, as explained by Dodet *et al*. (2010) who identified a decrease in the positive Hs trend from the northern latitudes towards the Equator in the North Atlantic Ocean. This result was corroborated by Wang *et al*. (2012) with the highest positive rates in the NE Atlantic Ocean and decreases in Hs in mid-latitudes. This type of latitudinal trend variation could be due to different proximities to storm paths or differences in wave generation areas (Masselink and Gehrels, 2014), as is the case for the study area.

Even though negative Hs trends have been detected in parts of the world, such as in the Western Tropical Pacific, the Eastern and South Indian Ocean, the Tasman Sea (Gulev and Grigorieva, 2004), the China Sea (Wu *et al*., 2014) and along the Italian coast (Martucci *et al*., 2010), positive trends represent the majority of the globe, including the North Pacific (Ruggiero *et al*., 2010), the North Atlantic (Dodet *et al*., 2010) and the Western Subtropical South Atlantic (Gulev and Grigorieva, 2004). Although, when compared to other regions, Hs trends are two to seven times smaller in the Southwest Atlantic Ocean (Table 16) and the Indian and Pacific sectors of the Southern Ocean have typically higher rates than the Atlantic sector (Hemer *et al*., 2010).

Table 16 Hs rates (m/yr; positive means increase) observed across the globe.

Study	Study area	Period studied	Hs rates (m/yr)
Present study	Southern Brazil	1970 - 2010	0.007
	Central Brazil		0.006
	Northern Brazil		0.003
Bacon and Carter (1991)	N Atlantic	1950 - 1988	0.02
Wang and Swail (2002)	NE Atlantic	1958 - 1997	0.005 - 0.025
Gulev and Grigorieva (2004)	NE Pacific	1950 - 2002	0.009
	N Atlantic		0.014
	SW Atlantic		0.007
Ruggiero *et al*. (2010)	NE Pacific	1970 - 2010	0.015
Harley *et al*. (2010)	Eastern Australia	1958 - 2002	0.003
Reguero *et al*. (2013)	S Atlantic	1948 - 2012	0.003
	Southern Brazil		0.006

5.5.1. Association to Climate Modes

A few studies have associated increasing Hs to climate modes. Bacon and Carter (1991), Gulev and Grigorieva (2004), Dodet *et al*. (2010) and Bertin *et al*. (2013) identified a correlation between positive Hs trends in the North Atlantic and the NAO. Reguero *et al*. (2013) associated the increase observed in Latin America with ENSO, which alongside with the North Pacific Oscillation explained long-term changes in wave height in the North Pacific Ocean (Gulev and Grigorieva, 2004).

However, several studies have detected a significant trend toward the positive phase of SAM since mid-1960s, with the greatest changes since late 1970s. This is associated with a southward shift of the Southern Ocean storm belt, which leads to stronger westerly winds around 50° S and 70° S (Marshall, 2003; Marshall *et al*., 2018). Consequently, there is an increase in storminess as a result of more tropical cyclones in the SAO driving larger wave heights in the southern latitudes (Dragani *et al*., 2010; Hemer *et al*., 2010).

As previously presented, the correlation analysis indicated a significantly positive relationship between SAM and Hs in the southern and central sectors with the correlation coefficients decreasing from higher to lower latitudes. Also, the trend analysis suggested higher Hs trends in these regions than in the northern region with the highest rates in the southern sectors. These results coincided with the period in which SAM has been trending toward its positive phase. Thus, the positive Hs trends detected in the southern and central sectors could be related to the positive trend SAM has been showing since mid-1960s. As a way to confirm these results, the trends of SAM were calculated for the entire time series available for this index and for the 1970-2010 period. Both rates were significant at a 95 % confidence level and a higher rate was identified in the 1970-2010 period (Figure 51; left).

In contrast, while the Hs trends in the southern and central sectors can be related to SAM, the positive Hs trends observed in the north region could be related with increased storm activity as described in the literature (Goldenberg *et al*., 2001; Bender *et al*., 2010). However, according to Goldenberg *et al*. (2001) the increase in hurricane activity in the Atlantic Ocean only started in the mid-1990s, with low activity from 1971 to 1994. When comparing the AMM trends for the whole time series (1948-2010) and for the 1970-2010 period, the shift to a positive phase in the latter is

clear (Figure 51; right). Thus, the linear regression models of AMM confirm the shift in the ocean-atmosphere variability of the tropical Atlantic Ocean towards a positive phase, which favors the development of tropical storms.

Yet, if AMM is the reason behind the Hs positive trends in the north region of Brazil, a significant Hs5 trend would be visible in both northern sectors, which is not the case. PN2 stands out given its significant Hs5 trend for 1970-2010 and significant AMM/Hs correlation (not observed in PN1). In other words, AMM could partially explain the trends in the northern sectors (only for PN2) but there are probably other complementary reasons.

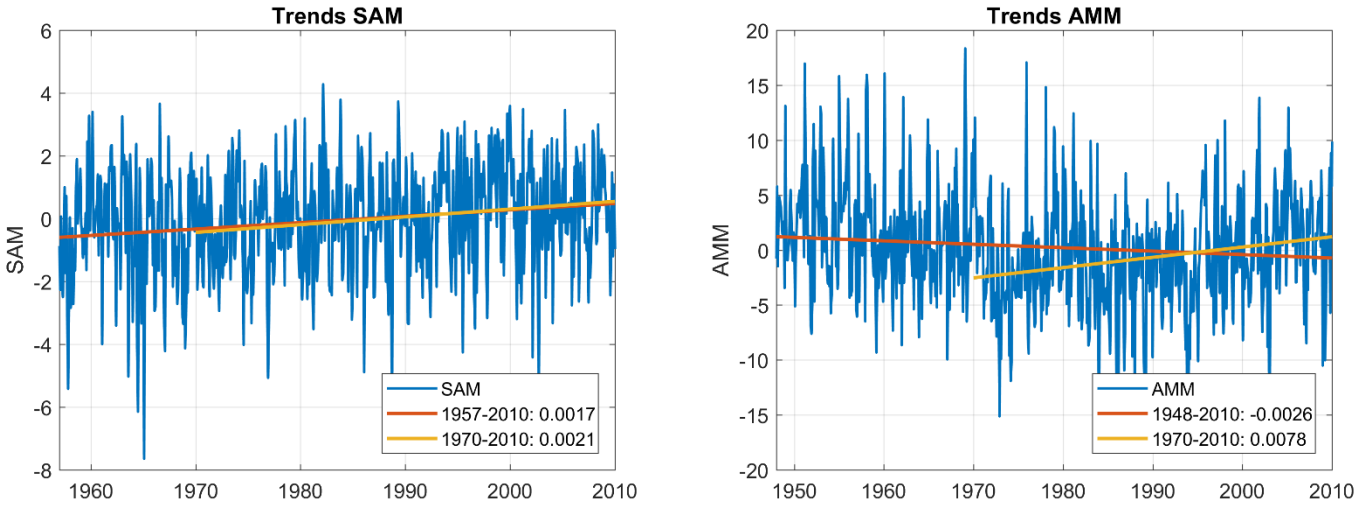

Figure 51 Left: SAM time series and linear regression models, with respective significant (95 % confidence level) rates per month, for the periods of 1957 to 2010 and 1970 to 2010. Right: AMM time series and linear regression models, with respective significant (95 % confidence level) rates per month, for the periods of 1948 to 2010 and 1970 to 2010.

5.5.2. Extreme Waves Trends

Another indication of increasing storminess are the extreme Hs trends, which generally presented a higher mean rate both in the present study and in the literature.

Just as observed for Hs trends analysis, the rates for NE Atlantic and NE Pacific Oceans are larger than the ones shown for the SAO, including the values found in this study (Table 17). When analyzing the Hs5 trends, the southern region shows an increasing rate that doubles the one observed for the Hs trend. When the Hs5 rate is higher than Hs one, it indicates that not only

waves are getting higher but that mostly storm waves are increasing, which could reflect more intense winds responsible for generating storms in the Atlantic Ocean as well as the increase in storm wave power hitting the coast.

The ongoing global trend of increased storminess reported by several studies (Wang and Swail, 2001; Mentaschi *et al*., 2017), would expose the Brazilian southeastern coast to increasing Hs by approximately 1 cm/yr (Young and Ribal, 2019). This study found that Hs5 increase can reach up to 11.9 mm/yr in the southern region of Brazil for the 1970-2010 period, which agrees with Reguero *et al*. (2013).

The difference in extreme Hs trend values between studies could be due to the different ways of calculating extreme waves. Here extreme Hs is computed as the average of the top 5 % highest waves for a given period. Meanwhile both Wang and Swail (2002) and Dodet *et al*. (2010) used the 90^{th} percentile as the indicator, Ruggiero *et al*. (2010) averaged the five highest Hs per year, Reguero *et al*. (2013) used Hs12 as an indicator of the tail of extreme annual wave heights and Izaguirre *et al*. (2013) considered extreme Hs as the monthly maxima. Additionally, the periods being examined were different, mainly when comparing studies within one region, such as Brazil.

Table 17 Extreme Hs rates (m/yr; positive means increase) observed across the globe.

Study	Study area	Period studied	Hs rates (m/yr)
Present study	Southern Brazil	1970 - 2010	0.008 - 0.012
	Central Brazil		0.006 - 0.008
	Northern Brazil		0.005
Wang and Swail (2002)	NE Atlantic	1958 - 1997	0.01 - 0.03
Dodet *et al*. (2010)	NE Atlantic	1953 - 2009	0.02
Ruggiero *et al*. (2010)	NE Pacific	1970 - 2010	0.071
Reguero *et al*. (2013)	S Atlantic	1948 - 2012	0.008
	Southern Brazil		0.030
Izaguirre *et al*. (2013)	Northern Brazil	1980 - 2008	-0.015
	Falkland Islands		0.065
	Pacific Basin of Central America		0.028
	Rio de La Plata		0.020

5.5.3. Association to Climate Change

Climate change impacts by human actions is mostly dominant after 1950s and upper oceanic warming observed by several studies has also been indicated as a possible reason for positive Hs trends. By statistically comparing global wave power and SST, Reguero *et al*. (2019) found significant positive correlation between the two and a positive trend of the former by 0.4 % per year since 1948. The authors based their conclusion on the fact that wind waves respond to wind regime, which in turn is critically influenced by SST. Therefore, an increase in SST would lead to an increase in wave power, implying an increase in either wave height or period or even both.

According to Bender *et al*. (2010), in a global warming scenario it is projected that there will be a significant increase in the frequency of intense Atlantic storms (mainly categories 4 and 5) as a result of anthropogenic impacts. However, they only predict this impact for the second half of the 21st century. This would then eliminate the hypothesis raised here as to increased Hs trends in the north region as a consequence of increased storm activity.

The possible increase in Hs can bring several consequences to the marine and coastal systems. Among them are the increase in the mean depth of the mixed layer and effects on littoral processes, such as variations in alongshore sand transport and an increase in wave set-up, which would then lead to an increase in coastal erosion (Dragani *et al*., 2010). Marcos et al. (2019) brought up the matter regarding the possibility of combined increase in frequency of storm surges and extreme wave heights as a result of climate change, which could lead to increased coastal flooding and hazards.

6. Conclusions

The wave climate along the coast of Brazil was characterized and analyzed for its temporal variability during the last century with ERA-20C data from six sectors off the Brazilian coast. In general, there was an agreement amongst the results found and the existing literature.

Even though only two sectors out of the six analyzed could be validated with buoy data, it was shown that ERA-20C represents the wave climate of Brazil well enough to be applied in this study. However, for a more local study this data might not be the best tool given its low horizontal resolution of 125 km.

This study presented a few limitations such as the shortage of observational data in order to validate ERA-20C for the entire study area, due to a lack of information regarding this topic in the South Atlantic Ocean. Additionally, all results should be considered with care given the different data quality of the reanalysis product from the beginning of the century until the latest years. Ultimately, it ought to be indicated that reanalyses products, while they attend to a critical disparity in oceanic and atmospheric sciences, they require further additional data in order to obtain improved models and hindcasts.

The principal conclusions of this study comprise:

1. A spatial variability of the wave climate in the form of latitudinal variation with three behavioral groups (South – PS and PSE; Central – PE and PNE; North – PN1 and PN2).
2. Each group showed different dominant Dir, representative of distinct wave formation and generation mechanisms, as well as different fetch. For PS, PSE, PE and PNE it was verified that waves from E to SW represent the dominant swell regime. On the other hand, for PN1 and PN2, swell regimes come mainly from N and NE.
3. A strong seasonality of waves in each sector of the coast was also observed and, in some cases, a bimodal pattern was detected, which could be a result of exposure to two distinct wave generation areas or climatic regions. The most energetic waves occurred during the Austral winter, with exception of the north region, which showed its most energetic waves in the Austral summer. The different patterns are due to the fact that the southern region is under the influence of polar front systems and seasonal oscillations of the intensity and

position of the SASA. Meanwhile, the wave climate of the northern region is influenced mainly by the ITCZ.

4. Hs peaks were observed in the 1910-20s in the southern and central sectors, which could be associated with ENSO and/or TSA. However, due to the lack of measured and validated wind field at the start of the century these peaks might not be real.
5. Hs time series also displayed peaks in the 1940s along the entire coast of Brazil, although they were not so abrupt in the northern region. Based on the climatic conditions described in the literature for the 1940s and the results found in the present work it is likely that ONI and AMO played a role in the occurrence of such peaks.
6. Just as observed for mean Hs, there were two peaks of Hs5 values (1910s and 1940s), with the exception of the north region. On the other hand, the temporal variability of Tp5 values showed high variability and trends were not clear.
7. The wave conditions in the southern and central regions of Brazil showed to be dominated by the variability of two climate indices (AMO and TSA), which are probably also related to each other. On the other hand, for PN1 and PN2 the situation is more complex and even though AMM explains partially the wave climate of the region, no climate index alone can explain well the variability of all wave parameters.
8. In addition to the previously mentioned climate indices, the study indicates that SAM has some influence over Hs in the SAO, with decreasing impact from south to north. Thus, SAM influences the southern sector the most. Additionally, this result could be linked to the storms generated in the Southern Ocean.
9. The trend analysis indicated trends of increase in Hs for the entire time series, with values between 1.3 mm/yr and 3.7 mm/yr for mean conditions and between 1.0 mm/yr and 7.4 mm/yr for extreme Hs. The higher increasing rates for extreme waves indicate that not only waves are getting higher but that mostly storm waves are increasing. This could then be a reflection of more intense winds responsible for generating storms in the Atlantic Ocean as well as the increase of storm wave power hitting the coast. In addition, the rates at which Hs and Hs5 have been changing decrease with latitude while the opposite is true for Tp and Tp5.

10. A temporal variability of the trends was also observed. Hence, when splitting the 110-year time series into three periods it was noted that even though the overall Hs trends were positive in all sectors, most of the coast presented either a negative trend or no trend at all until 1969.
11. Positive Hs trends from the 1970s were identified for the entire coast and all Hs and Hs5 rates were higher for the last four decades than the overall rates (1901-2010). However, the highest rates were detected in the southern sectors (8 mm/yr for Hs and 11.9 mm/yr for Hs5 in PS) and the lowest in the northern (2.4 mm/yr for Hs in PN1 and 4.6 mm/yr for Hs5 in PN2). The positive wave height trends since the 1970s could be related to one or more of the following theories:
    a. SAM's positive trend since the 1960s controlling the Hs trends in the southern and central sectors, especially the storm waves and Hs5 trends.
    b. Increased storm activity in the Northern Hemisphere reflected in the AMM and the Hs trends in the northern sectors, even though these showed the lowest Hs rates.
    c. Upper oceanic warming as a result of climate change providing more energy to the atmosphere and as a consequence, to the wind waves as well.

A possible existence of correlations between the wave climate of the study area with the Atlantic Niño (ATL3) and the Southeastern Tropical Atlantic (SETA) might better explain how and why changes on the wave climate of SAO have been occurring in the last decades. Future perspective studies could also include an analysis focused on mean wave direction. For example, how this parameter has changed over the years and how it is impacted by the different climate indices as pointed out in the literature. In addition, a more precise analysis of extreme wave conditions could further benefit coastal management and hazard studies given the increased storm activity as one of the consequences of climate change. As a final recommendation, the advancement of data validation and multifactorial analysis could help to improve the different data quality observed in long-term reanalysis products.

Overall, this study represents a substantial advance regarding wave climate analysis in the South Atlantic Ocean and can be an important reference for coastal and marine planning and management in the area, considering climate change implications on wave conditions.

References

Aarnes, O. J., Abdalla, S., Bidlot, J. R., & Breivik, Ø. (2015). Marine wind and wave height trends at different ERA-interim forecast ranges. *Journal of Climate*, *28*(2), 819–837. https://doi.org/10.1175/JCLI-D-14-00470.1

Alexander, M. A., Kilbourne, K. H., & Nye, J. A. (2014). Climate variability during warm and cold phases of the Atlantic Multidecadal Oscillation (AMO) 1871-2008. *Journal of Marine Systems*, *133*, 14–26. https://doi.org/10.1016/j.jmarsys.2013.07.017

Almeida, L. R. de, Amaro, V. E., Marcelino, A. M. T., & Scudelari, A. C. (2015). Avaliação do clima de ondas da Praia de Ponta Negra (RN, Brasil) através do uso do SMC-Brasil e sua contribuição Ã gestão costeira. *Journal of Integrated Coastal Zone Management*, *15*(2), 135–151. https://doi.org/10.5894/rgci532

Alves, J. H. G. de M., Ribeiro, E. O., Matheson, G. S. G., Lima, J. A. M., & Ribeiro, C. E. P. (2009). Reconstituição do clima de ondas no sul-sudeste Brasileiro entre 1997 e 2005. *Revista Brasileira de Geofisica*, *27*(3), 427–445. https://doi.org/10.1590/S0102-261X2009000300010

Araujo, C. E. S., Franco, D., Melo, E., & Pimenta, F. (2003). Wave Regime Characteristics of the Southern. *International Conference on Coastal and Port Engineering in Developing Countries*, *097*, 1–15.

Araújo Junior, L. M., Da Silva, E. M., Costa, A. A., Sales, D. C., Guimarães, S. O., & Vasconcelos Junior, F. D. C. (2014). Assessment of the wind resources simulated over the Ceará state: A case study for the El Niño 97/98 and for the La Niña 98/99. *Revista Brasileira de Meteorologia*, *29*(1), 139–152. https://doi.org/10.1590/S0102-77862014000100013

Assunção, R. V. (2017). Variabilidade sazonal da dinâmica oceânica na região do mar de dentro do Arquipélago de Fernando de Noronha, PE. In *Curso de Pós-Graduação em Oceanografia*. Universidade Federal de Pernambuco.

Bacon, S., & Carter, D. J. T. (1991). Wave climate changes in the North Atlantic and North Sea. *International Journal of Climatology*, *11*(5), 545–558. https://doi.org/10.1002/joc.3370110507

Baines, P. G., & Folland, C. K. (2007). Evidence for a rapid global climate shift across the late 1960s. *Journal of Climate*, *20*(12), 2721–2744. https://doi.org/10.1175/JCLI4177.1

Barbariol, F., Bidlot, J. R., Cavaleri, L., Sclavo, M., Thomson, J., & Benetazzo, A. (2019). Maximum wave heights from global model reanalysis. *Progress in Oceanography*, *175*, 139–160. https://doi.org/10.1016/j.pocean.2019.03.009

Befort, D. J., Wild, S., Kruschke, T., Ulbrich, U., & Leckebusch, G. C. (2016). Different long-term trends of extra-tropical cyclones and windstorms in ERA-20C and NOAA-20CR reanalyses. *Atmospheric Science Letters*, *17*(11), 586–595. https://doi.org/10.1002/asl.694

Bender, M. A., Knutson, T. R., Tuleya, R. E., Sirutis, J. J., Vecchi, G. A., Garner, S. T., & Held, I. M. (2010). Modeled impact of anthropogenic warming on the frequency of intense Atlantic hurricanes. *Science*, *327*(5964), 454–458. https://doi.org/10.1126/science.1180568

Bertin, X., Prouteau, E., & Letetrel, C. (2013). A significant increase in wave height in the North Atlantic Ocean over the 20th century. *Global and Planetary Change*, *106*, 77–83. https://doi.org/10.1016/j.gloplacha.2013.03.009

Beserra, E. R., Mendes, A. L. T., Estefen, S. F., & Parente, C. E. (2007). Wave climate analysis for a wave energy conversion application in Brazil. *Proceedings of the International Conference on Offshore Mechanics and Arctic Engineering - OMAE*, *1*(January), 897–902. https://doi.org/10.1115/OMAE2007-29597

Bigg, G. R. (2003). *The oceans and climate* (2nd ed.). Cambridge University Press. New York, 286p.

Bird, E. (2008). *Coastal Geomorphology: An Introduction* (2nd ed.). John Wiley & Sons. West Sussex, 536p. https://doi.org/10.1029/01eo00219

Bittencourt, A. C. D. S. P., Dominguez, J. M. L., Martin, L., & Silva, I. R. (2000). Patterns of sediment dispersion coastwise the State of Bahia - Brazil. *Anais Da Academia Brasileira de Ciencias*, *72*(2), 271–287. https://doi.org/10.1590/S0001-37652000000200012

Buizza, R., Brönnimann, S., Haimberger, L., Laloyaux, P., Martin, M. J., Fuentes, M., Alonso-Balmaseda, M., Becker, A., Blaschek, M., Dahlgren, P., De Boisseson, E., Dee, D., Doutriaux-Boucher, M., Feng, X., John, V. O., Haines, K., Jourdain, S., Kosaka, Y., Lea, D., … Ziese, M. (2018). The EU-FP7 ERA-CLIM2 project contribution to advancing science and production of earth system climate reanalyses. *Bulletin of the American Meteorological Society*, *99*(5), 1003–1014. https://doi.org/10.1175/BAMS-D-17-0199.1

Campos, R. M. (2009). *Análise dos extremos de onda no Rio de Janeiro associados a ciclones extratropicais no Atlântico Sul*. Universidade Federal do Rio de Janeiro.

Campos, R. M., Alves, J. H. G. M., Guedes Soares, C., Guimaraes, L. G., & Parente, C. E. (2018). Extreme wind-wave modeling and analysis in the south Atlantic ocean. *Ocean Modelling*, *124*(January), 75–93. https://doi.org/10.1016/j.ocemod.2018.02.002

Carvalho, B. C., Dalbosco, A. L. P., & Guerra, J. V. (2020). Shoreline position change and the relationship to annual and interannual meteo-oceanographic conditions in Southeastern Brazil. *Estuarine, Coastal and Shelf Science*, *235*(2019), 10. https://doi.org/10.1016/j.ecss.2020.106582

Castro, B., Brandini, F., Pires-Vanin, A., & Miranda, L. (2006). Multidisciplinary oceanographic processes on the Western Atlantic continental shelf between 4 N and 34 S. *The Sea*, *14*, 259–293.

Cavalcanti, I. F. A., Ferreira, N. J., Silva, M. G. A. J., & Dias, M. A. F. S. (2009). *Tempo e Clima no Brasil*. Oficina de Textos. São Paulo, 468p.

Cecilio, R. O., & Dillenburg, S. R. (2019). An ocean wind-wave climatology for the Southern Brazilian Shelf. Part II: Variability in space and time. *Dynamics of Atmospheres and Oceans*, *88*, 14. https://doi.org/10.1016/j.dynatmoce.2019.101103

Cecilio, R. O., & Dillenburg, S. R. (2020). An ocean wind-wave climatology for the Southern Brazilian Shelf. Part I: Problem presentation and model validation. *Dynamics of Atmospheres and Oceans*, *89*, 19. https://doi.org/10.1016/j.dynatmoce.2019.101101

Chawla, A., Spindler, D. M., & Tolman, H. L. (2013). Validation of a thirty year wave hindcast using the Climate Forecast System Reanalysis winds. *Ocean Modelling*, *70*, 189–206. https://doi.org/10.1016/j.ocemod.2012.07.005

Compo, G. P., Whitaker, J. S., & Sardeshmukh, P. D. (2006). Feasibility of a 100-year reanalysis using only surface pressure data. *American Meteorological Society*, 175–190.

Contel, F. B. (2014). As divisões regionais do IBGE no século XX (1942, 1970 e 1990). *Terra Brasilis (Nova Série)*, *3*. https://doi.org/10.4000/terrabrasilis.990

Cuchiara, D., Fernandes, E. H., Strauch, J. C., & Calliari, L. J. (2006). Modelagem numérica do comportamento das ondas na costa do Rio Grande do Sul. *II Seminário e Workshop Em Engenharia Oceânica*, 15. Rio Grande, Brazil.

D'Agostino, R., & Lionello, P. (2016). Evidence of global warming impact on the evolution of the Hadley Circulation in ECMWF centennial reanalyses. *Climate Dynamics*, *48*, 3047–3060. https://doi.org/10.1007/s00382-016-3250-0

Davidson-Arnott, R. (2010). *Introduction to Coastal Processes and Geomorphology*. Cambridge University Press. New York, 458p.

Dee, D. P., Balmaseda, M., Balsamo, G., Engelen, R., Simmons, A. J., & Thépaut, J. N. (2014). Toward a consistent reanalysis of the climate system. *Bulletin of the American Meteorological Society*, *95*(8), 1235–1248. https://doi.org/10.1175/BAMS-D-13-00043.1

Dee, D. P., Källén, E., Simmons, A. J., & Haimberger, L. (2011). Reanalyses suitable for characterizing long-term trends. *Bulletin of the American Meteorological Society*, *92*(1), 65–70. https://doi.org/10.1175/2010BAMS3070.1

Dodet, G., Bertin, X., & Taborda, R. (2010). Wave climate variability in the North-East Atlantic Ocean over the last six decades. *Ocean Modelling*, *31*(3–4), 120–131. https://doi.org/10.1016/j.ocemod.2009.10.010

Dominguez, J. M. L. (2013). The Coastal Zone of Brazil: an Overview. *Journal of Coastal Research*, *39*, 16–20.

Dragani, W. C., Martin, P. B., Simionato, C. G., & Campos, M. I. (2010). Are wind wave heights increasing in south-eastern south American continental shelf between 32°S and 40°S? *Continental Shelf Research*, *30*(5), 481–490. https://doi.org/10.1016/j.csr.2010.01.002

Enfield, D. B., Mestas-Nuñez, A. M., & Trimble, P. J. (2001). The Atlantic multidecadal oscillation and its relation to rainfall and river flows in the continental U.S. *Geophysical Research Letters*, *28*(10), 2077–2080.

Enfield, D. B., Mestas-Nuñez, A. M., Mayer, D. A., & Cid-Serrano, L. (1999). How ubiquitous is the dipole relationship in tropical Atlantic sea surface temperatures? *Journal of Geophysical Research*, *104*(C4), 7841–7848. https://doi.org/10.1029/1998jc900109

Espindola, R. L., & Araújo, A. M. (2017). Wave energy resource of Brazil: An analysis from 35 years of ERA-Interim reanalysis data. *PLoS ONE*, *12*(8), 1–28. https://doi.org/10.1371/journal.pone.0183501

Farias, E.G.G. and Souza, J. M. A. C. (2012). Chegada Dispersiva de Campos de Ondas Swell na Costa Oeste do Estado Ceará – Brasil. *Arquivo de Ciências Do Mar*, *45*(1), 69–74. https://doi.org/10.32360/acmar.v45i1.145

Ferreira, J. A., & Guedes Soares, C. (2002). Modelling bivariate distributions of significant wave height and mean wave period. *Applied Ocean Research*, *24*(1), 31–45. https://doi.org/10.1016/S0141-1187(02)00006-8

Gilliland, J. M., & Keim, B. D. (2018). Position of the South Atlantic anticyclone and its impact on surface conditions across Brazil. *Journal of Applied Meteorology and Climatology*, *57*(3), 535–553. https://doi.org/10.1175/JAMC-D-17-0178.1

Goldenberg, S. B., Landsea, C. W., Mestas-Nuñez, A. M., & Gray, W. M. (2001). The recent increase in Atlantic hurricane activity: Causes and implications. *Science*, *293*(5529), 474–479. https://doi.org/10.1126/science.1060040

Gomes, G., & Silva, A. C. da. (2018). Nearshore wave analysis in the Brazilian Northeast based on observations and numerical models. *Journal of Operational Oceanography*, *11*(1), 44–53. https://doi.org/10.1080/1755876X.2018.1438567

Gulev, S. K., & Grigorieva, V. (2004). Last century changes in ocean wind wave height from global visual wave data. *Geophysical Research Letters*, *31*(24), 1–4. https://doi.org/10.1029/2004GL021040

Harley, M. D., Turner, I. L., Short, A. D., & Ranasinghe, R. (2010). Interannual variability and controls of the Sydney wave climate. *International Journal of Climatology*, *30*(9), 1322–1335. https://doi.org/10.1002/joc.1962

Haver, S. (1985). Wave climate off Northern Norway. *Applied Ocean Research*, *7*(2), 85–92.

Hemer, M. A., Church, J. A., & Hunter, J. R. (2010). Variability and trends in the directional wave climate of the Southern Hemisphere. *International Journal of Climatology*, *30*(4), 475–491. https://doi.org/10.1002/joc.1900

Hersbach, H., Peubey, C., Simmons, A., Berrisford, P., Poli, P., & Dee, D. (2015). ERA-20CM: A twentieth-century atmospheric model ensemble. *Quarterly Journal of the Royal Meteorological Society*, *141*(691), 2350–2375. https://doi.org/10.1002/qj.2528

Holthuijsen, L. H. (2007). *Waves in Oceanic and Coastal Waters*. Cambridge University Press. New York, 458p.

Hounsou-Gbo, G. A., Servain, J., Araujo, M., Caniaux, G., Bourlès, B., Fontenele, D., & Martins, E. S. P. R. (2019). SST indexes in the tropical South Atlantic for forecasting rainy seasons in Northeast Brazil. *Atmosphere*, *10*(6). https://doi.org/10.3390/atmos10060335

Hughes, S.A. and Miller, H. C. (1987). Transformation of Significant Wave Heights. *Journal of Waterway, Port, Coastal, and Ocean Engineerin*, *113*(6), 588–605.

Izaguirre, C., Méndez, F. J., Espejo, A., Losada, I. J., & Reguero, B. G. (2013). Extreme wave climate changes in Central-South America. *Climatic Change*, *119*(2), 277–290. https://doi.org/10.1007/s10584-013-0712-9

Kayano, M. T., & Capistrano, V. B. (2014). How the Atlantic multidecadal oscillation (AMO) modifies the ENSO influence on the South American rainfall. *International Journal of Climatology*, *34*(1), 162–178. https://doi.org/10.1002/joc.3674

Kerr, R. A. (2000). A North Atlantic climate pacemaker for the centuries. *Science*, *288*(June), 1984–1986.

Killick, R., Eckley, I. A., Ewans, K., & Jonathan, P. (2010). Detection of changes in variance of oceanographic time-series using changepoint analysis. *Ocean Engineering*, *37*(13), 1120–1126. https://doi.org/10.1016/j.oceaneng.2010.04.009

Knight, J. R., Folland, C. K., & Scaife, A. A. (2006). Climate impacts of the Atlantic Multidecadal Oscillation. *Geophysical Research Letters*, *33*(17), 4. https://doi.org/10.1029/2006GL026242

Kossin, J. P., & Vimont, D. J. (2007). A more general framework for understanding atlantic hurricane variability and trends. *Bulletin of the American Meteorological Society*, *88*(11), 1767–1781. https://doi.org/10.1175/BAMS-88-11-1767

Kumar, P., Kaur, S., Weller, E., & Min, S. K. (2019). Influence of Natural Climate Variability on the Extreme Ocean Surface Wave Heights Over the Indian Ocean. *Journal of Geophysical Research: Oceans*, *124*(8), 6176–6199. https://doi.org/10.1029/2019JC015391

Kumar, P., Min, S. K., Weller, E., Lee, H., & Wang, X. L. (2016). Influence of climate variability on extreme ocean surface wave heights assessed from ERA-interim and ERA-20C. *Journal of Climate*, *29*(11), 4031–4046. https://doi.org/10.1175/JCLI-D-15-0580.1

Lourenço, T. de S. (2012). *Variabilidade interanual do clima de ondas e sua influência no litoral Sudeste e Sul do Brasil*. Universidade de São Paulo. São Paulo, 108p.

Marcos, M., Rohmer, J., Vousdoukas, M. I., Mentaschi, L., Le Cozannet, G., & Amores, A. (2019). Increased Extreme Coastal Water Levels Due to the Combined Action of Storm Surges and Wind Waves. *Geophysical Research Letters*, *46*(8), 4356–4364. https://doi.org/10.1029/2019GL082599

Marshall, A. G., Hemer, M. A., Hendon, H. H., & McInnes, K. L. (2018). Southern annular mode impacts on global ocean surface waves. *Ocean Modelling*, *129*(June), 58–74. https://doi.org/10.1016/j.ocemod.2018.07.007

Marshall, G. J. (2003). Trends in the Southern Annular Mode from observations and reanalyses. *Journal of Climate*, *16*(24), 4134–4143. https://doi.org/10.1175/1520-0442(2003)016<4134:TITSAM>2.0.CO;2

Martucci, G., Carniel, S., Chiggiato, J., Sclavo, M., Lionello, P., & Galati, M. B. (2010). Statistical trend analysis and extreme distribution of significant wave height from 1958 to 1999 - An application to the Italian Seas. *Ocean Science*, *6*(2), 525–538. https://doi.org/10.5194/os-6-525-2010

Masselink, G., & Gehrels, R. (2014). *Coastal Environments & Global Change*. American Geophysical Union and John Wiley & Sons, Ltd. www.wiley.com/go/masselink/coastal

Mentaschi, L., Vousdoukas, M. I., Voukouvalas, E., Dosio, A., & Feyen, L. (2017). Global changes of

extreme coastal wave energy fluxes triggered by intensified teleconnection patterns. *Geophysical Research Letters*, *44*(5), 2416–2426. https://doi.org/10.1002/2016GL072488

Miyasaka, T., & Nakamura, H. (2010). Structure and mechanisms of the Southern Hemisphere summertime subtropical anticyclones. *Journal of Climate*, *23*(8), 2115–2130. https://doi.org/10.1175/2009JCLI3008.1

Moura, M. R. (2012). Aspectos Climáticos versus Variação Sazonal do Perfil Morfodinâmico das Praias do Litoral Oeste de Aquiraz, Ceará, Brasil. *Revista Brasileira de Climatologia*, *11*, 208–222.

NOAA, National Oceanic and Atmospheric Administration, C. P. C. (CPD). (2017). *Description of Changes to Ocean Nino Index (ONI)*. https://www.cpc.ncep.noaa.gov/products/analysis_monitoring/ensostuff/ONI_change.shtml. Accessed on 23rd of December 2019.

NOAA, National Oceanic and Atmospheric Administration, P. S. D. (ESRL). (2019). *El Niño Southern Oscillation (ENSO)*. https://www.esrl.noaa.gov/psd/enso/. Accessed on 23rd of December 2019.

Nobre, P. and Shukla, J. (1996). Variations of Sea Surface Temperature, Wind Stress, and Rainfall over the Tropical Atlantic and South America. *Journal of Climate*, *9*, 2464–2479.

Oliveira, B. A., Sobral, F., Fetter, A., & Mendez, F. J. (2019). A high-resolution wave hindcast off Santa Catarina (Brazil) for identifying wave climate variability. *Regional Studies in Marine Science*, *32*, 15. https://doi.org/10.1016/j.rsma.2019.100834

Pecher, A. and Kofoed, J. P. (2017). *Handbook of Ocean Wave Energy*. Springer Open. Aalborg, 305p.

Pereira, N. E. S., & Klumb-Oliveira, L. A. (2015). Analysis of the influence of ENSO phenomena on wave climate on the central coastal zone of Rio de Janeiro (Brazil). *Journal of Integrated Coastal Zone Management*, *15*(3), 353–370. https://doi.org/10.5894/rgci570

Pianca, C., Mazzini, P. L. F., & Siegle, E. (2010). Brazilian offshore wave climate based on NWW3 reanalysis. *Brazilian Journal of Oceanography*, *58*(1), 53–70.

Poli, P., Hersbach, H., Dee, D. P., Berrisford, P., Simmons, A. J., Vitart, F., Laloyaux, P., Tan, D. G. H., Peubey, C., Thépaut, J. N., Trémolet, Y., Hólm, E. V., Bonavita, M., Isaksen, L., & Fisher, M. (2016). ERA-20C: An atmospheric reanalysis of the twentieth century. *Journal of Climate*, *29*(11), 4083–4097. https://doi.org/10.1175/JCLI-D-15-0556.1

Poli, P., Hersbach, H., Tan, D., Dee, D., Thépaut, J. N., Simmons, A., Peubey, C., Laloyaux, P., Komori, T., Berrisford, P., Dragani, R., Trémolet, Y., Hólm, E., Bonavita, M., Isaksen, L., & Fisher, M. (2013). ERA report series. The data assimilation system and initial performance evaluation of the ECMWF pilot reanalysis of the 20th-century assimilating surface observations only (ERA-20C). In *ERA Report Series No. 14*.

Reboita, M. S., Ambrizzi, T., Silva, B. A., Pinheiro, R. F., & Rocha, R. P. da. (2019). The south atlantic subtropical anticyclone: Present and future climate. *Frontiers in Earth Science*, *7*, 1–15. https://doi.org/10.3389/feart.2019.00008

Reguero, B. G., Menéndez, M., Méndez, F. J., Mínguez, R., & Losada, I. J. (2012). A Global Ocean Wave (GOW) calibrated reanalysis from 1948 onwards. *Coastal Engineering*, *65*, 38–55. https://doi.org/10.1016/j.coastaleng.2012.03.003

Reguero, B. G., Méndez, F. J., & Losada, I. J. (2013). Variability of multivariate wave climate in Latin America and the Caribbean. *Global and Planetary Change*, *100*, 70–84. https://doi.org/10.1016/j.gloplacha.2012.09.005

Reguero, B. G., Losada, I. J., & Méndez, F. J. (2019). A recent increase in global wave power as a consequence of oceanic warming. *Nature Communications*, *10*(1), 1–14. https://doi.org/10.1038/s41467-018-08066-0

Rodríguez-Fonseca, B., Polo, I., García-Serrano, J., Losada, T., Mohino, E., Mechoso, C. R., & Kucharski, F. (2009). Are Atlantic Niños enhancing Pacific ENSO events in recent decades? *Geophysical Research Letters*, *36*(20). https://doi.org/10.1029/2009GL040048

Ruggiero, P., Komar, P. D., & Allan, J. C. (2010). Increasing wave heights and extreme value projections: The wave climate of the U.S. Pacific Northwest. *Coastal Engineering*, *57*(5), 539–552. https://doi.org/10.1016/j.coastaleng.2009.12.005

Seymour, R.J.; Strange, R.R.; Cayan, D.R.; Nathan, R. A. (1984). Influence of El Ninos on Claifornia's Wave Climate. In *Coastal Engineering* (Issue 1, pp. 577–592). ASCE.

Silva, A. C. da, Façanha, P., Bezerra, C., Araujo, A., & Pitombeiras, E. (2011). Características das Ondas "Sea" and "Swell" Observadas no Litoral do Ceará-Brasil: Variabilidade Anual e Inter-anual. *Tropical Oceanography*, *39*(2), 123–132. https://doi.org/10.5914/to.2011.055

Silva, Alex C. da, Bezerra, C. S., Barcellos, R. L., Araújo, M., Bouchonneau, N., & Manso, V. (2016). Seasonal and Intraseasonal Variability of Wave Climate on the NE Brazilian Coast using a Nautical Radar System. *Journal of Coastal Research*, *75*, 927–931. https://doi.org/10.2112/si75-186.1

Silva, P. G., Klein, A. H. F., González, M., Gutierrez, O., & Espejo, A. (2015). Performance assessment of the database downscaled ocean waves (DOW) on Santa Catarina coast, South Brazil. *Anais Da Academia Brasileira de Ciencias*, *87*(2), 623–634. https://doi.org/10.1590/0001-3765201520140329

Sprovieri, F. C. (2018). *Clima de Ondas , Potencial Energético e o Transporte de Sedimentos no Litoral Norte do Rio Grande do Sul*. Universidade Federal do Ri o Grande do Sul, 142p.

Stech, J. L., & Lorenzzetti, J. A. (1992). The Response of the South Brazil Night to the Passage of Wintertime Cold Fronts. *Journal of Geophysical Research*, *97*(C6), 9507–9520.

Stewart, R. H. (2005). *Introduction to Physical Oceanography*. Department of Oceanography, Texas A&M University. https://doi.org/10.1119/1.1941791

Sun, X., Cook, K. H., & Vizy, E. K. (2017). The South Atlantic subtropical high: Climatology and interannual variability. *Journal of Climate*, *30*(9), 3279–3296. https://doi.org/10.1175/JCLI-D-16-0705.1

Talley, L. D., Pickard, G. L., Emery, W. J., & Swift, J. H. (2011). *Descriptive Physical Oceanography:*

an introduction (6th ed.). Elsevier. London, 983p.

Tessler, M. G., & Goya, S. C. (2005). Processos Costeiros Condicionantes do Litoral Brasileiro. *Revista Do Departamento de Geografia*, *17*, 11–23.

Torrence, C., & Compo, C. (1998). A Practical Guide to Wavelet Analysis. *Bulletin of the American Meteorological Society*, *79*(1), 61–78. https://doi.org/10.1016/j.biopha.2017.10.142

Trenberth, Kevin, Zhang, R. & N. C. for A. R. S. (2019). *The Climate Data Guide: Atlantic Multi-decadal Oscillation (AMO)*. https://climatedataguide.ucar.edu/climate-data/atlantic-multi-decadal-oscillation-amo. Accessed on 7th of April 2020.

Utida, G., Cruz, F. W., Etourneau, J., Bouloubassi, I., Schefuß, E., Vuille, M., Novello, V. F., Prado, L. F., Sifeddine, A., Klein, V., Zular, A., Viana, J. C. C., & Turcq, B. (2019). Tropical South Atlantic influence on Northeastern Brazil precipitation and ITCZ displacement during the past 2300 years. *Scientific Reports*, *9*(1), 1–8. https://doi.org/10.1038/s41598-018-38003-6

Venegas, S. A., Mysak, L. A., & Straub, D. N. (1998). An interdecadal climate cycle in the South Atlantic and its links to other ocean basins. *Journal of Geophysical Research: Oceans*, *103*(C11), 24723–24736. https://doi.org/10.1029/98JC02443

Vieira, L. A. de A., Pitombeira, E. da S., & Souza, R. O. de. (2007). Análise Estatística do Regime de Ondas ao Longo da Região Marítima do Porto do Pecém. *XVII Simpósio Brasileiro de Recursos Hídricos*, *85*, 1–20.

Vimont, D. J., & Kossin, J. P. (2007). The Atlantic Meridional Mode and hurricane activity. *Geophysical Research Letters*, *34*(7), 1–5. https://doi.org/10.1029/2007GL029683

Vizy, E. K., & Cook, K. H. (2016). Understanding long-term (1982–2013) multi-decadal change in the equatorial and subtropical South Atlantic climate. *Climate Dynamics*, *46*(7–8), 2087–2113. https://doi.org/10.1007/s00382-015-2691-1

Vujkov, B., Dumnić, B., Grbić, T., Popadić, B., Vukajlović, N., & Medić, S. (2019). Spectral analysis of ocean waves for determination of fundamental energy parameters. *EUROCON 2019 - 18th International Conference on Smart Technologies*, 1–5. https://doi.org/10.1109/EUROCON.2019.8861877

Wainer, I., & Venegas, S. A. (2002). South Atlantic multidecadal variability in the climate system model. *Journal of Climate*, *15*(12), 1408–1420. https://doi.org/10.1175/1520-0442(2002)015<1408:SAMVIT>2.0.CO;2

Wang, C. (2019). Three-ocean interactions and climate variability: a review and perspective. *Climate Dynamics*, *53*(7–8), 5119–5136. https://doi.org/10.1007/s00382-019-04930-x

Wang, X. L., & Swail, V. R. (2001). Changes of extreme Wave Heights in northern Hemisphere Oceans and related atmospheric circulation regimes. *Journal of Climate*, *14*(10), 2204–2221. https://doi.org/10.1175/1520-0442(2001)014<2204:COEWHI>2.0.CO;2

Wang, X. L., & Swail, V. R. (2002). Trends of Atlantic wave extremes as simulated in a 40-yr wave hindcast using kinematically reanalyzed wind fields. *Journal of Climate*, *15*(9), 1020–1035. https://doi.org/10.1175/1520-0442(2002)015<1020:TOAWEA>2.0.CO;2

Wang, Xi. L., Feng, Y., & Swail, V. R. (2012). North atlantic wave height trends as reconstructed from the 20th century reanalysis. *Geophysical Research Letters*, *39*(17), 1–6. https://doi.org/10.1029/2012GL053381

Wells, N. C. (2012). *The Atmosphere and Ocean: a physical introduction* (3rd ed.). John Wiley & Sons, Ltd.

WMO, World Meteorological Organization (1998). Guide to Wave Analysis and Forecasting. In *World Meterological Organization (WMO-No. 702)* (2nd ed., Issue 702).

Wu, L., Wang, X. L., & Feng, Y. (2014). Historical wave height trends in the South and East China Seas, 1911-2010. *Journal of Geophysical Research: Oceans*, *119*, 4399–4409. https://doi.org/10.1002/2014JC010087

Young, I. R. (1999). Seasonal variability of the global ocean wind and wave climate. *International Journal of Climatology*, *19*(9), 931–950. https://doi.org/10.1002/(SICI)1097-0088(199907)19:9<931::AID-JOC412>3.0.CO;2-O

Young, I. R., & Ribal, A. (2019). Multiplatform evaluation of global trends in wind speed and wave height. *Science*, *364*(6440), 548–552. https://doi.org/10.1126/science.aav9527

Zampieri, M., Russo, S., di Sabatino, S., Michetti, M., Scoccimarro, E., & Gualdi, S. (2016). Global assessment of heat wave magnitudes from 1901 to 2010 and implications for the river discharge of the Alps. *Science of the Total Environment*, *571*, 1330–1339. https://doi.org/10.1016/j.scitotenv.2016.07.008

Annex A

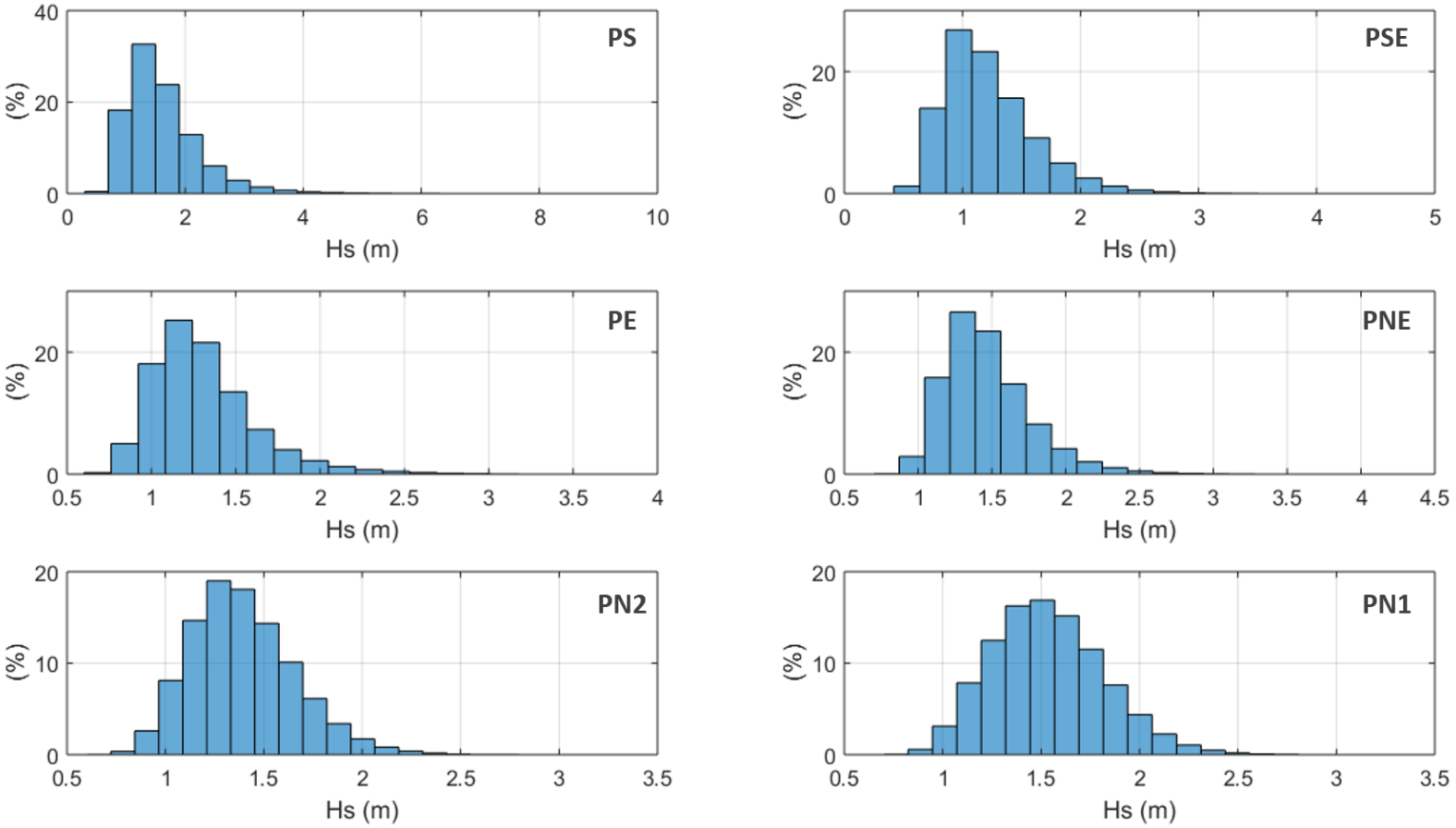

Figure 52 Hs frequency distribution histograms for each sector of the Brazilian coast.

Annex B

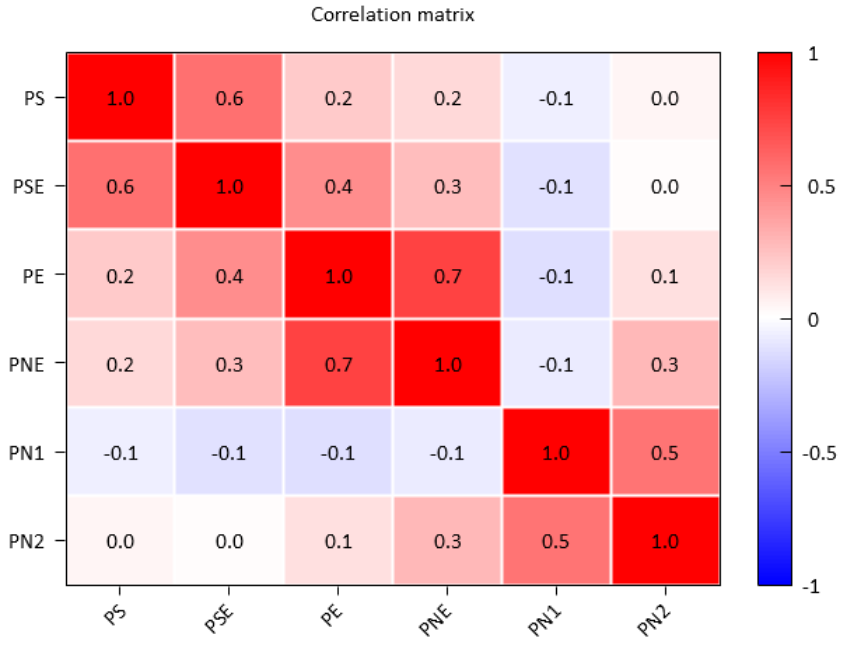

Figure 53 Correlation matrix referring to the relationship between sectors of the Brazilian coast, based on Hs (m).

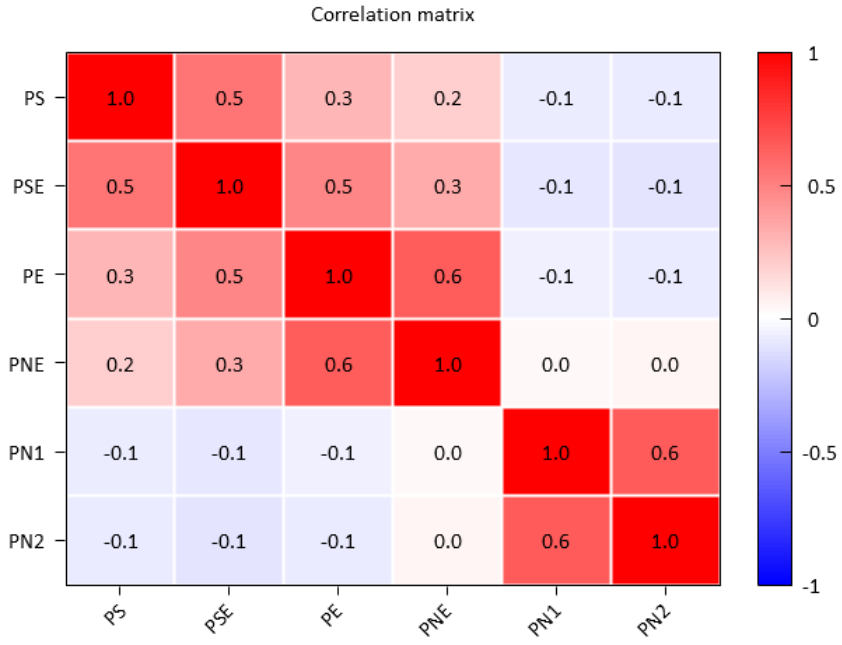

Figure 54 Correlation matrix referring to the relationship between sectors of the Brazilian coast, based on Tp (s).

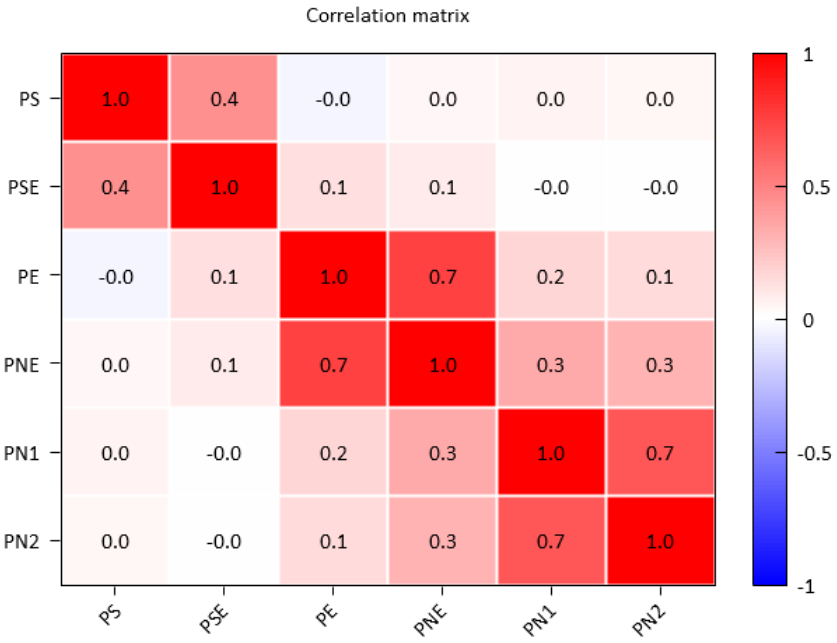

Figure 55 Correlation matrix referring to the relationship between sectors of the Brazilian coast, based on Dir (°).

Annex C

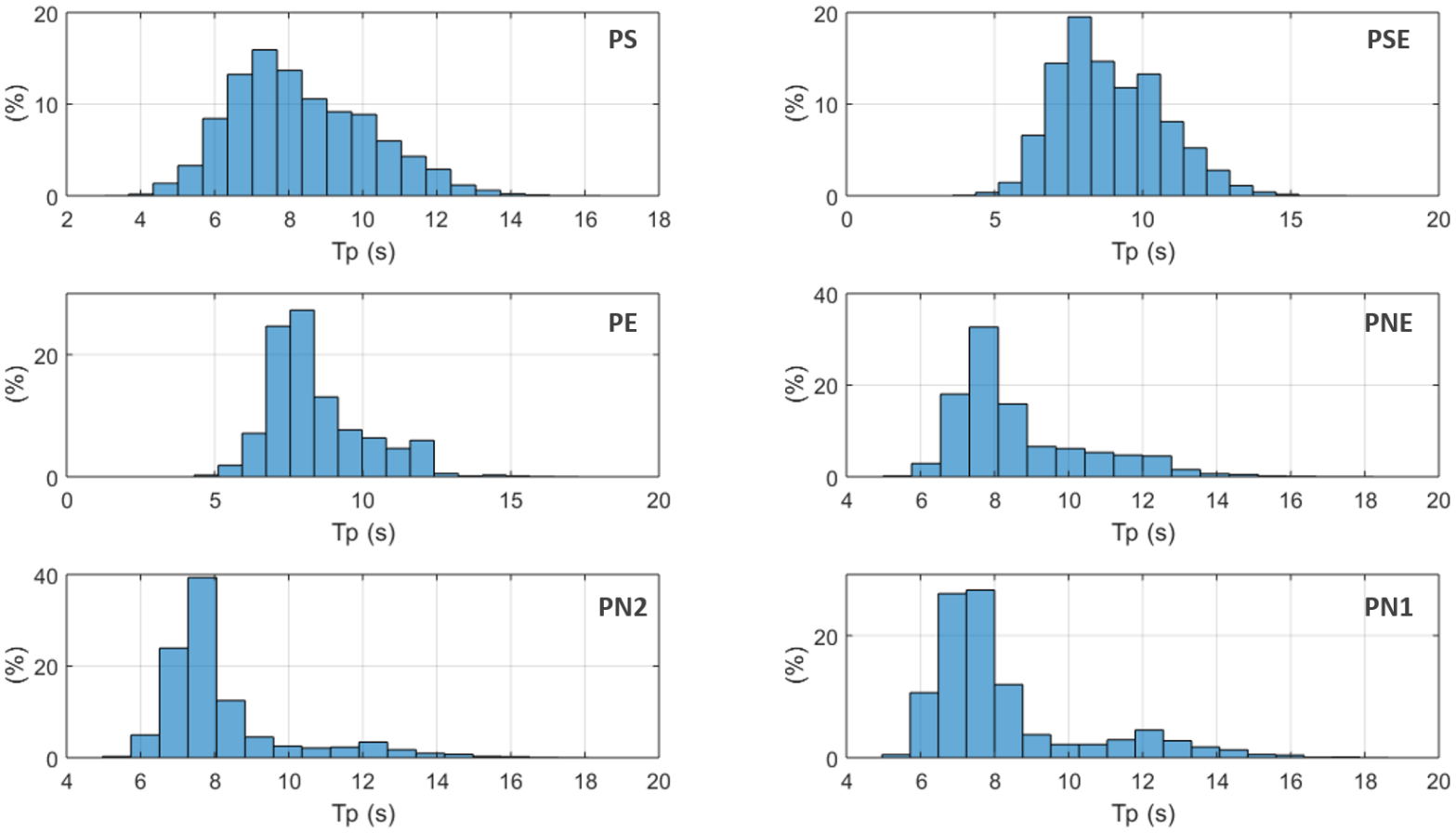

Figure 56 Tp frequency distribution histograms for each sector of the Brazilian coast.

Annex D

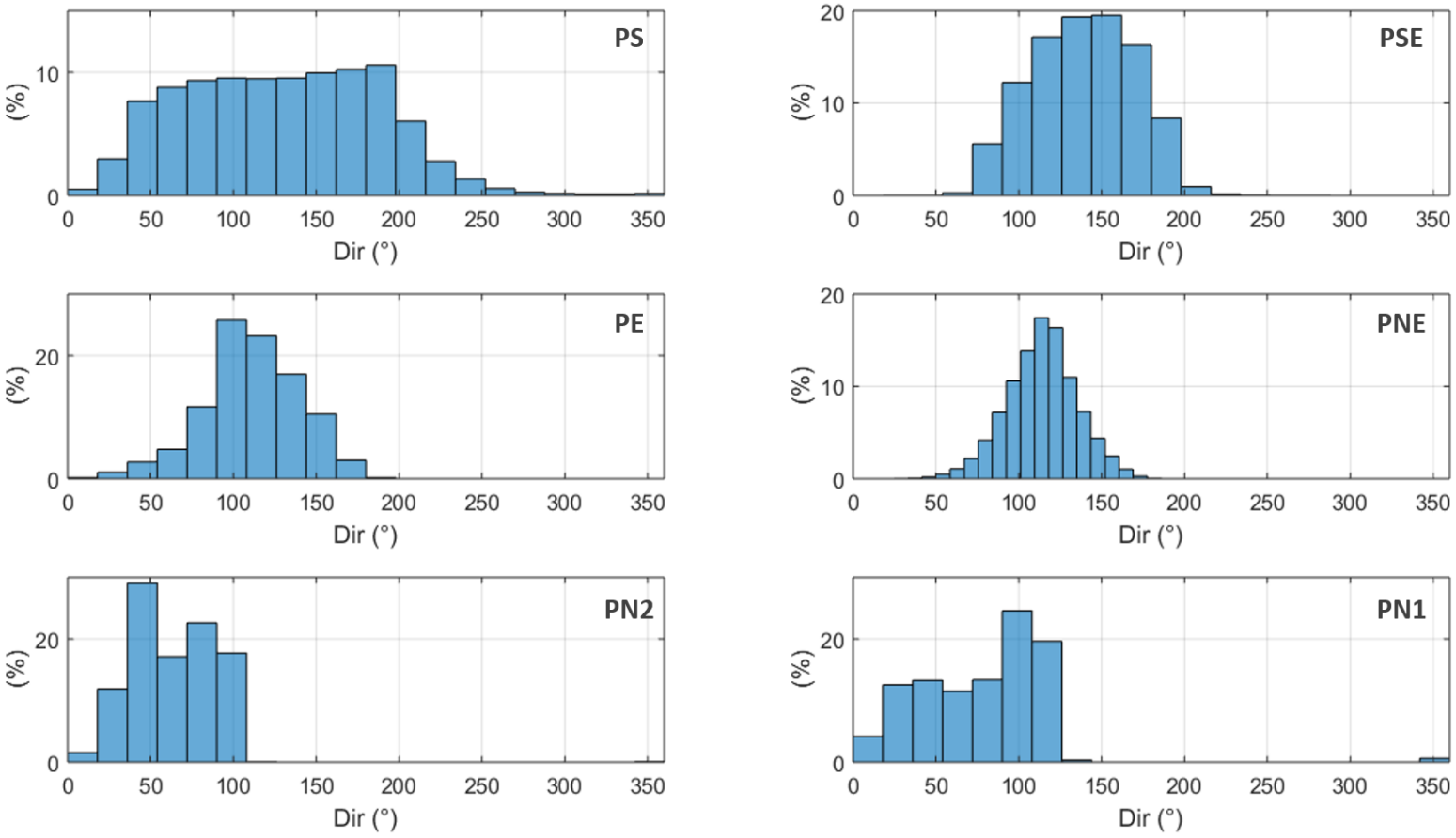

Figure 57 Dir frequency distribution histograms for each sector of the Brazilian coast.

Annex E

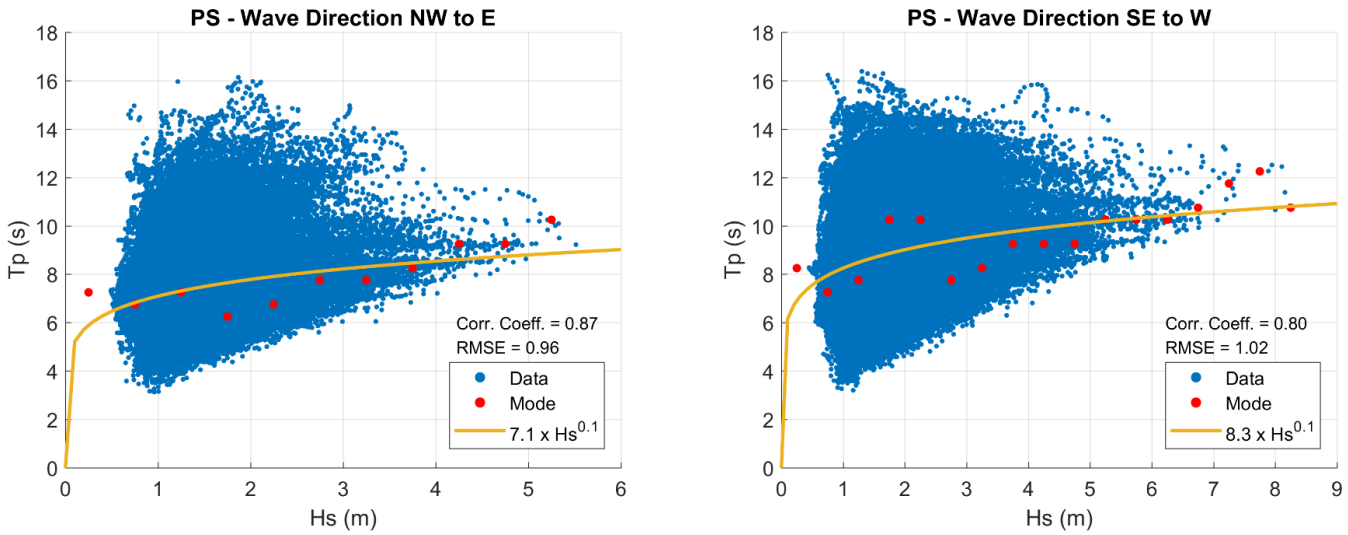

Figure 58 Exponential fits between Hs and Tp for waves with Dir from NW to E (left) and SE to W (right) in PS, including RMSE values and significant correlation coefficients (99 % confidence level).

Annex F

Table 18 Pearson correlation coefficients between Hs and AAO and Tp and AAO for each sector of the coast.

Index	Parameter	PS	PSE	PE	PNE	PN1	PN2
AAO	Hs	0.09	0.09	0.08	-0.01	-0.04	-0.06
	Tp	0.04	0.00	0.01	0.05	0.00	-0.01